CSULB MARS Project (Monterey and Related Sediments)
2015 Field Trip

Overview of the Monterey Formation:
Understanding Stratigraphy, Lithology, Diagenesis and Deformation by Examination of Classic Locations in Santa Barbara County, California

Field Trip Leader: Rick Behl
California State University Long Beach
with contributions by Michael Gross

2015 MARS Project Field Trip Study Locations

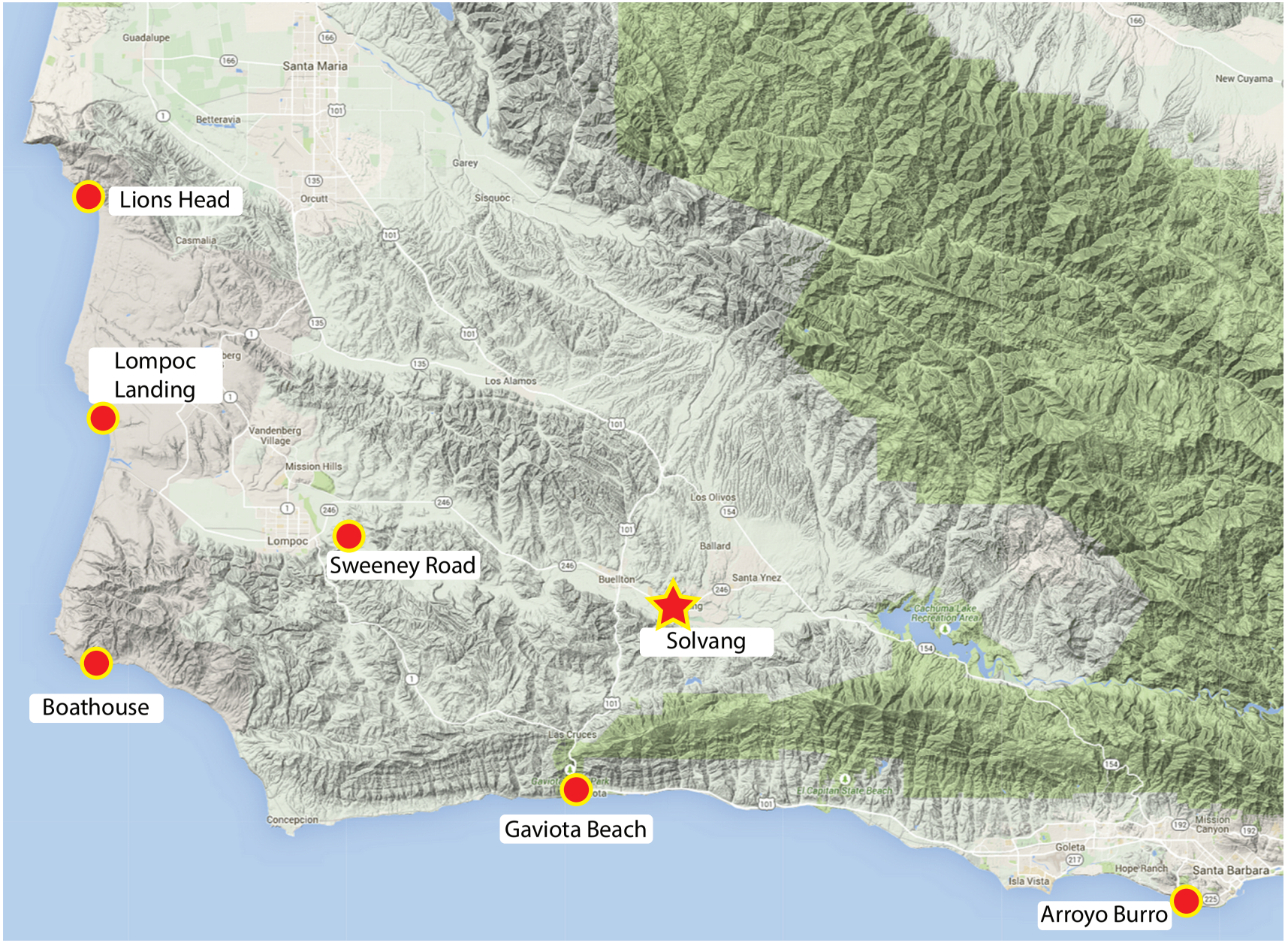

2015 MARS Project Field Trip Itinerary

Day 1: Monday, July 20.

Drive to and assemble in Solvang, CA.
Venue: Hadsen House, 1450 Mission Dr., Solvang, 93463, CA
Meet at 12:00 Noon for lunch in meeting room at Hadsen House.
Overview presentations on the Monterey Formation and field areas.
Check-in to hotel.
Field trip depart about 2:30 PM.
Sweeney Road. ~30 minute drive. (Opal-A diatomite, opal-CT porcelanite, opal-CT chert, cyclic stratigraphy, silica diagenesis, deformational style).
Return to Hadsen House by about 6 PM.
7:30 PM. Group dinner at the Succulent Café (~5 minute walk from Hadsen House).

Day 2: Tuesday, July 21.

Breakfast at hotel.
Field Trip. Assemble at CSULB vehicles for 7:30 AM departure.
Pick up lunches in Buellton on route to Gaviota Beach (~30 minutes).
Gaviota Beach State Beach. No sample collecting permitted. (Monterey stratigraphy, diverse lithologies (opal-CT phase, calcareous, phosphatic and organic-rich rocks), submarine slope gulley channels reservoirs. ~2.5-mile round trip walk on beach. Lunch at Gaviota Beach.
Arroyo Burro Beach. Drive to Mesa Lane Stairs in Santa Barbara (~35 minutes). (Lateral facies changes, axis-parallel extension, mechanical stratigraphy, fracture networks, fault scaling, permeable faults, fluid flow).
~ 1.5-mile round trip walk on beach, including 100' of stairs.
Return to Hadsen House by ~5 PM.
Dinner in informal groups.

Day 3: Wednesday, July 22.

Breakfast at hotel.
Check-out of hotel for most participants.
Field Trip. Assemble at CSULB vehicles for 7:30 AM departure.
Some participants may wish to drive their own cars and leave at Vandenberg Air Force Base gate instead of returning to Solvang at end of day.
Drive to Vandenberg gate (~40 minutes).
Check-in to get base badges (unknown military time?).
Boat House section. ~45 minute drive. (quartz-phase porcelanite, chert and dolomite, bedding-parallel slip, early shortening of intrastratal contorted chert fold; timing of deformation and diagenesis vs. oil migration).
Lompoc Landing/Wall Beach. ~45 minute drive. (exhumed charged oil field in opal-CT to quartz transition, fracture networks, bed-confined and multi-layer fractures, chert breccias); possibly Lions Head (but unlikely to have sufficient time).

Field day will end at approximately 3:30 PM and participants can either drive back to Solvang or return to their homes if they brought their cars to Vandenberg.

2015 CSULB MARS Project Annual Field Trip Participants List

CSULB MARS Team
Rick Behl (Professor and Director)
Pam Hill (Post-doc and Lecturer)
Tessfalidet Kassa (Graduate student)
Yannick Wirtz (Graduate student)
Maia Davis (Graduate student)
Alex Sedlak (Graduate student)
Ryan Weller (Graduate student)

MARS Corporate Affiliates Professional Participants
David Brewster, Bayswater
Stan Obernyer, Bayswater
Kevin F. Kane, Bayswater
David Lowe, ExxonMobil
Jim McNabb, ExxonMobil
Brady Barto, Signal Hill Petroleum
Mitchell Barklage, Signal Hill Petroleum
Donald Clarke, Signal Hill Petroleum
Yucqiang (Richard) Chang, California Resources Corporation
Courtney Libben, California Resources Corporation
Chris Sine, California Resources Corporation
Veronika Riaboukha, California Resources Corporation
Lisa Alpert, Aera Energy
David Miner, Aera Energy
Chad Severson, Aera Energy
Greg Gordon, Aera Energy
Christian Aguilar, BreitBurn/PCEC
Ivan Aburto, BreitBurn/PCEC
Conor James O'Toole, BreitBurn/PCEC
Jireh Groenow, BreitBurn/PCEC
Neal Livingston, Freeport McMoRan
Michael Quilliam, Freeport McMoRan
Olawale Olabisi, Freeport McMoRan

2015 MARS Project Annual Monterey Formation Field Trip

Monterey Formation Overview, Santa Maria and Santa Barbara Counties
Monday-Wednesday, July 20-22, 2015
Field Leader: Rick Behl
Structural material contributed by Michael Gross, now with Shell.

INTRODUCTION PART 1 - GENERAL OVERVIEW

This 2.5-day field trip will examine several classic locations of the Miocene Monterey Formation in the Santa Maria and Santa Barbara basins in order to gain insight into the stratigraphic, lithologic, and diagenetic character of siliceous rocks. At multiple sites, we will address the following themes:

- Lithofacies characterization, focusing on silica-rich rocks, but including carbonates and mixed biogenic-siliciclastic lithofacies
- Reservoir significance of lithology, silica diagenetic stage, and timing of diagenesis
- Styles of faulting and folding that vary with scale, lithology, silica phase, and timing.
- Fracture networks and mechanical stratigraphy

Field trip stops will be coordinated with low tides. Please keep safety in mind when traversing wet, slippery rocks or examining outcrops with your back to the surf.

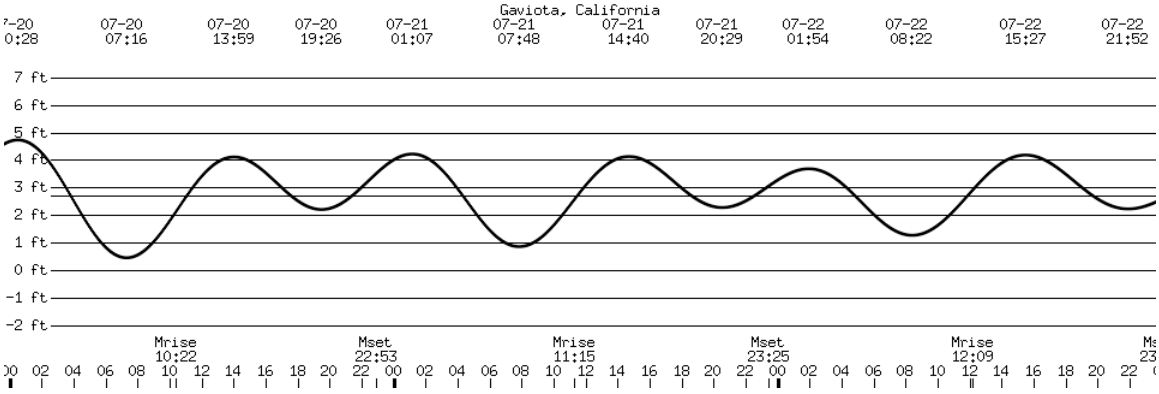

Figure I-01. Tide chart for field trip.

THE MONTEREY FORMATION

The Miocene Monterey Formation is spread across much of onshore California and the offshore California margin (Bramlette, 1946; Behl, 1999), and equivalents extend around the Pacific Rim. It is a largely bio-siliceous, fine-grained deposit that accumulated in small basins that formed in the early to middle Miocene in response to the subduction of the Pacific-Farallon spreading center and development of the San Andreas transform margin (Blake *et al*., 1978; Pisciotto & Garrison, 1981; Isaacs, *et al*., 1983;

Atwater, 1989; Nicholson *et al*., 1994). The Monterey is primarily known as a diatomaceous, organic-rich hemipelagic unit deposited mostly beneath a strong upwelling zone and well-developed oxygen minimum zone (Ingle, 1981; Pisciotto & Garrison, 1981). However, the conditions of its deposition led it to also be unusually enriched in phosphate, or dolomite or limestone in certain locations or stratigraphic levels – this serves as the basis for separating different members or units within the Monterey overall (Fig. I-03). Typical Monterey lithologies are: diatomite, diatomaceous and siliceous shale, porcelanite, chert, calcareous and phosphatic shale, dolostone and limestone. These rocks are differentiated by composition, texture, and their physical properties.

Silica diagenesis

The Monterey Formation has been buried and uplifted to different depths, consequently it contains all silica phases (Fig. I-04) (Bramlette, 1946; Murata & Larson, 1975; Pisciotto, 1981; Isaacs, 1981a; Pisciotto & Garrison, 1981). These silica phases include: biogenic opal-A (hydrous silica with an X-ray amorphous structure) which makes up the shells of diatoms and radiolarians; metastable opal-CT (hydrous silica with crystal structure similar to mixed cristobalite and tridymite) which forms with increased temperature or time from dissolved opal-A; and the stable end-product, diagenetic quartz, which forms by another dissolution/reprecipitation step with further burial or time. Field and geochemical evidence indicates that cherts can form earlier than porcelanite (Murata & Nakata, 1974; Behl & Garrison, 1994: Behl, 1998). In addition to temperature and time, compositional variations in clay, organic matter, and calcium carbonate content are also important in controlling the rates of silica diagenesis. The presence of clay and organic matter retards the opal-A to opal-CT transformation (Fig. I-04; Kastner *et al*., 1977; Isaacs, 1981a, 1982; Hinman, 1990), whereas the presence of calcium carbonate increases the rate of opal-CT nucleation (Kastner *et al*., 1977) and possibly quartz.

Chert and porcelanite are distinguished by their physical characteristics as observable in the field or in core. Chert is identified as the pure, fine-grained siliceous rock that is hard and dense, has a smooth, conchoidal or splintery fracture, and a glassy or waxy luster. It is usually composed of >90% diagenetic silica (Behl & Garrison, 1994). In contrast, porcelanite is the rock composed of 50 to 85% diagenetic silica that is less hard and dense than chert, has a blocky to splintery fracture and a matte surface texture similar to that of unglazed porcelain (Isaacs, 1981b). The principal difference between chert and porcelanite is clay content and/or porosity (Isaacs, 1981b, 1982; Dunham & Blake, 1987; Behl & Smith, 1992; Behl & Garrison, 1994). Identification of a rock as chert or porcelanite is made independently of the silica phase, i.e., a dense vitreous chert can be composed of either, or both, opal-CT or quartz silica phases, and a porcelanite, similarly, can contain either opal-CT and/or quartz phases. Other more detrital-rich, organic-rich, calcareous or dolomitic rocks have different physical and mechanical properties, such as ductility, rock strength, porosity, permeability, characteristic bed thickness, etc. that are key to reservoir evaluation (Fig I-06).

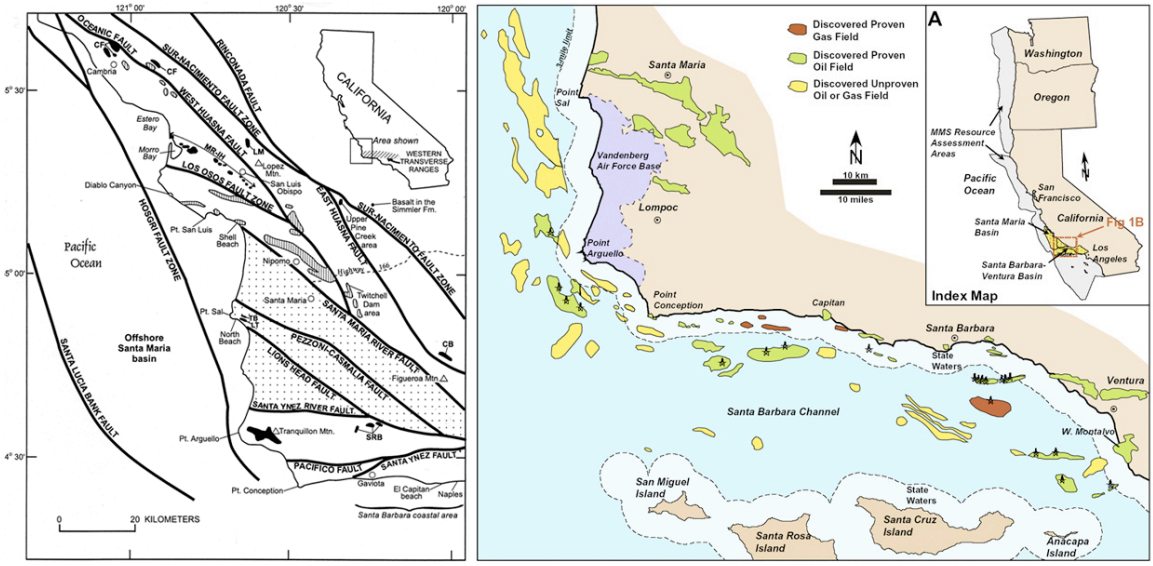

Figure I-02. Major faults of field trip area (left), and related oil fields (right).

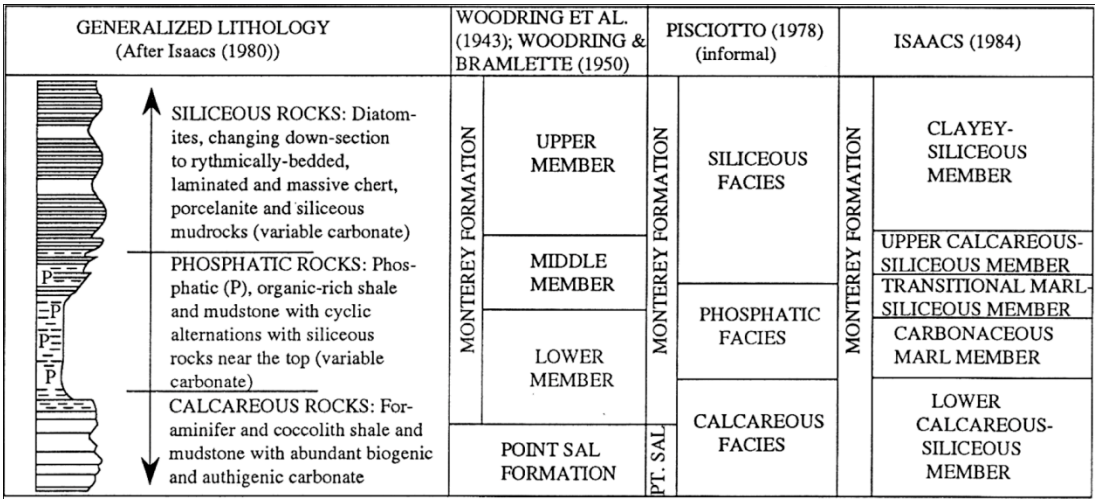

Figure I-03. Comparison of lithostratigraphic zonations (informal members) of the Monterey Formation in the Santa Barbara-Santa Maria areas (after Pisciotto, 1981).

Figure I-04. (next page) Diagrams and scanning electron microscope (SEM) photomicrographs depicting steps in silica diagenesis. A. Mixed clay and diatom fragments (opal-A) in a muddy diatomite. B. Nearly pure opal-A diatomite (penate diatoms). C. Large centric diatom simultaneously being dissolved and infilled with opal-CT lepispheres. D. Close-up of opal-CT lepispheres ("spheres of blades"). E. Nearly completely cemented opal-CT chert showing lost intercrystalline microporosity and remaining moldic porosity. F. Silica phase diagram (Keller and Isaacs, 1985 as modified by Behl and Garrison, 1994) showing that the transition of opal-A to opal-CT and opal-CT to quartz is a function of both temperature and composition. Note that the purest cherts form at considerably lower temperature than the silica phase transitions in less-pure porcelanite and siliceous mudrocks. G. Sequence of diagenesis for the timing of formation of various siliceous rocks (Behl and Garrison, 1994).

A.

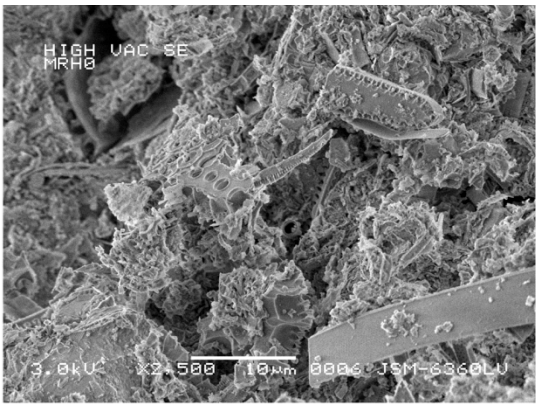
HIGH VAC SE
MRH0
3.0kV X2,500 10µm 0006 JSM-6360LV

B.

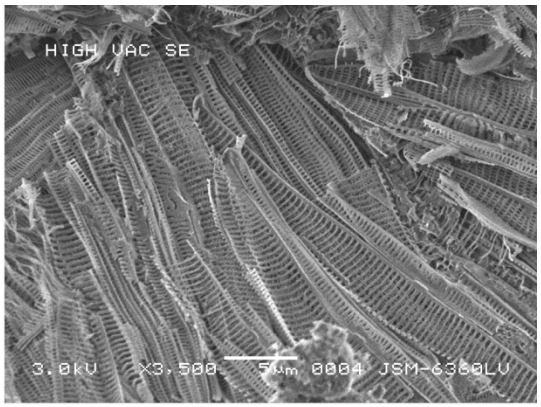
HIGH VAC SE
3.0kV X3,500 5µm 0004 JSM-6380LV

C.

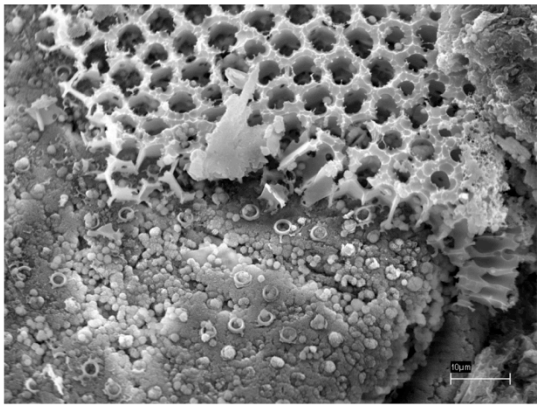

D.

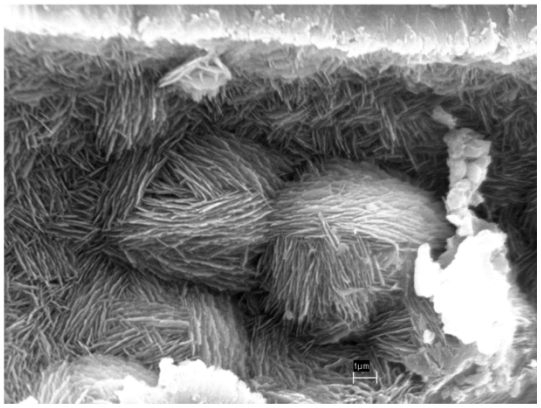

E.

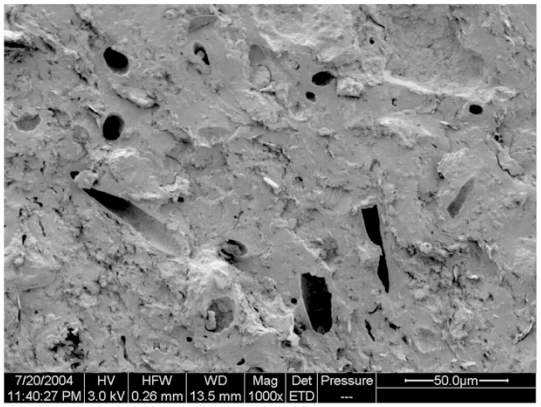
7/20/2004 11:40:27 PM
HV 3.0 kV
HFW 0.26 mm
WD 13.5 mm
Mag 1000x
Det ETD
Pressure ---
50.0µm

F.

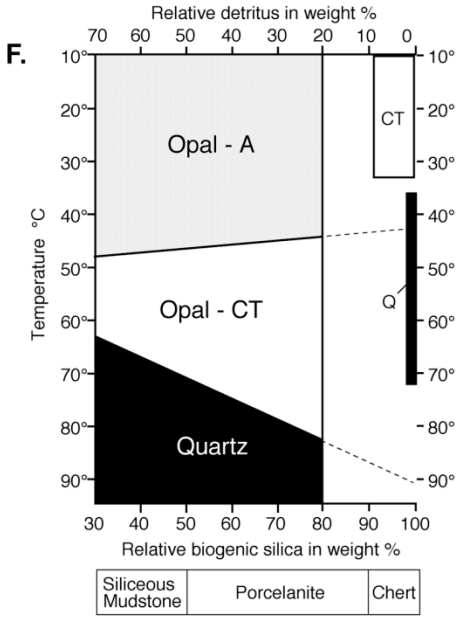
Relative detritus in weight %
70 60 50 40 30 20 10 0
Temperature °C
10° 20° 30° 40° 50° 60° 70° 80° 90°
Opal - A
Opal - CT
Quartz
CT
Q
30 40 50 60 70 80 90 100
Relative biogenic silica in weight %
Siliceous Mudstone
Porcelanite
Chert

G.

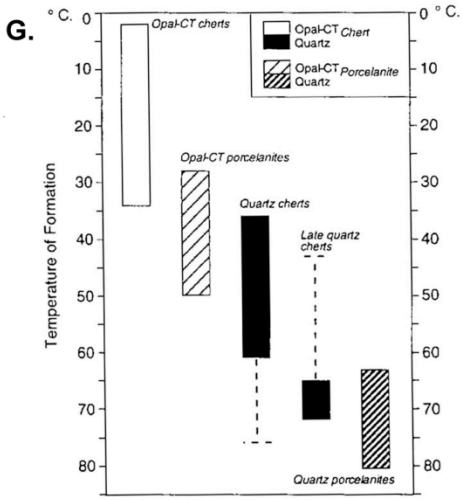
° C.
0 10 20 30 40 50 60 70 80
Temperature of Formation
Opal-CT cherts
Opal-CT Chert
Quartz
Opal-CT Porcelanite
Quartz
Opal-CT porcelanites
Quartz cherts
Late quartz cherts
Quartz porcelanites

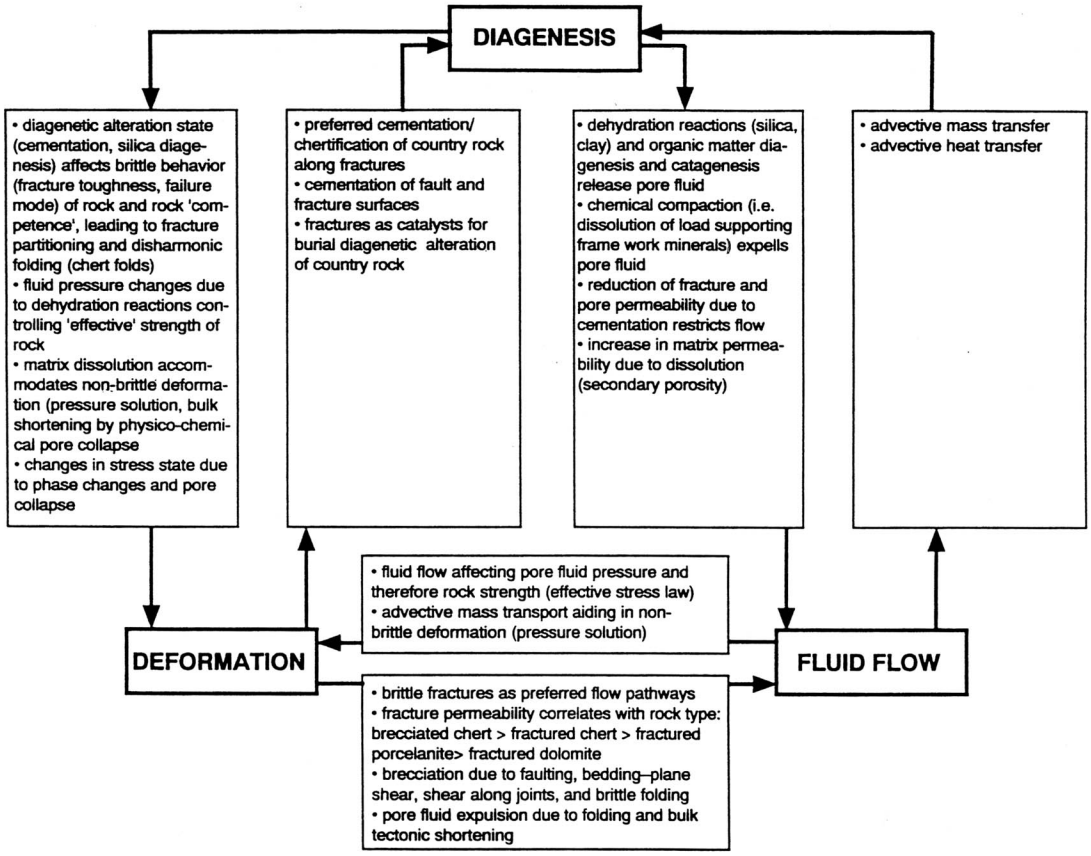

Figure I-05. Potential relationships between diagenesis, deformation, and fluid flow as inferred from observations of the Monterey Formation (Eichhubl & Behl, 1998).

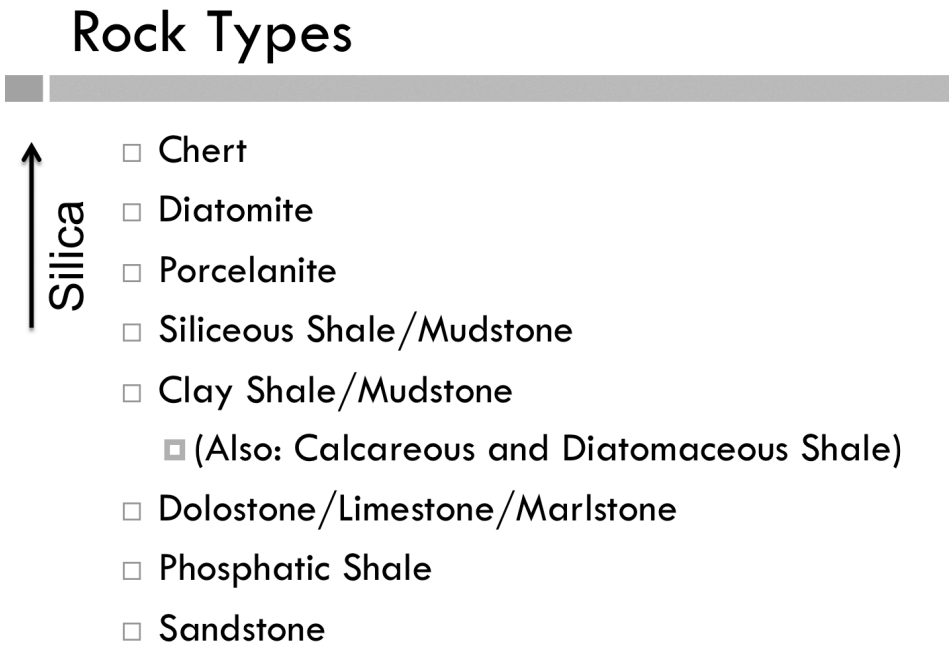

Figure I-06. Monterey lithologies.

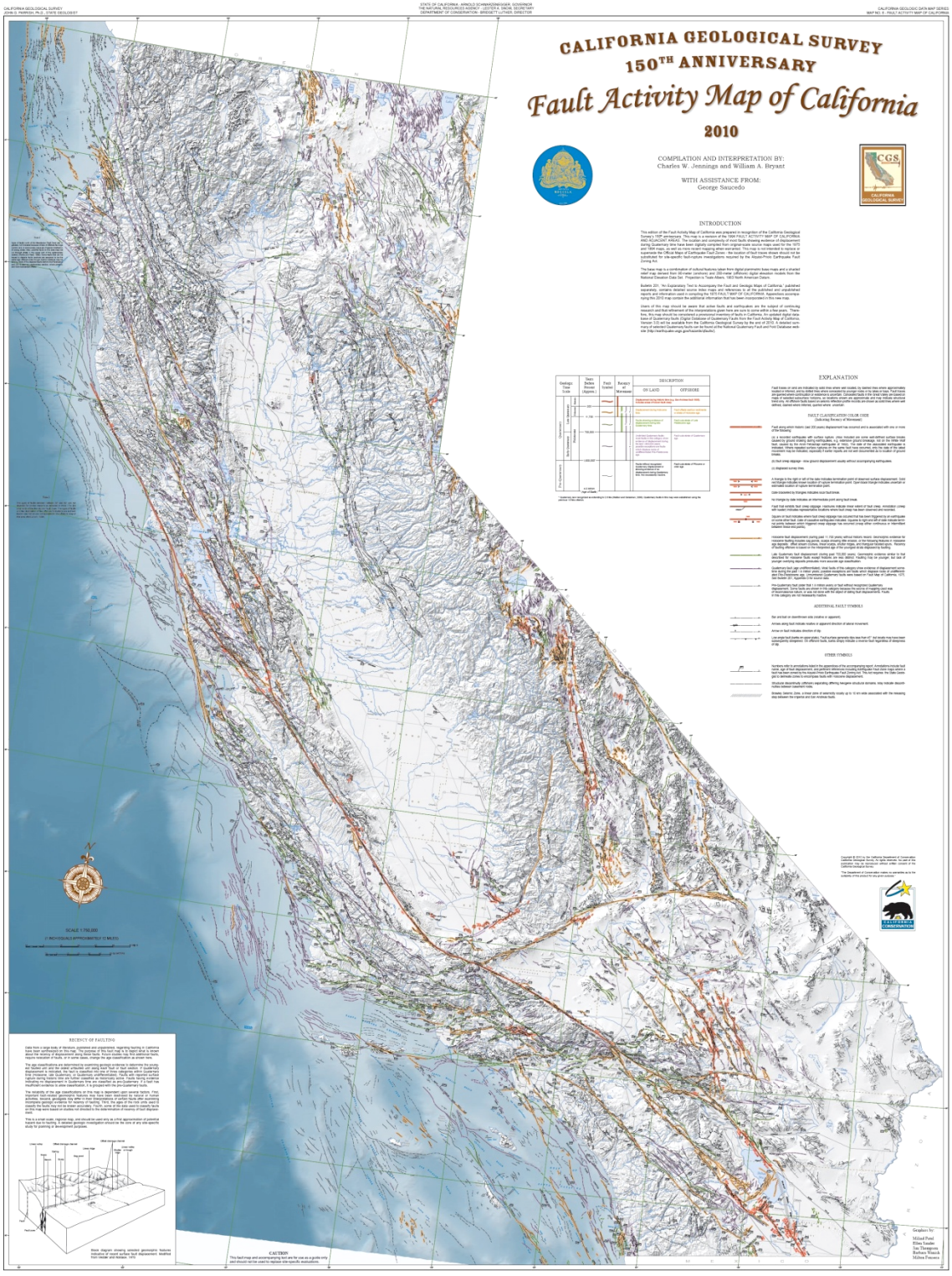

Figure I-07. Map of active faults in California (California Geological Survey). The San Andreas Fault (SAF) is a right-lateral transform the marks the boundary between the Pacific and North American tectonic plates. Estimate the locations of Bakersfield, Santa Barbara and field stops.

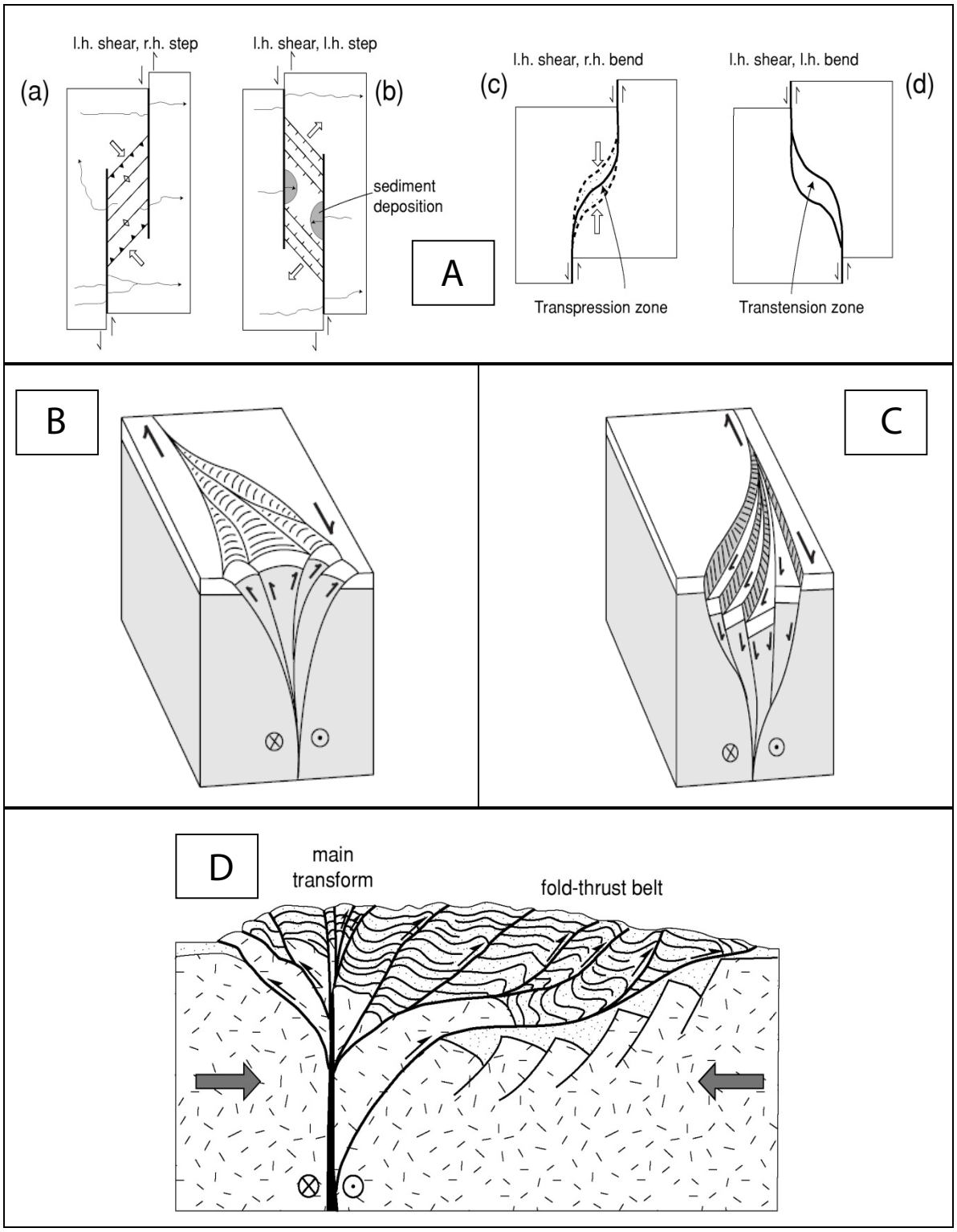

Figure I-08. Deformation associated with strike slip faults. (A) Bends and en-echelon step-overs in strike-slip faults resulting in localized contraction and extension (Ramsay and Huber, 1987); (B) Contractional strike-slip duplex ("positive flower structure"); (C) extensional strike-slip duplex ("negative flower structure")(B & C from van der Pluijm and Marshak, 2004); (D) Contractional fold and thrust belt adjacent to plate boundary transform, due to transform-normal tectonic shortening (Marshak and Wilkerson, 2004).

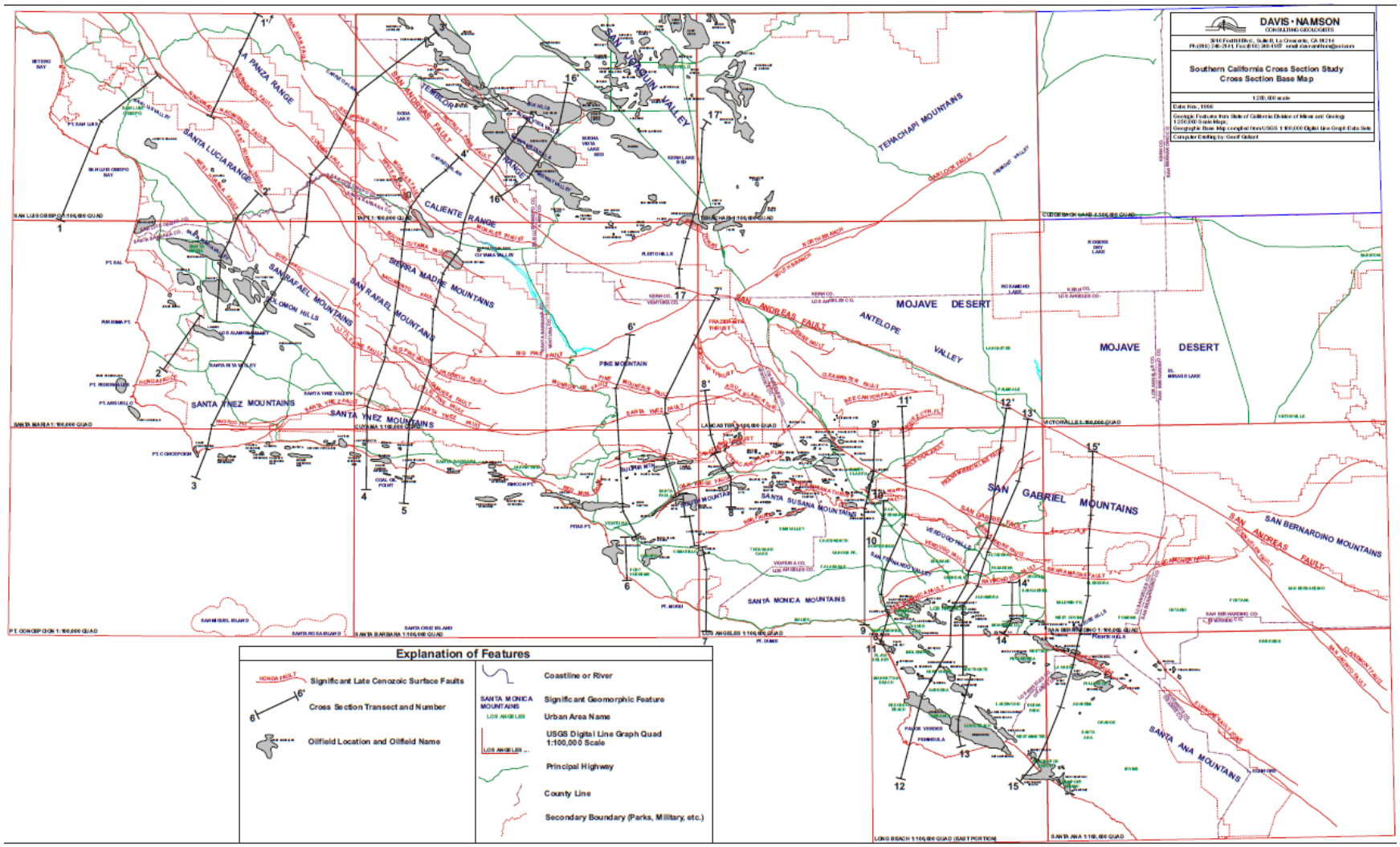

Figure I-09. Base map for Namson and Davis USGS cross sections. Main faults shown in red and oil fields shaded gray.

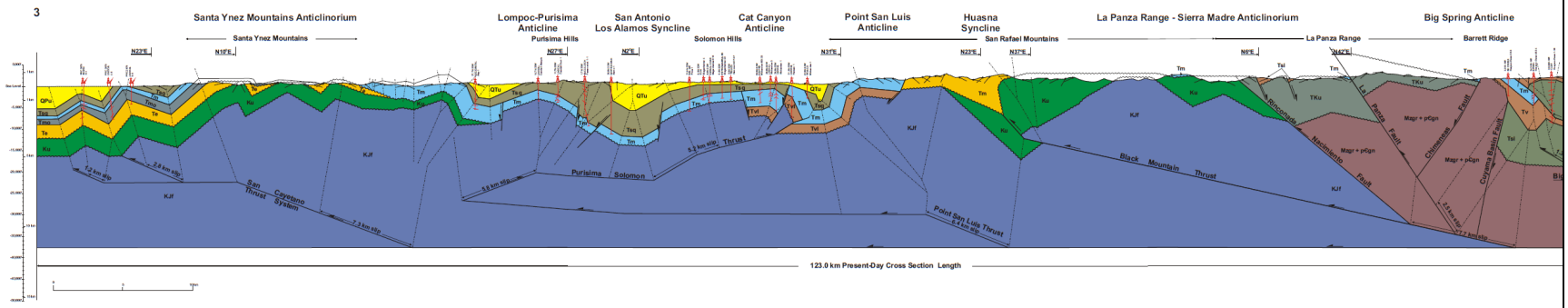

Figure I-10..Namson and Davis USGS cross section #3 (1988).

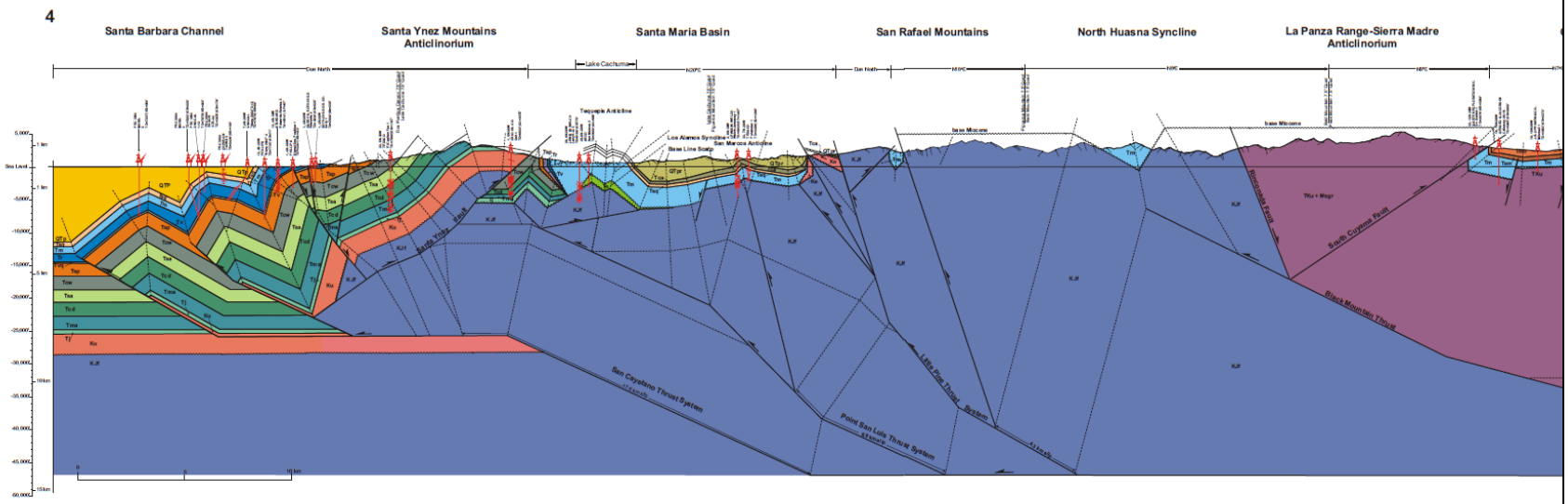

Figure I-11..Namson and Davis USGS cross section #4 (1988).

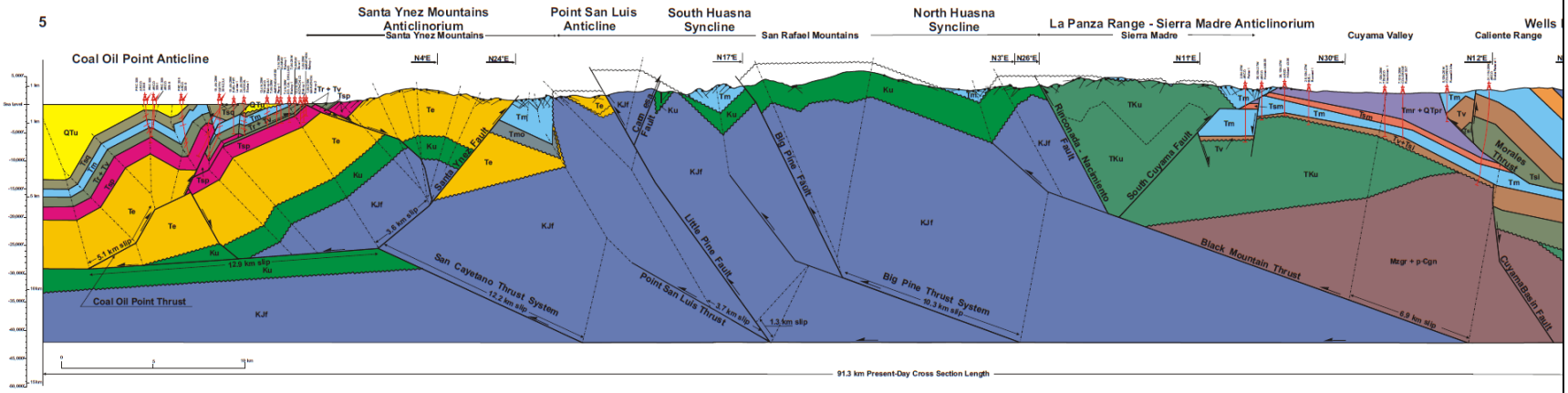

Figure I-12..Namson and Davis USGS cross section #5 (1988).

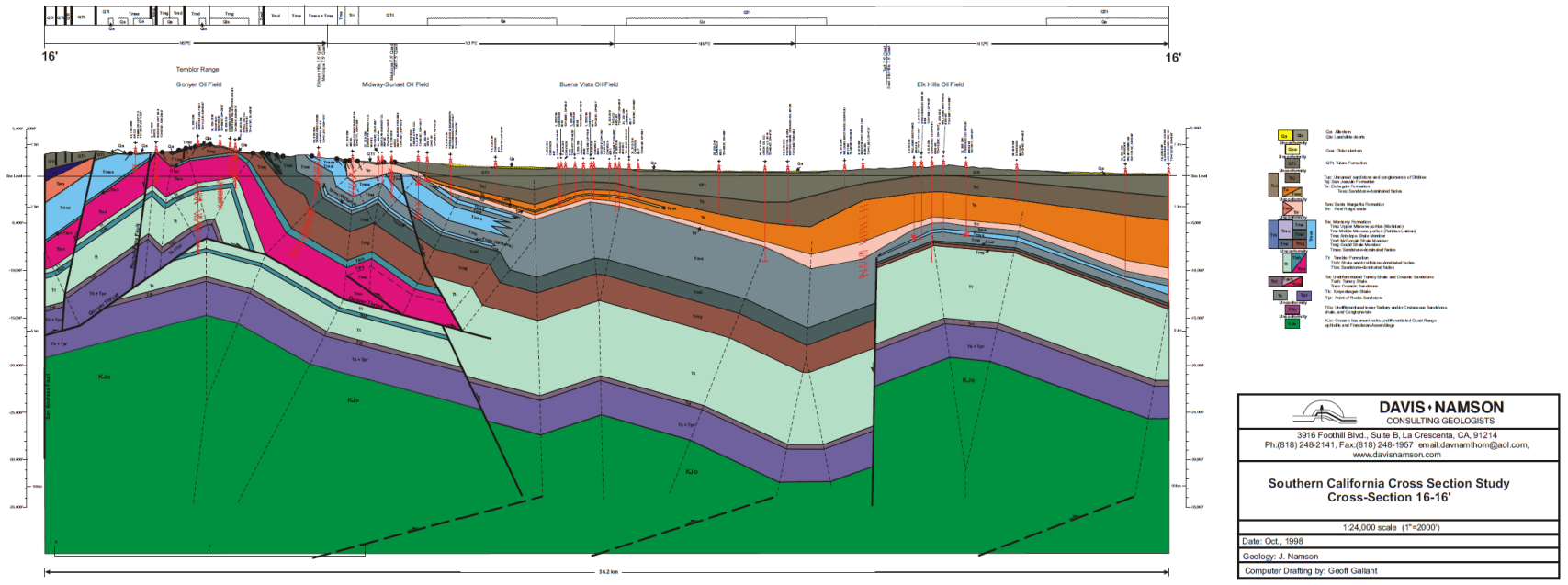

Figure I-13..Namson and Davis USGS cross section #16 (1988).

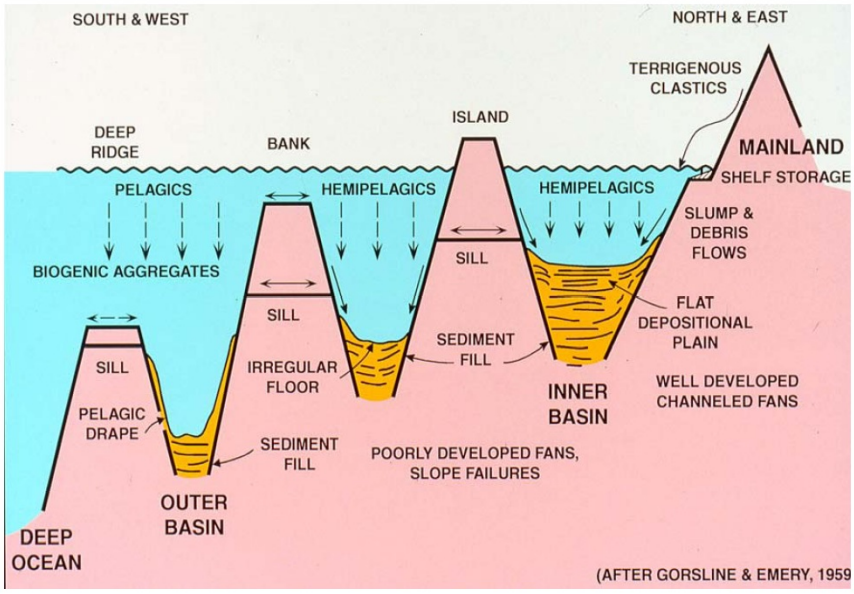

Figure 2. Schematic cross section of margin configuration of the California Continental Borderland after Gorsline and Emery (1959). Blake (1981) suggested this topographic arrangement could account for many characteristics of Monterey Formation depositional systems.

Figure I-14. Depositional setting for Monterey Formation basins (from Schwalbach et al, 2007).

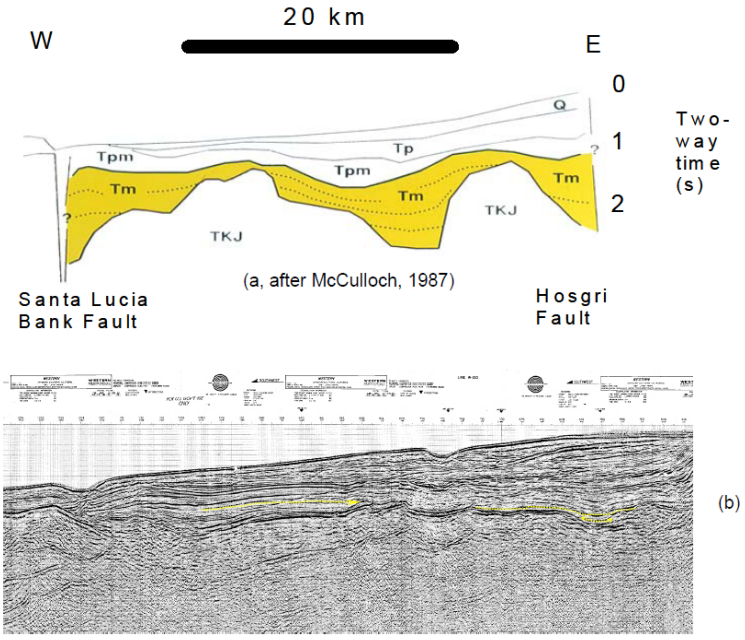

Figure 3. (a) Seismic line drawing after McCulloch (1987) from offshore Santa Maria Basin the illustrates onlap of lower units filling basin topography and generally planar, parallel reflectors for younger Monterey strata (Tm). (b) Migrated seismic data from offshore Santa Maria Basin - different location and scale from (a). Similar onlap and depositional geometry as depicted in line drawing. Neither example shows evidence of seismic-scale progradation.

Figure I-15. Seismic expressions of offshore Miocene basins (from Schwalbach et al, 2007).

INTRODUCTION PART 2: FRACTURE & MECHANICAL STRATIGRAPHY

By Michael Gross, PhD, now with Shell Exploration and Production

Throughout the course of our field trip we will relate specific field observations to four main themes related to brittle deformation. Our goal is to initiate discussions that will incorporate the fracture patterns and geometries we observe in outcrop with the expertise and experience of the field trip participants. The four main themes are:

1.) The relationship between fracture development and structural style (i.e., regional tectonics, fold geometry and stress fields).

Fracture development is strongly controlled by regional tectonics and the style of structural deformation. The large folds and faults that define many hydrocarbon traps are a product of regional deformation, thus their geometries and internal strains often reflect a broader tectonic framework (Fig. I-16). Mechanisms of fold development, in turn, will have a profound influence on fracture development, both in terms of orientation and intensity (Fig. I-17).

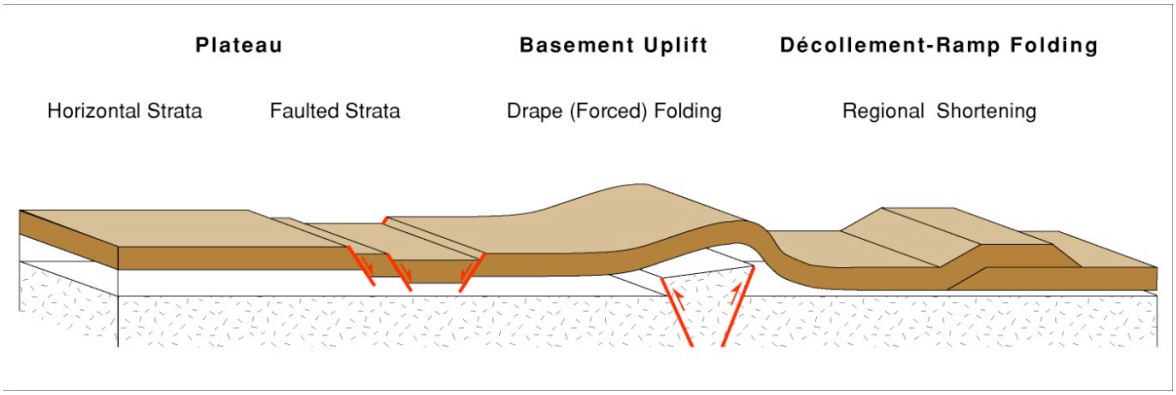

Figure I-16. Various tectonic settings that lead to regional fracture development.

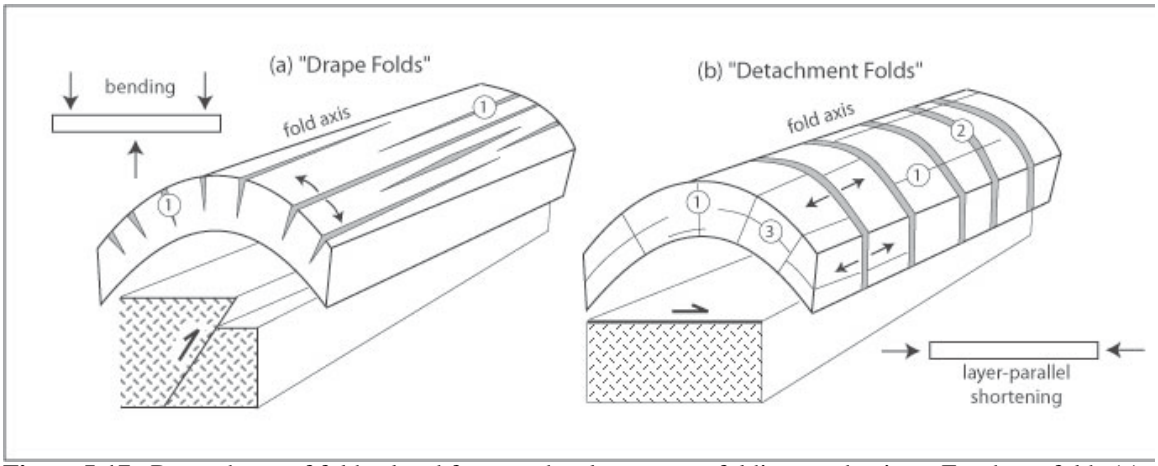

Figure I-17. Dependence of fold-related fracture development on folding mechanism. For drape folds (a) the dominant opening-mode fracture set is often hinge-parallel, whereas for detachment folds (b) the most prominent set is perpendicular to the fold hinge. The main fracture sets are (1) hinge (strike) parallel, (2) hinge (strike) perpendicular, and (3) bed parallel. The numbers do not imply relative timing.

Questions to consider:

- What is the dominant fracture set observed in the Monterey Formation with respect to regional and local folding?
- How are these fractures related to fold geometry and tectonic contraction?
- Why and how is extension accommodated by brittle fracturing in the Monterey Formation?
- What is the magnitude of this fracture-related extension, and how does it contribute to porosity and permeability?

2.) The influence of mechanical stratigraphy on fracture development and distribution

Mechanical stratigraphy refers to the elements within a stratigraphic section that control structural deformation. In our case, we focus primarily on brittle deformation, though you will note that intraformational folding in the Monterey Formation is also strongly controlled by mechanical stratigraphy. Important elements within the mechanical stratigraphy that influence fracture development and distribution in the Monterey Formation include lithology, bed thickness and bed boundaries.

In the Monterey Formation, fracture type (faults versus joints) is often dependent upon lithology. The more competent beds such as cherts, porcelanites and dolostones tend to develop joints and veins, whereas the less competent beds such as mudstones and shales often fail by faulting (Fig. I-18a). This dependence of failure mode on lithology is referred to as "fracture partitioning". Portions of the stratigraphic section therefore display a different type of fracture in alternating beds (Fig. I-18b).

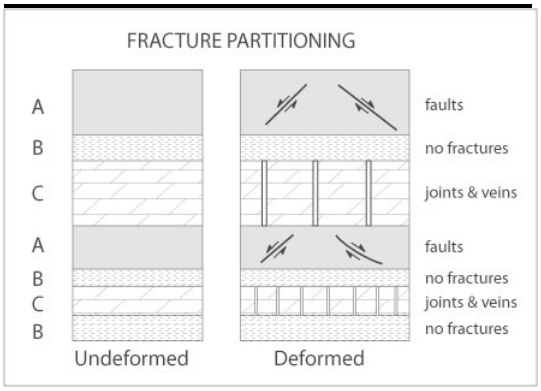

Figure I-18a. The concept of fracture partitioning, where the type of fracture (faults versus joints) is controlled by lithology (from Gross, 1995).

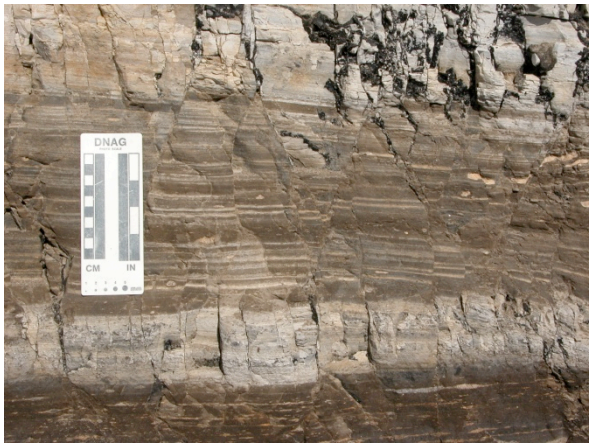

Figure I-18b. Photo of Monterey Fm at Arroyo Burro with small faults in laminated mudstone and joints in the porcelanite.

The boundaries between mechanical units, referred to as mechanical layer boundaries, have a profound influence on fracture development in the Monterey Formation. Fractures often terminate at discrete bed boundaries, thus restricting their vertical dimensions and leading to highly elliptical fracture shapes. The fracture height,

which often corresponds to the thickness of one or several stratigraphic beds, thus defines the mechanical layer thickness (Fig. I-19). Fractures confined to discrete mechanical units are observed at a variety of scales in outcrop, core and image logs.

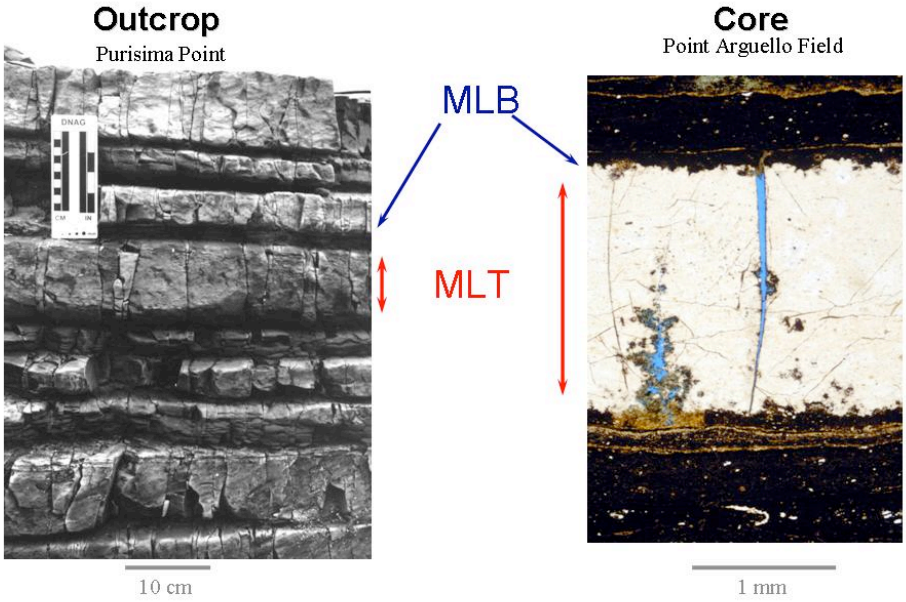

Figure I-19. Bed-confined fractures in outcrop and core of the Monterey Formation. Note discrete mechanical layer boundaries (MLB) and how the fracture height defines the mechanical layer thickness (MLT). From Gross et al (1995).

Mechanical stratigraphy is also one of several factors that control fracture spacing in the Monterey Formation. Several studies of bed-confined fractures in the Monterey Formation have shown a strong correlation between fracture spacing and bed thickness (Narr and Suppe, 1991; Gross et al., 1995). The linear relationship is thought to result from the stress reduction shadow that develops in the vicinity of a pre-existing fracture, whose dimensions scale with fracture height. Thus, thin beds tend to have more closely-spaced fractures, whereas fracture spacing is greater in thicker beds (Fig. I-20). Other factors that control fracture spacing include structural position (strain magnitude) and lithology (mechanical properties).

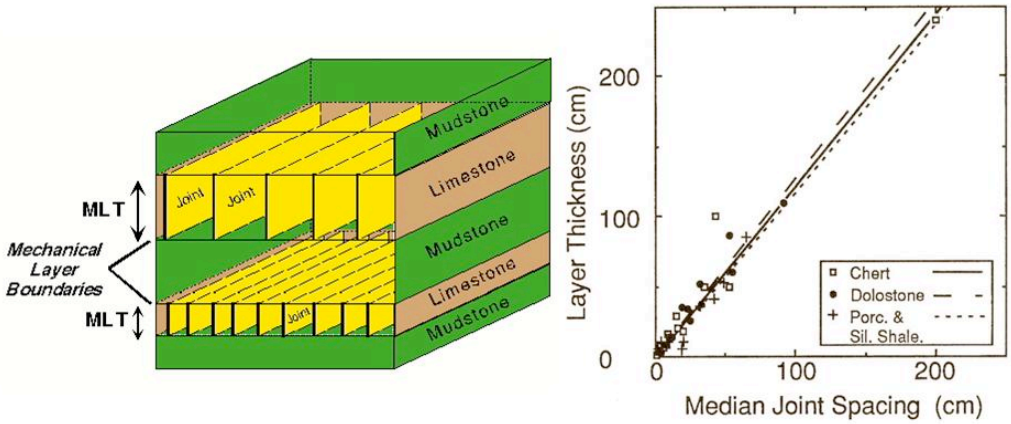

Figure I-20. Schematic to left showing relationship between fracture spacing and mechanical layer thickness (Gross et al., 1995). On right, plot of layer thickness versus joint spacing for fractures measured in the Monterey Formation (from Narr and Suppe, 1991).

Questions to consider:

- How important is mechanical stratigraphy for characterizing and modeling fractures at the reservoir scale?
- What methods can be used to quantify effects of mechanical stratigraphy on fracture distribution in the Monterey Formation?
- What kind of impact does fracture partitioning (alternating units of faults and joints) have on fluid flow?

3.) Fracture scaling in the Monterey Formation.

Fractures in the Monterey Formation occur at a variety of scales. For example, opening-mode fractures belonging to the same set (i.e., fractures of the same orientation that formed in response to the same episode of deformation) can be observed at the microscale in thin section, confined to single beds, spanning multiple beds and as throughgoing features that extend across the entire outcrop. A similar scaling relationship is observed for faults. The result is a hierarchical fracture-fault architecture consisting of "nested" fractures that correspond to mechanical units of varying dimensions (Fig. I-21).

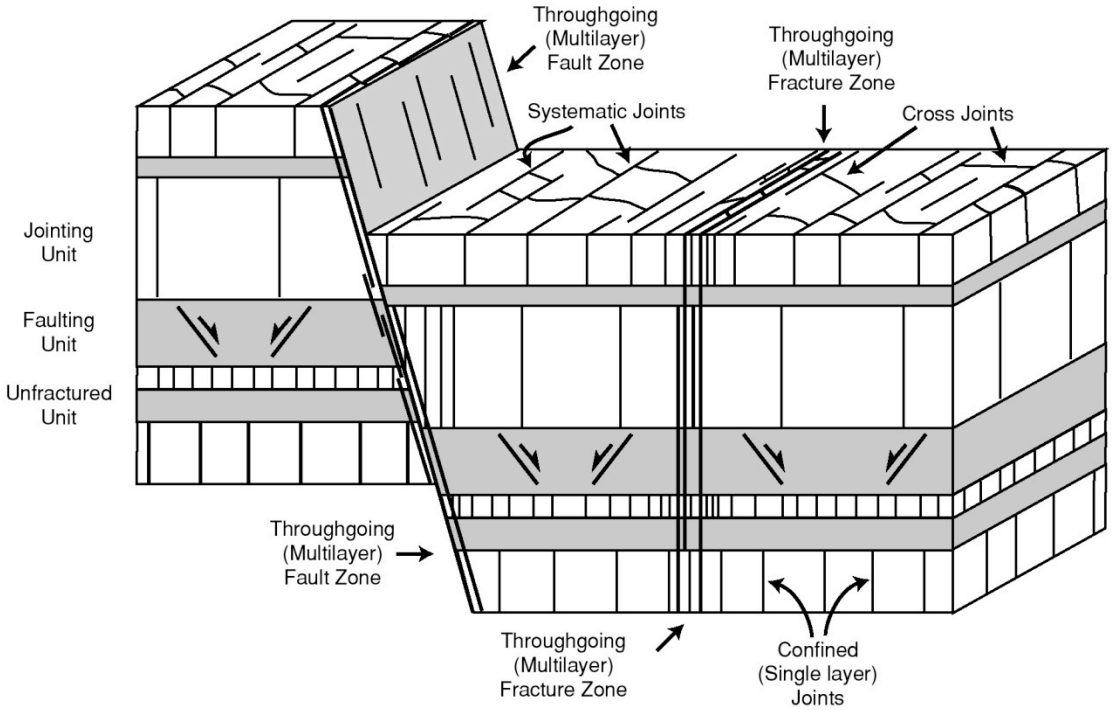

Figure I-21. Schematic of fracture architecture commonly observed in layered sedimentary rocks such as the Monterey Formation (from Gross and Eyal, in press).

The photographs in Figure I-22 show opening-mode fractures in the Monterey Formation at different scales.

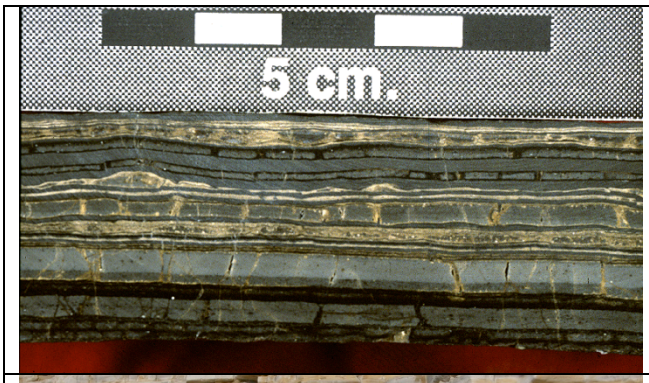

Figure I-22a. Small fractures confined to thin laminae of the Monterey Formation. Sample taken from well in Point Arguello field.

Figure I-22b. Bed-confined fractures at Point Buchon. Note alternating fractured and unfractured beds.

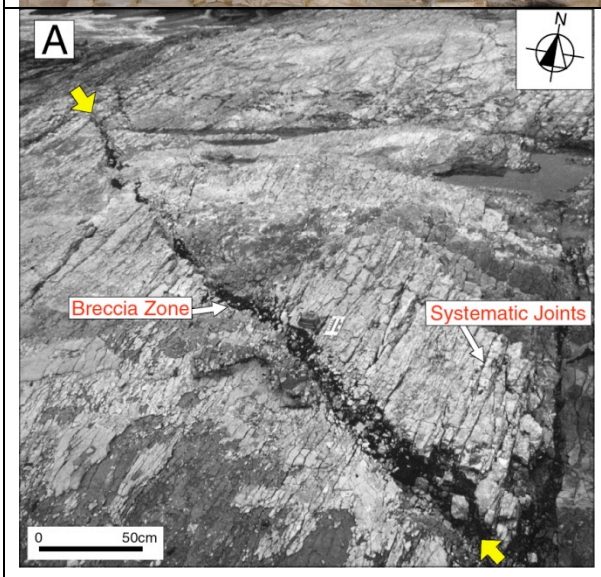

Figure I-22c. A multi-layer, tar-filled breccia zone (between arrows) at Lompoc Landing. These are intermediate-size structures that provide access to hydrocarbons stored in the smaller bed-confined fractures. In the Monterey Formation they have heights ranging from 10-25 feet and lengths from 50-80 feet. (From Finn et al., 2003).

Figure I-22d. Large, throughgoing fractures at Point Buchon. These represent major pathways for fluid flow and provide vertical connectivity among fracture populations confined to smaller mechanical units.

Questions to consider:

- At what scale do fractures and faults become significant hydrologic features?
- Can populations of the more abundant, small fractures contribute to our understanding of the larger fractures? How?
- How is fracture connectivity achieved among the various mechanical-flow units?
- What is the mechanism for the formation of multilayer faults and fractures, and are they genetically related to the smaller bed-confined features?

4.) Reservoir characterization and extrapolating field observations to the subsurface.

The first step in modeling fractured Monterey reservoirs involves developing a conceptual model of how the fractures and faults are distributed with respect to mechanical stratigraphy (Fig. I-23), and incorporating subsurface data from core and well logs that shed light on fracture orientations and intensity. Primary data required to characterize fracture populations include fracture type (faults, joints, fracture zones, etc.), fracture intensity (e.g., spacing or its inverse frequency, clustering), fracture orientation (to determine major trends and division into discrete sets), fracture aperture, mineral fill, timing of fracture set development (with respect to other fracture sets and structural/tectonic history), dimensions (length and height to estimate aspect ratio) and porosity.

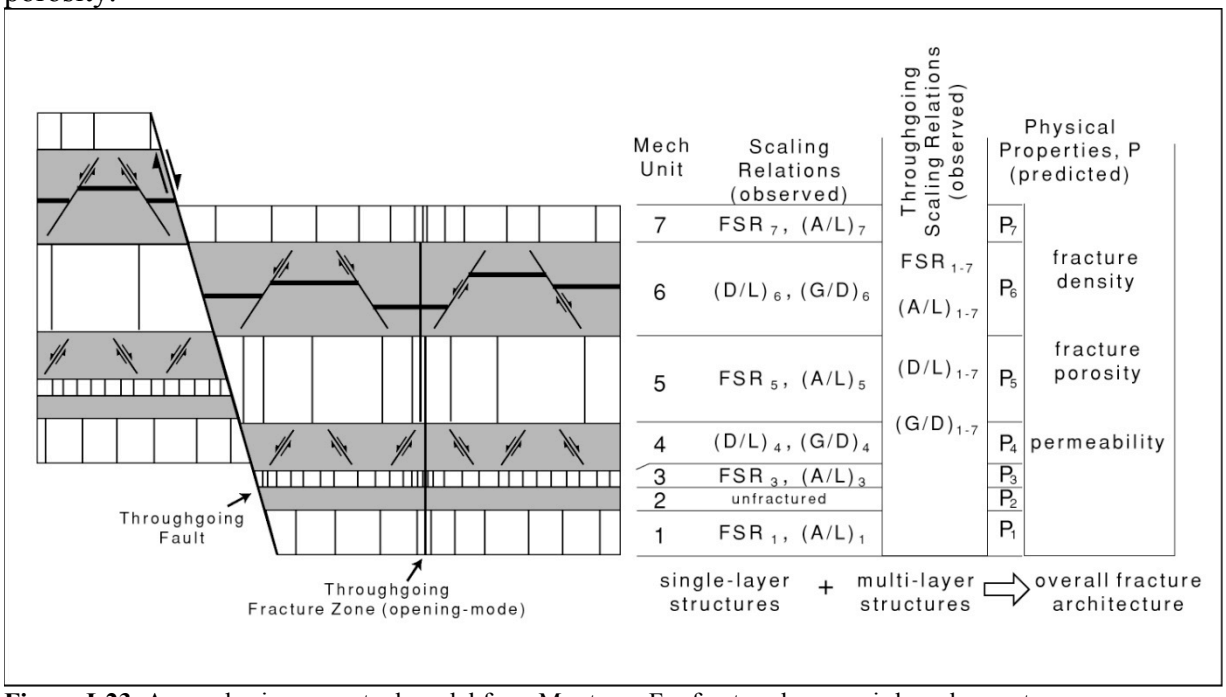

Figure I-23. A very basic conceptual model for a Monterey Fm fractured reservoir based on outcrop observations, showing how fracture scaling relations can be used to estimate petrophysical properties.

Outcrop analogs offer considerable insight for understanding fractured reservoirs, especially important concepts such as mechanical stratigraphy, scaling of fracture populations and associations with structural geometry and tectonics. In frontier settings results from outcrop surveys may formulate the strategy for initial exploratory drilling.

However, in production settings there is no substitute for collecting fracture data directly from the reservoir. In the latter case, the outcrop analogs serve as a framework for building the conceptual model based on the inherently limited datasets derived from subsurface data sources. It is therefore useful to incorporate as much subsurface techniques and data as possible, including sonic logs, image logs, well tests, tracer tests mud loss/lost circulation, production logs, core and seismic. Knowledge of the structure (geometries, mechanisms and kinematics) and state of stress (orientations and magnitudes) will provide valuable constraints.

Questions to consider:

- How many of the fractures observed in outcrop are actually found at depth under reservoir pressures, and how many represent near-surface weathering processes?
- What are the dimensions of the fractures and mechanical units that can be used to generate discrete fracture models at the reservoir scale, and what do they look like in outcrop?
- What is the contribution of the numerous small fractures and faults to overall porosity and permeability of the formation, and how can it be captured in reservoir models?
- What kind of techniques have been used successfully by field trip participants to characterize fractured reservoirs (e.g., seismic anisotropy, sonic logs, scaling relations)?

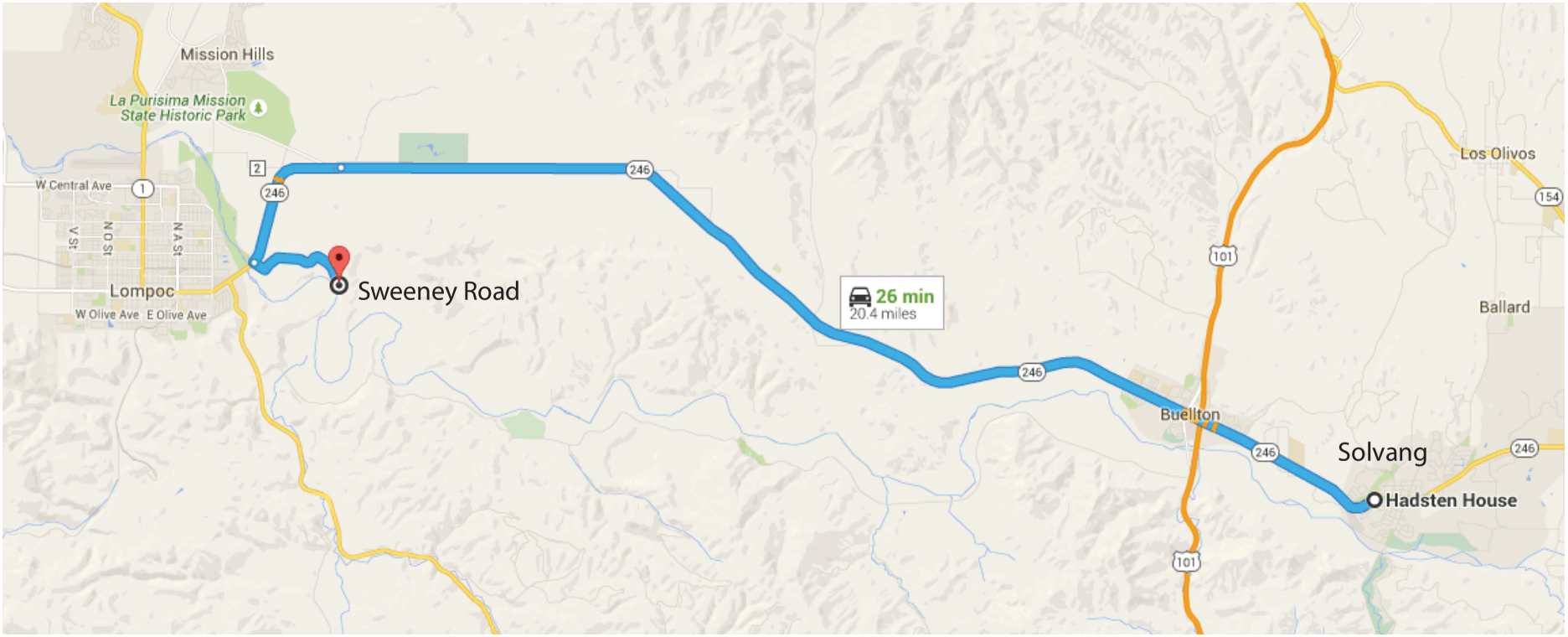

Day 1. Solvang to Sweeney Road.

Sweeney Road

Basin: Southern edge of Santa Maria Basin.

Formation/Members:

Monterey

- clayey siliceous (Isaacs, MacKinnon)
  (siliceous, Pisciotto)

Sisquoc

- lower banded/laminated facies

Notes & Questions:

- Sweeney Road is one of the classic sections of the Monterey Formation where Murata and Nakata (1974) first observed the progressive crystallographic ordering of opal-CT with increased burial depth and temperature. Ramirez and Barron studied it for stratigraphic refinement of the Monterey-Sisquoc boundary. Gutierrez-Alonzo and Gross (1997) studied the deformational style here and across the Santa Maria basin.
- Opal-A to opal-CT transition occurs near the formational boundary between the Monterey and Sisquoc formations (~6.0-6.7 Ma).
- Formation boundary is gradational due to continuous sedimentation in a basinal setting, in contrast to the unconformable contact that exists elsewhere on paleo-submarine highs.
- Ribbon-bedded opal-CT chert and porcelanite in Monterey.
- Interbedded laminated and massive intervals of diatomaceous mudstone in Sisquoc.
- Reservoir-scale anticlines and synclines are oriented E-W and include 1-10m-wavelength folds that appear to have formed as a result of blind thrusts splaying off detachment horizons at depth. Bedding-plane detachments themselves are folded progressively during deformation. Folding of faults indicated the ongoing nature of the contractional deformation.
- Localized brecciated opal-CT chert with hard bitumen coatings.
- Compare fold orientations and geometries at different scales, from (1) hinges of small folds (cm to m scale wavelengths, to (2) axes of mesoscale folds (10-20 m wavelengths) to (3) regional folds that extend across the basin (see geologic maps and sections). Are the trends of folds at different scales similar or different?
- Based on your analysis of regional and outcrop scale folds, can you predict the fold geometry and structural style in the subsurface reservoir? What type of fracture pattern would you expect? How would you deviate a horizontal wellbore with respect to the predicted fold orientation?
- What engineering challenges and problems will you face when drilling through intensely folded and contorted beds of the Monterey Formation? Would they vary depending upon lithology and degree of diagenesis?

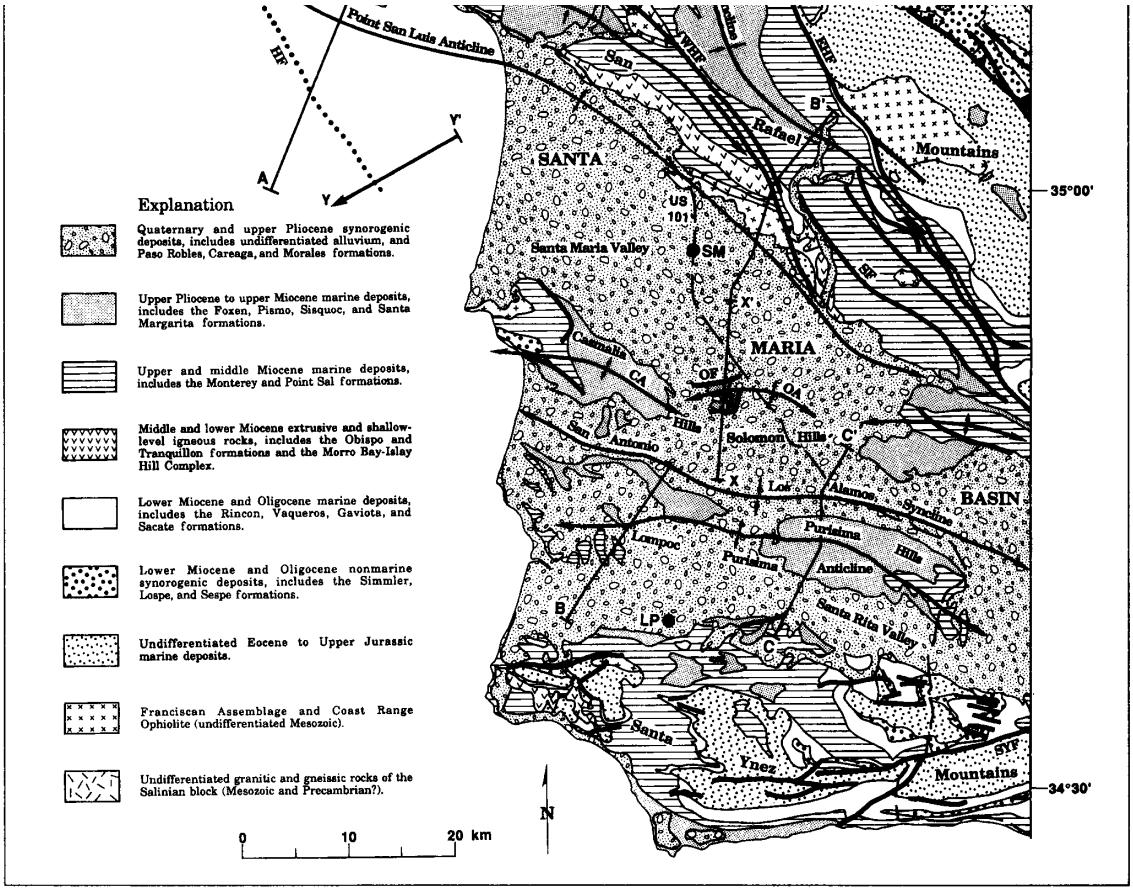

Figure 3-01. Simplified geologic map of the Santa Maria Basin. Sweeney Road is located in the southern part of the basin. (Namson and Davis, 1990).

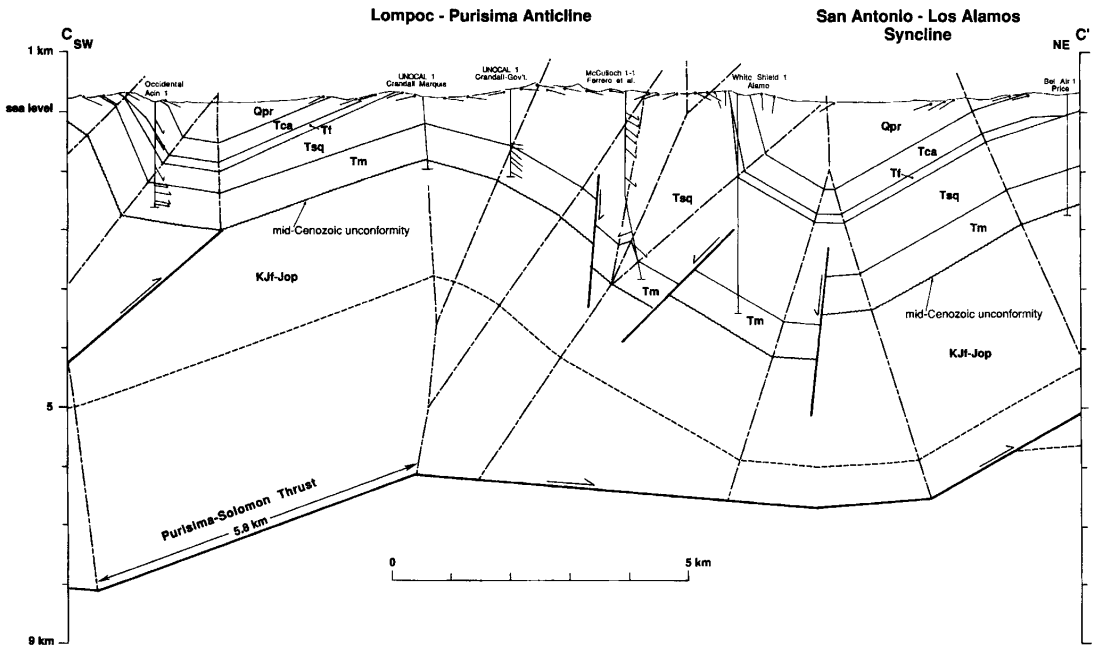

Figure 3-02. Cross section across Lompoc-Purisima anticline in southern Santa Maria Basin. Note fault-bend fold geometry due to reverse slip on buried Purisima-Solomon thrust (Namson and Davis, 1990).

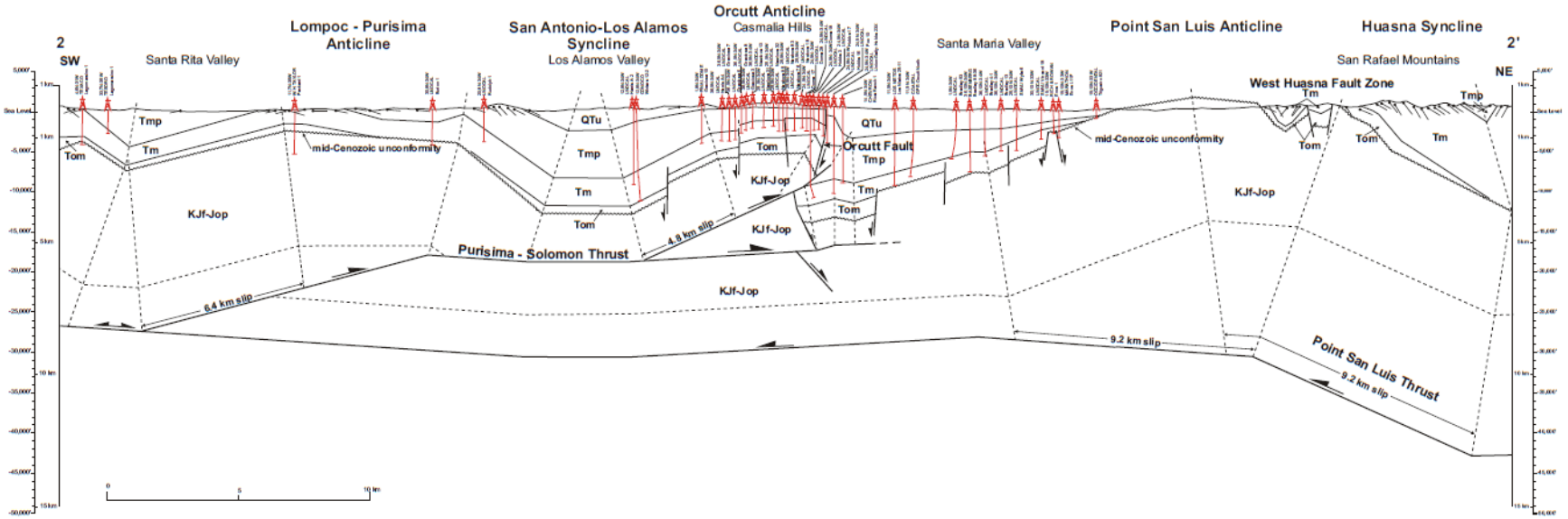

Figure 3-03. Namson & Davis Cross Section #2 through the Santa Maria Basin, USGS funded study.

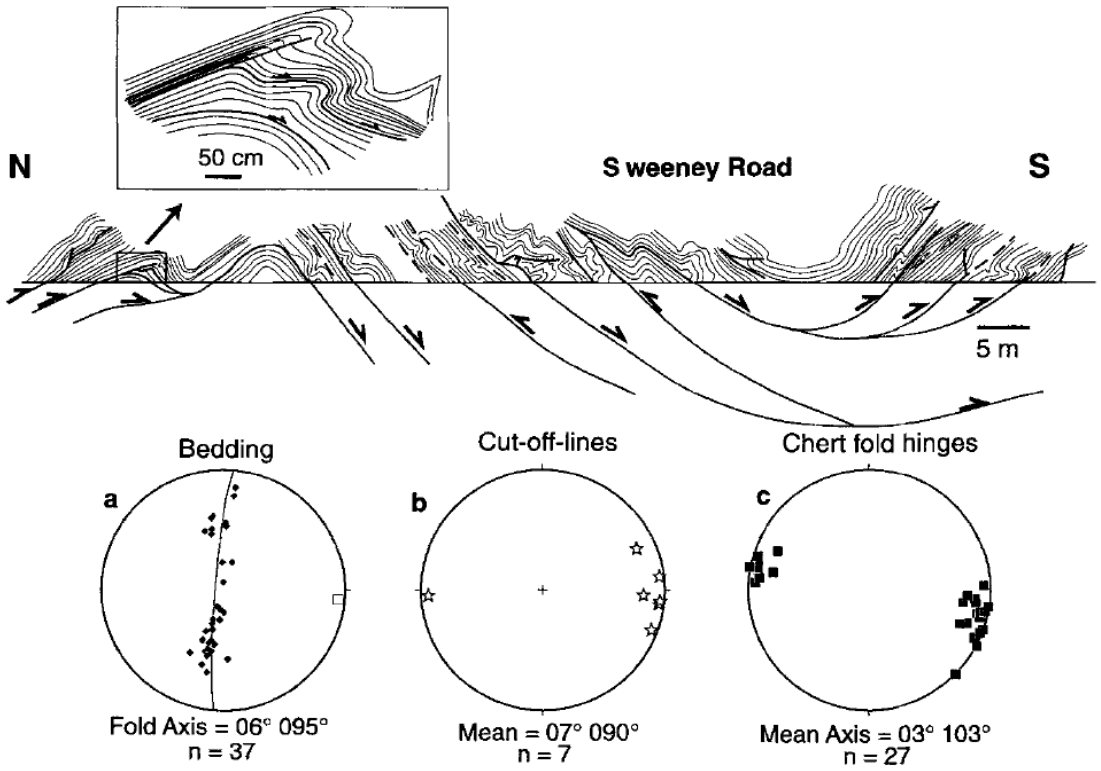

Figure 3-04. Structural cross section and data of Monterey strata exposed at Sweeney Road cut. Note the numerous bed-parallel fault zones that serve as detachments, as well as the small fold hinges within the larger anticline and syncline. Compare these structures to regional map and cross section in Figs. 3-01, 3-02 and 3-03. From Gutierrez-Alonso and Gross (1997).

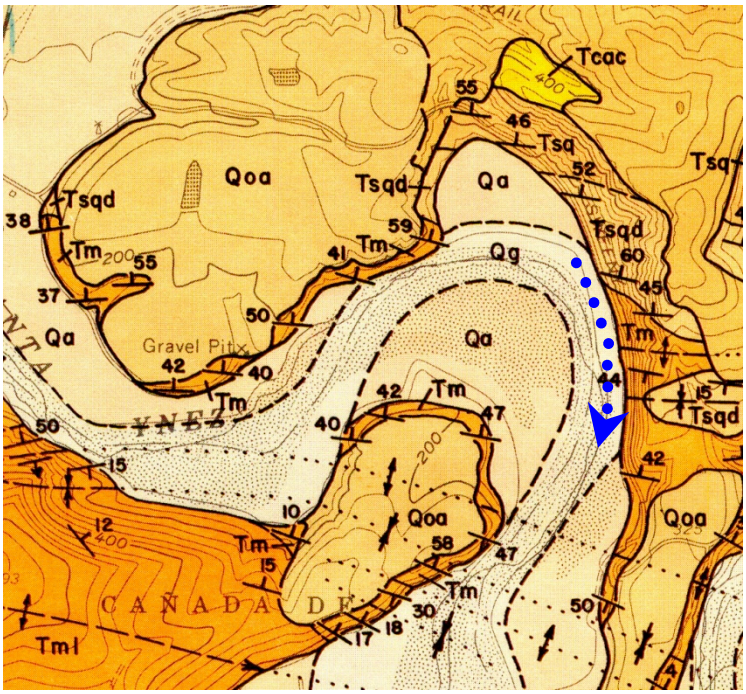

Figure 3-05. Geologic map showing structures and field trip transect from Sisquoc to Monterey formations and from opal-A diatomite to opal-CT porcelanite and chert (Dibblee, 1988).

Figure 3-06. Ribbon-bedded opal-CT chert, porcelanite, and siliceous shale of upper clayey siliceous member of the Monterey Formation. Subtle and distinct bedding-plane detachments cut off strata and fold beds.

Figure 3-07. Uppermost opal-CT chert lenses that formed within opal-A diatomite near the silica phase boundary and formational contact. Note that chert formation requires localized addition of silica to fill open porosity.

Figure 3-08. Outcrop photo of bedding-plane detachment folds at Sweeney Road. Located near center of structural cross-section shown in Fig. 3-04.

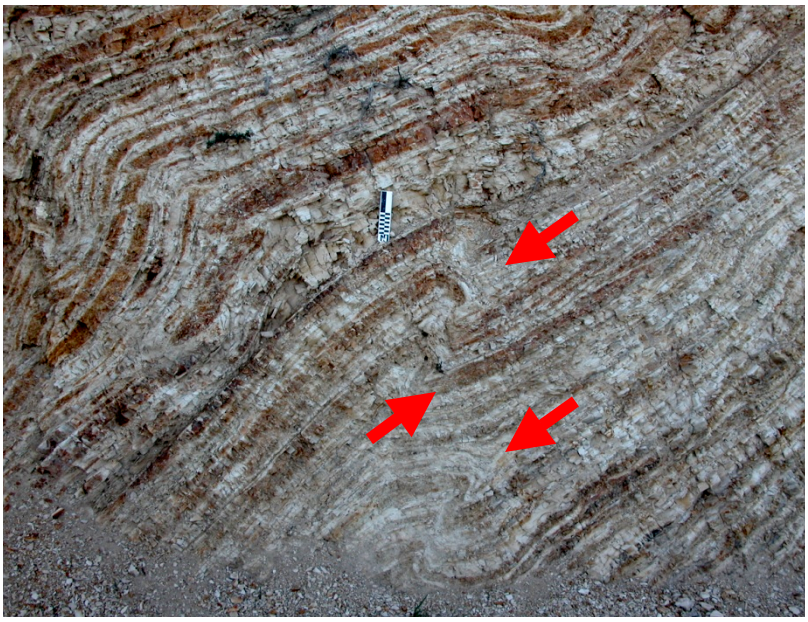

Figure 3-09. Close-up photo of small folds in the Monterey Formation along Sweeney Road. What are the trends of the fold hinges? How are they related to the regional folds?

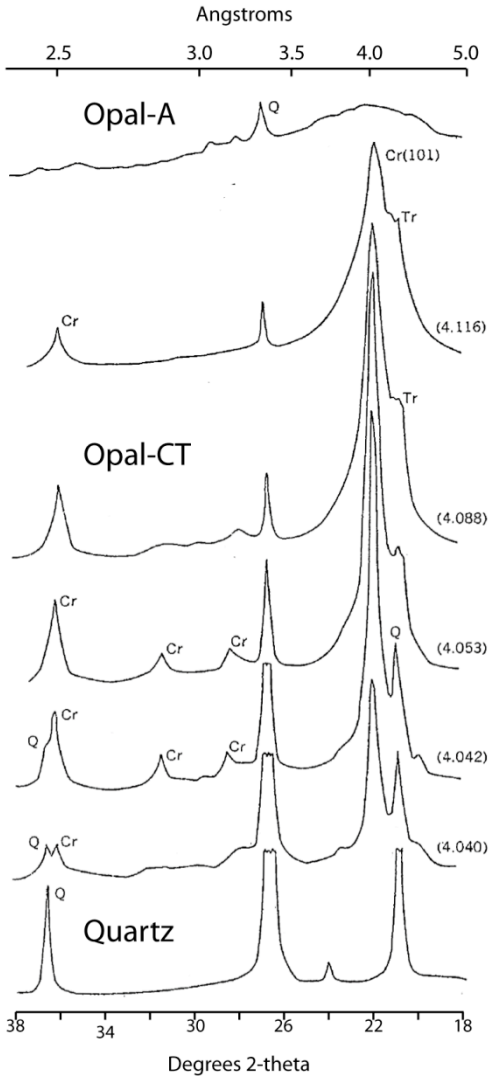

Figure 3-10. Typical X-ray difractometer patterns showing the progressive transition from opal-A to opal-CT to diagenetic quartz silica phases. Cr, Q, and Tr indicate the diffraction peaks of cristobalite, quartz, and tridymite, respectively. The numbers in parentheses are the d101-spacing of cristobalite in angstroms indicated by position of the major cristobalite peak. Modified from Murata and Larson (1975). Progressive solid-state crystallographic ordering of opal-CT with burial was first demonstrated here at Sweeney Road and at Chico Martinez Creek.

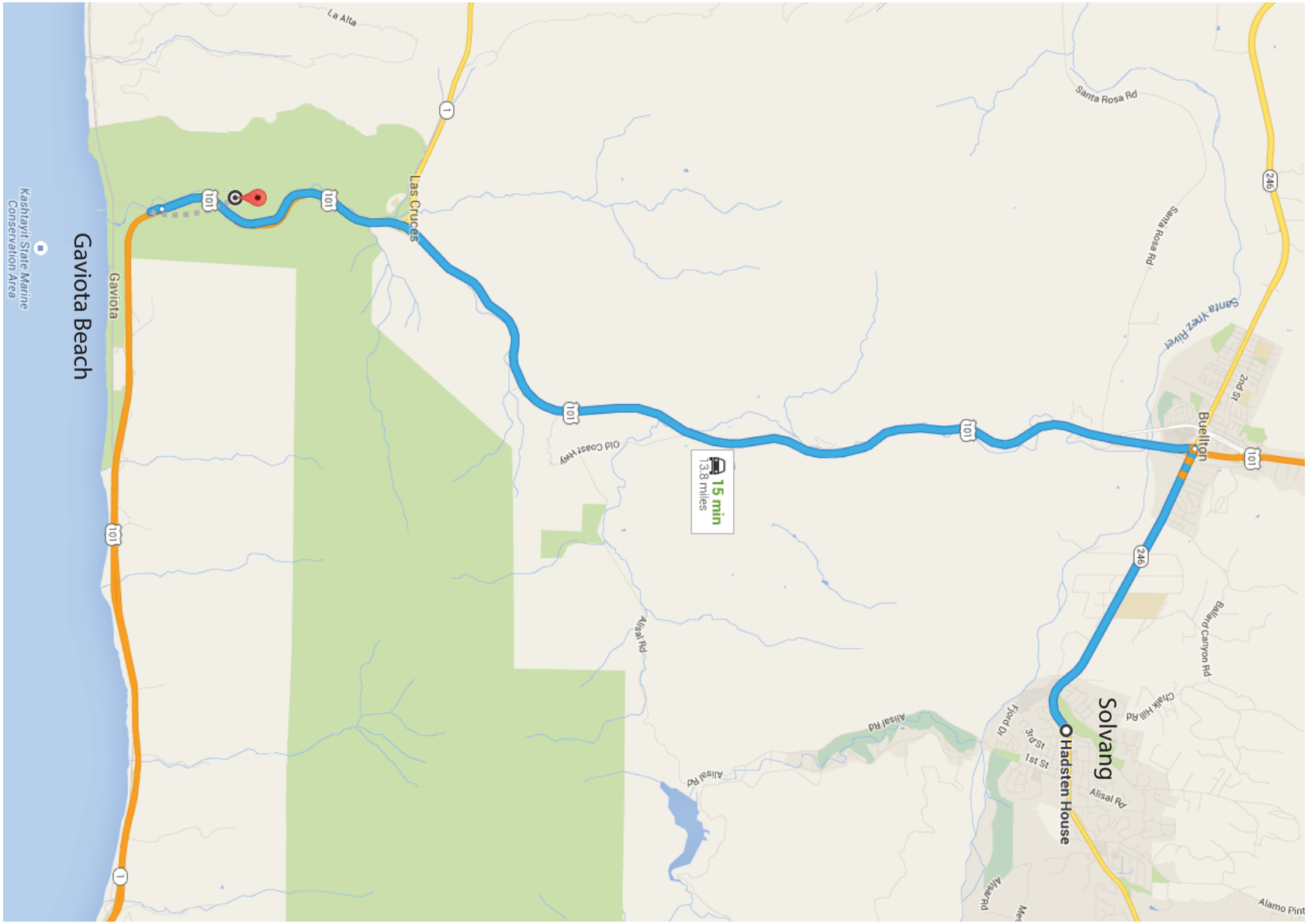

Day 2. Solvang to Gaviota Beach.

Gaviota State Beach

Basin: Santa Barbara

Formation/Members:

Monterey

- clayey-siliceous (upper siliceous)
- upper calcareous-siliceous member
- transitional marl-siliceous
- carbonaceous marl

Notes & Questions:

- Slope channel deposits to west, Rest of Monterey Formation stratigraphic section to east.
- Submarine slope gulley/channel deposits of sandstone and conglomerate interrupt and cut the upper Monterey Formation. Larger clasts derived from uplifted and eroded middle Monterey lithologies. Oil-saturated. Intercalated overbank thin sandstone beds.
- Vertically oriented clastic dikes cut hemipelagic strata. Do these provide cross-stratigraphic conduits in subsurface?
- All siliceous rocks here are opal-CT phase, except for quartz chert clasts included in the conglomerate.
- 1-2 m thick packages of thin-bedded, laminated porcelanite interbedded with massive siliceous mudstone.
- How does joint spacing and intensity relate to lithology? To bed thickness?
- Monterey stratigraphy here (west of Santa Barbara) differs from Arroyo Burro (next stop) by not having a significant massive chert/porcelainte member. Instead of siliceous sediments, an organic-rich, phosphatic, calcareous shale slowly accumulated.

Watch for surf and slippery rocks!!!

Figure GB-01. Tar-saturated sandstone and conglomerate gully/channels cut into the clayey-siliceous upper Monterey Formation (left). Various orientations and spacings of spaced joint sets in porcelanite of the upper Monterey Formation.

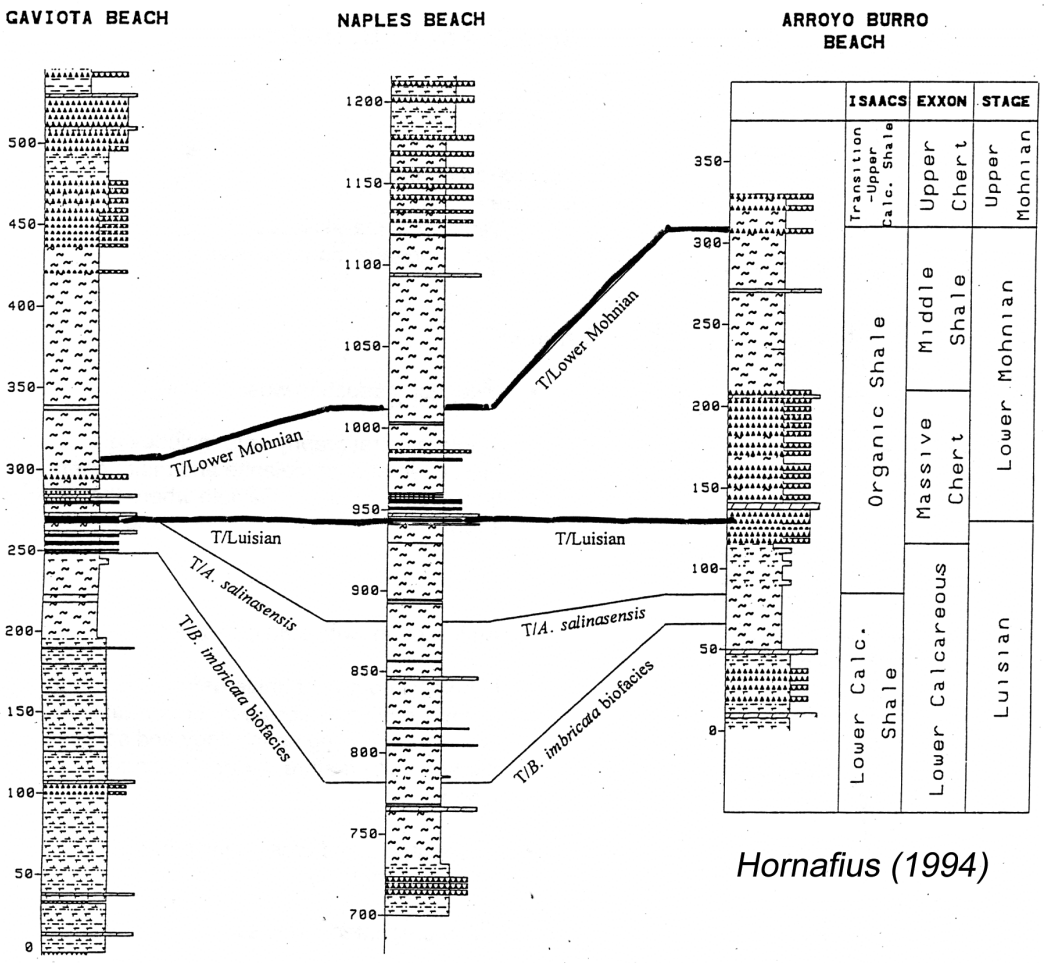

Figure GB-02. Dramatic variation in thickness and character of portions of the Monterey Formation between Arroyo Burro Beach and Gaviota Beach (Hornafius, 1994).

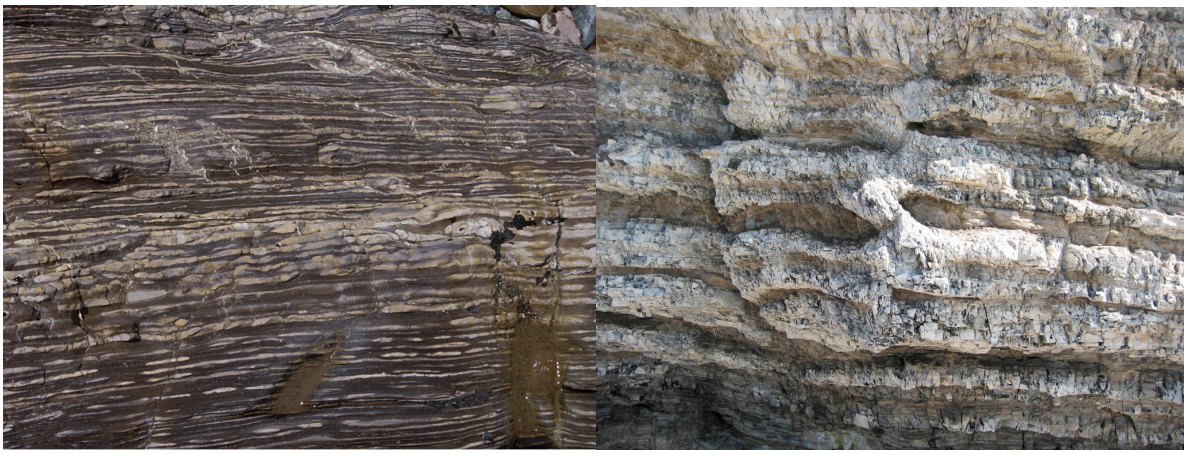

Figure GB-03. Organic-rich, phosphatic shale (carbonaceous marl) was deposited at Gaviota Beach (left) during the same interval that sediments converting to porcelanite and siliceous shale were deposited at Arroyo Burro (right). Gaviota was likely a shallower, current-winnowed banktop, whereas Arroyo Burro was in a deeper slope or basin setting.

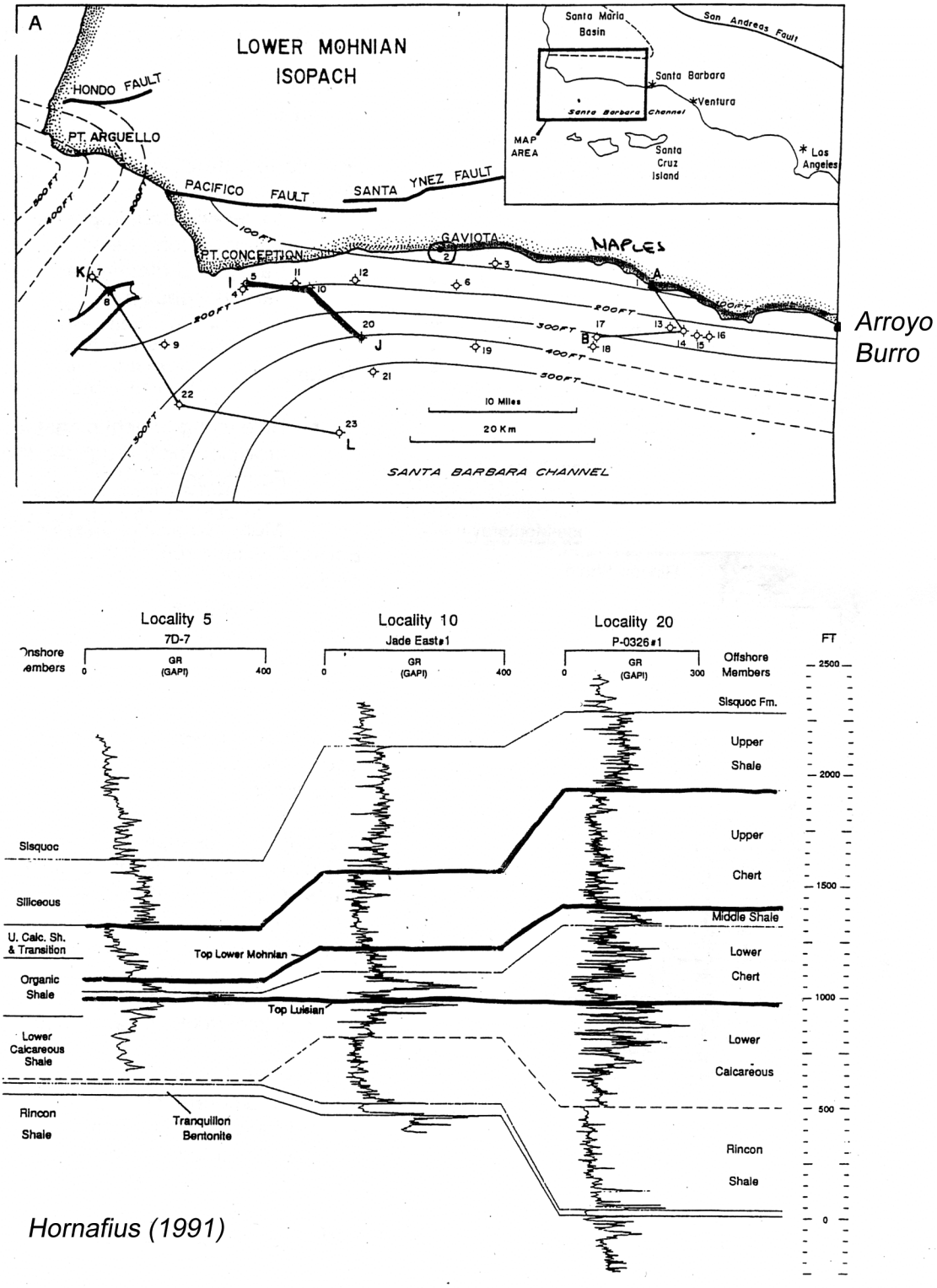

Figure GB-04. Lateral variation in thickness of different members of the Monterey Formation shown by well logs (Hornafius, 1991).

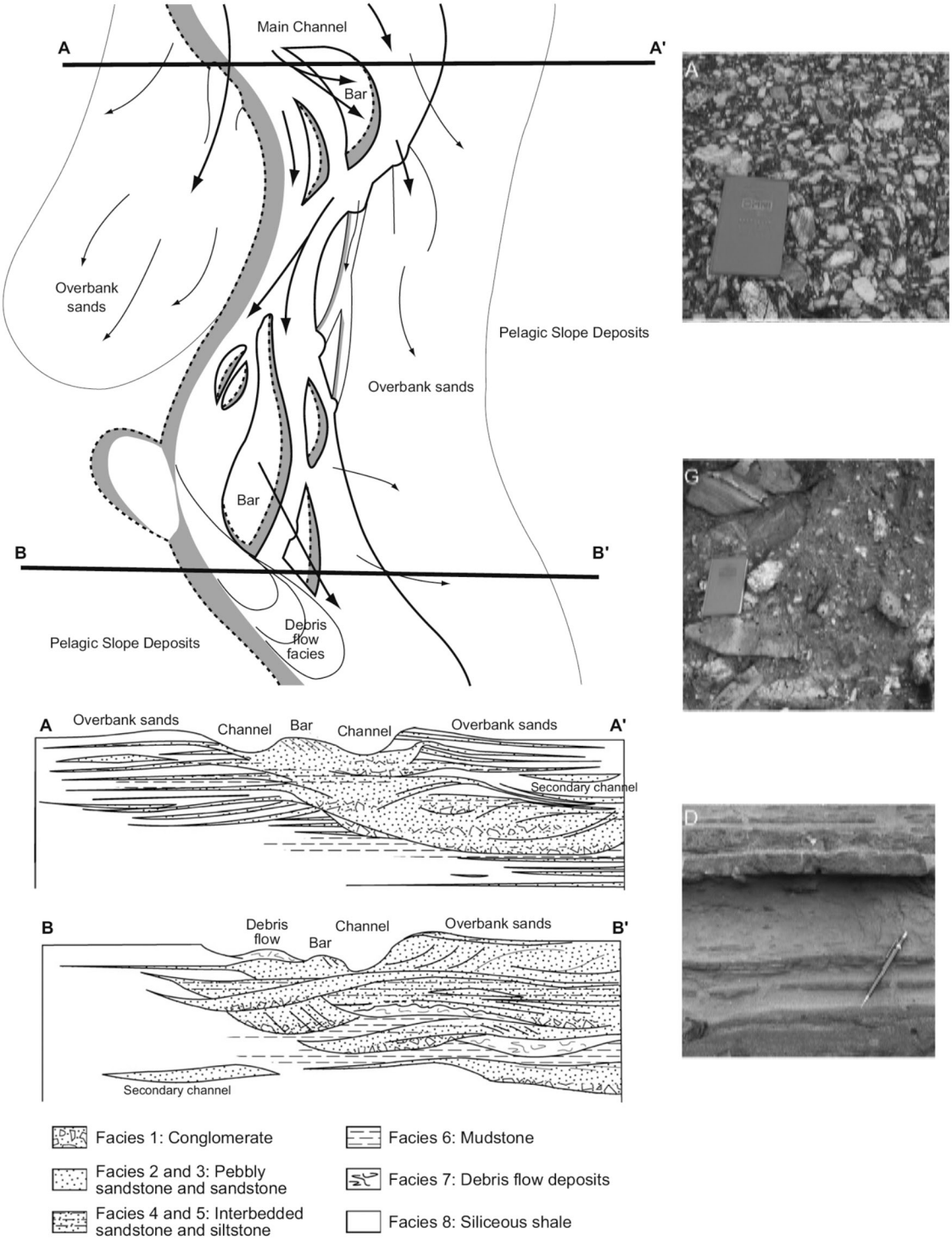

Figure GB-05. Schematic plan view and cross-sections of the Gaviota slope gully deposits, illustrating the fairly straight, braided course of the channelized flows (Surpless et al., 2008)

GAVIOTA BEACH

Locality: Gaviota 7.5 minute quadrangle, section at latitude 34°28.2' N. between longitude 120°13.5' W. and 120°12.2' W. This section is exposed along the beach east of the pier. On the east side of the canyon mouth and along the beach to the east, the siliceous member is well exposed. The top of the upper calcareous shale member occurs just beyond a concrete drain, about 0.8 km east of the pier. Farther east is the transition member (exposed in cliffs and rock ledges on the beach) and the upper part of the organic shale member (exposed in beach cliffs protected by resistant ledges). The lower calcareous shale member is located east and west of the mouth of the Canada del Cementerio.

Diagenetically, the silica phase at Gaviota Beach is mainly opal-CT; diagenetic quartz is present in a few detrital-rich rocks in the lower two members (see fig. 15):

Siliceous member (fig. 11)	All opal-CT.
Upper calcareous shale member (fig. 12)	All opal-CT.
Transition member	All opal-CT.
Organic shale member (fig. 13)	Mainly opal-CT with some diagenetic quartz in detrital-rich rocks.
Lower calcareous shale member (fig. 14)	Mainly opal-CT with diagenetic quartz in detrital-rich rocks

Note the following features in this section:

** 1- to 2-m-thick units of laminated porcelanites and cherty porcelanites interbedded with 1- to 2-m-thick units of massive siliceous mudstone--siliceous member;

** Dolomite nodules in preferred layers within siliceous mudstone units--siliceous member;

** Fracture patterns on dip-slope exposures--siliceous member;

** Blockiness of porcelanite fragments--siliceous member;

** Thin beds with varying resistance to erosion--top of upper calcareous shale member (fig. 12A);

** 1- to 2-m-thick units grading upward from detrital-rich calcareous shale to detrital-poor calcareous cherty porcelanites, forming resistant ledges along the beach--upper calcareous shale member (fig. 12B);

** Dark shales with phosphatic layers and blebs--transition member and organic shale member;

** Nodular dolomite layers in organic-rich phosphatic calcareous shale--organic shale member;

** Distinct layering in shales and porcelanites--upper part of lower calcareous shale member; and

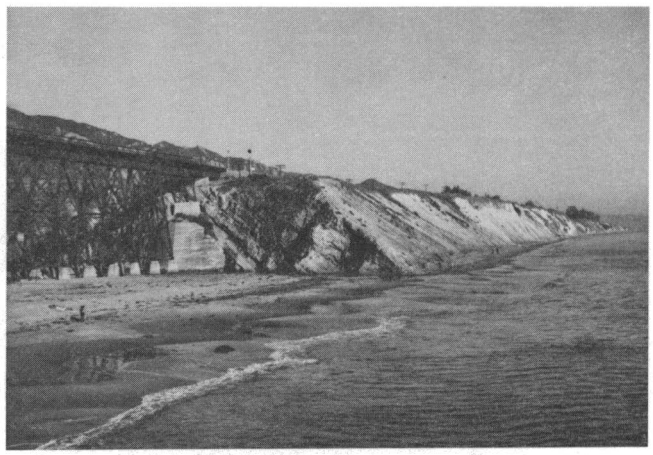

Figure 11A. Siliceous member on the east side of the mouth of Gaviota Canyon, showing porcelanite units exposed in dip slopes. Cliff is about 25 m high.

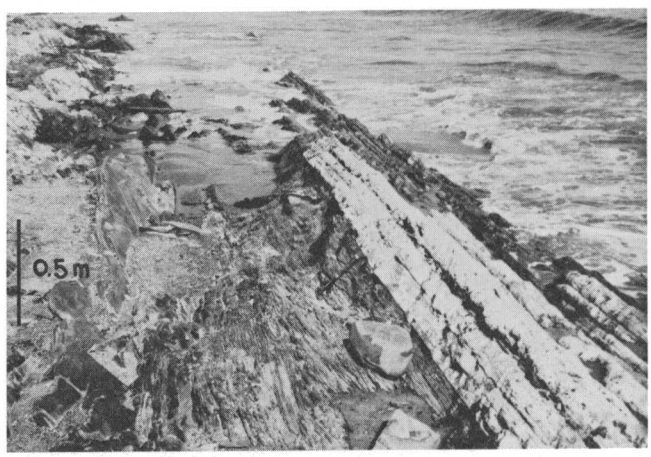

Figure 11B. A unit of porcelanite (light-colored, resistant beds on right) overlying a unit of dark siliceous mudstone in the siliceous member at Gaviota Beach.

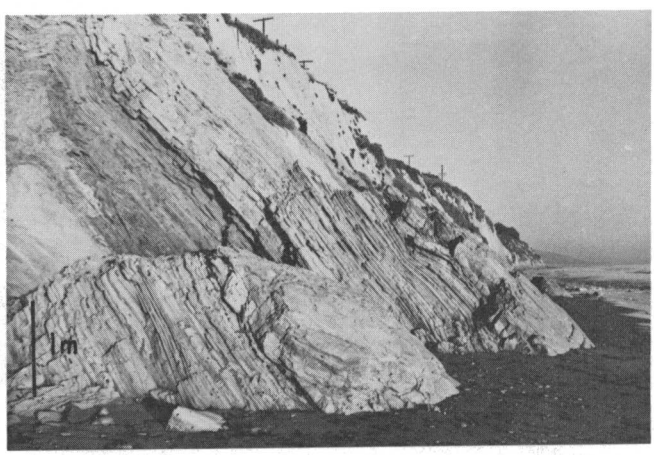

Figure 12A. Upper calcareous shale member at Gaviota Beach, showing thin beds of calcareous porcelanites and calcareous shales near the top of the member. At the top of the exposure (right) is a thick dolomite bed.

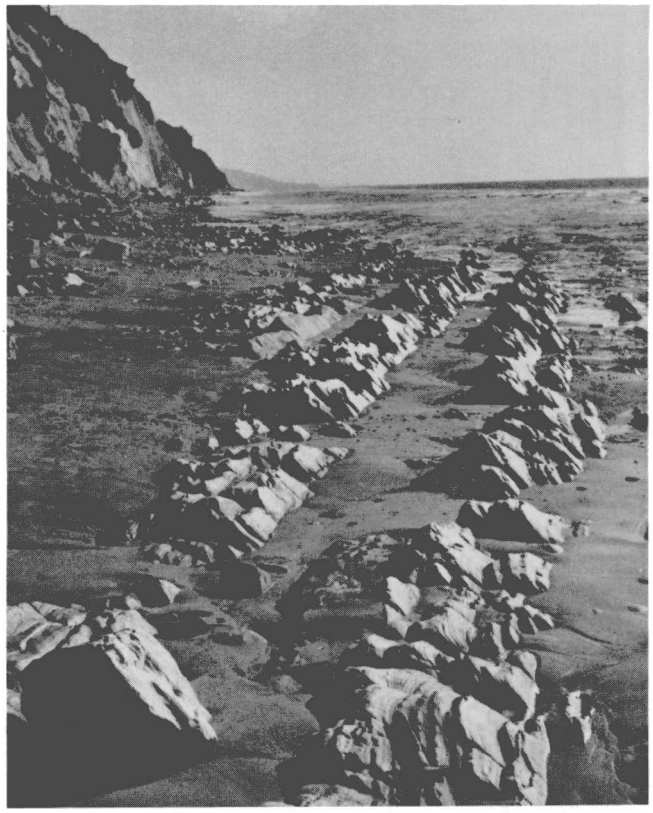

Figure 12B. Resistant ledges of calcareous porcelanite along the beach in the upper calcareous shale member at Gaviota Beach.

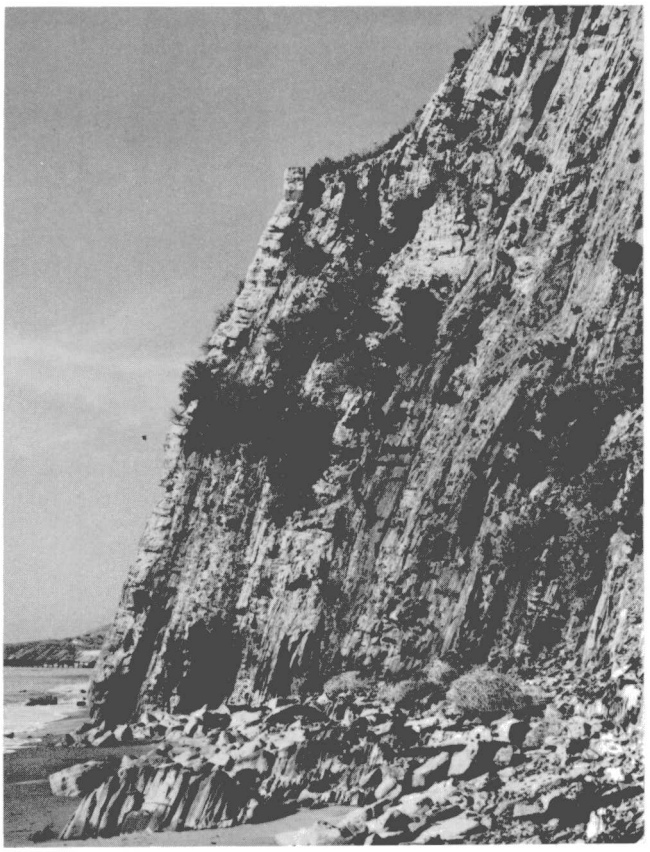

Figure 13. Organic shale member at Gaviota Beach protected by a resistant ledge (at far left). Cliff is about 25 m high.

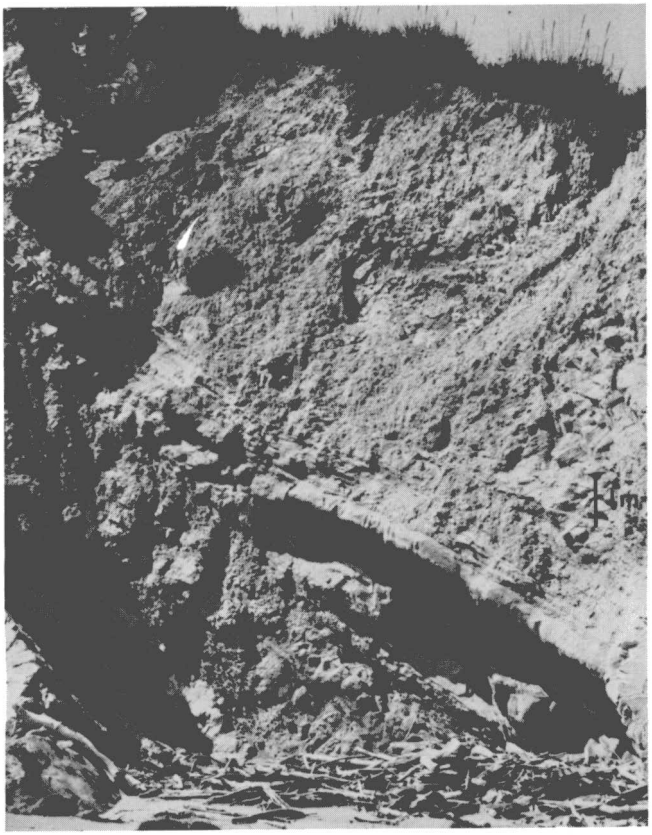

Figure 14A. Lower calcareous shale member at Gaviota Beach just west of Canada del Cementerio.

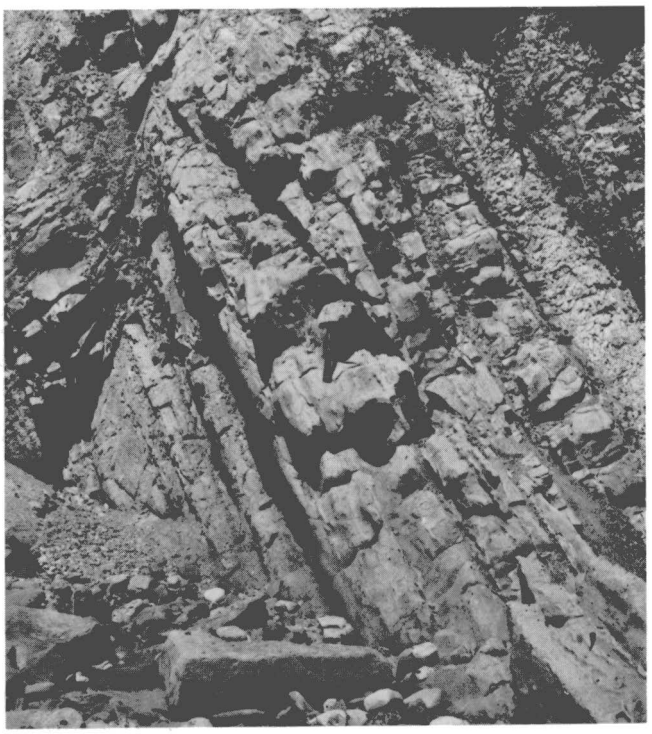

Figure 14B. Thick-bedded calcareous rocks in the lower calcareous shale member just east of Canada del Cementerio.

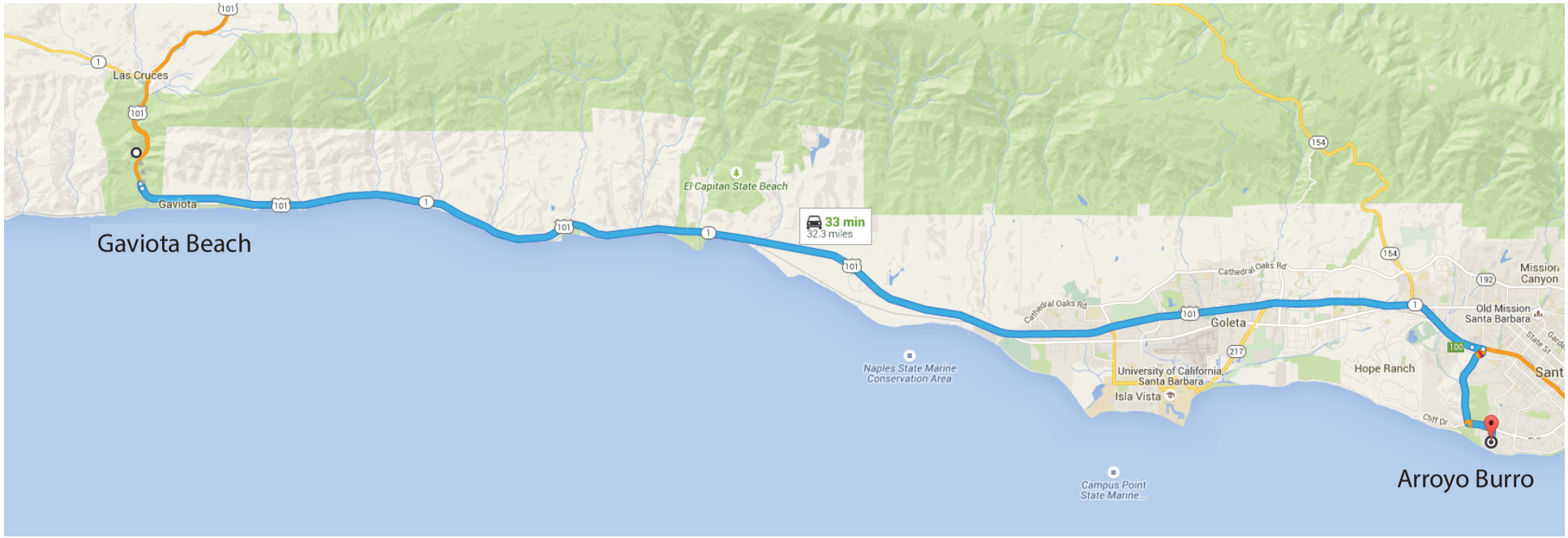

Day 2. Gaviota Beach to Arroyo Burro Beach.

Arroyo Burro County Beach (aka Hendry's Beach)

ARROYO BURRO PART 1 - GENERAL OVERVIEW

Structural content by Michael Gross, now with Shell

Basin: Ventura-Santa Barbara

Formation/Members:

Monterey,

- transitional marl-siliceous (Isaacs)
- carbonaceous marl/organic shale

Notes:

- Walk west along beach from Mesa Lane stairs to Arroyo Burro parking lot.

- Stratigraphy here includes a 100'-thick interval of porcelanite and minor chert not present to west along Santa Barbara coast where, instead, there is a relatively condensed, organic-rich, phosphatic marl facies.

- Nearly all siliceous rocks here are in the opal-CT phase. Crystallographic ordering indicates that they barely formed at maximum burial depth.

- Reservoir-scale Mesa Anticline with smaller-scale parasitic folds, bounded to north by Lavigia and La Mesa faults. Outcrop is on south flank of structure.

- Lithologic control of brittle deformation, with distinct jointing, brecciation, or normal faulting depending on lithology and scale of the structural feature. Extension parallel to hinge.

- Stratigraphically controlled and cross-cutting breccias in siliceous lithologies.

- Oil-impregnated fractures.

- Sequence of different carbonate veins and oil emplacement relate to evolution and expulsion of basin fluids.

- Major fault with massive layered calcite veins, recording alternate oil migration and calcite precipitation/cementation and large volumes of fluid flow

- Dolomite concretions that nucleated on whale bones.

Watch for surf and slippery rocks!!!

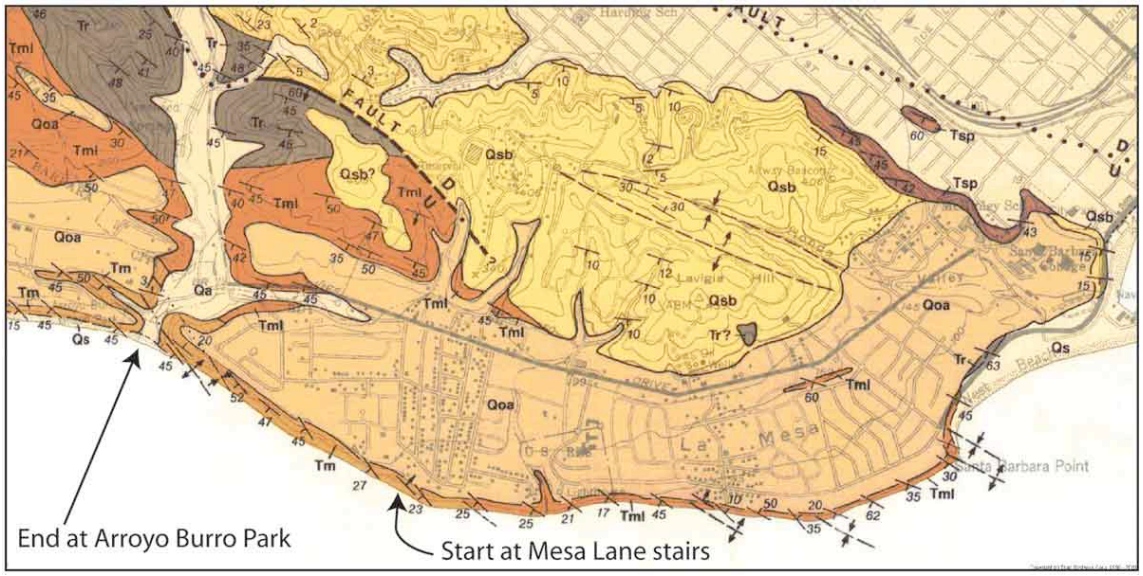

Figure AB-01. Geologic map of the Arroyo Burro field trip stop and the Santa Barbara Mesa area. Modified from (Dibblee and Ehrenspeck, 1986).

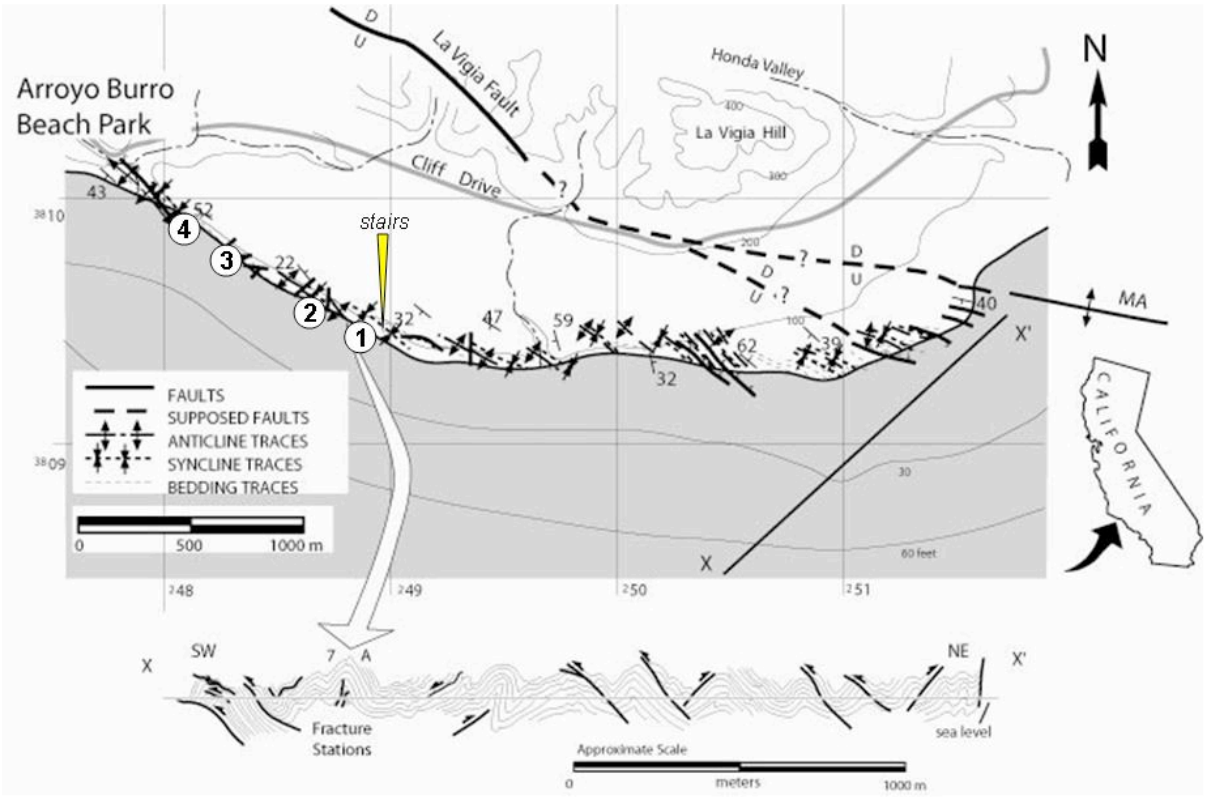

Figure AB-02. Map and cross section of Arroyo Burro showing the four stops on our field trip (after Gross et al., 1997).

Figure AB-03. Outcrop expressions of three common lithologies in the Arroyo Burro locality: dolostone, phosphatic, calcareous shale (also called carbonaceous marl), and porcelanite.

Figure AB-04. Interbedded carbonaceous marl and opal-CT porcelanite showing lithologic control of deformational style and reservoir potential , opening-mode fractures in porcelanite, and lithologic control of fracture density.

Figure AB-05. Normal faults crosscutting interbedded clay shale, siliceous shale, and fractured porcelanite. Dead oil stains fractures in porcelanite, but clean offset along faults results in low continuity of permeability along offset strata.

Figure AB-06. Brecciated and stretched beds of brittle lithologies enhance permeability across and along normal fault that cuts shale, porcelanite, and chert. Note oil stain on breccia fragments and rotated dolomite concretion in fault zone.

Figure AB-07. Through-going fault breccia cutting siliceous dolomite bed. Fractured dolomite is an important reservoir in the Monterey Formation. Dolomite breccias are generally composed of larger and more equant fragments than chert or porcelanite breccias, giving larger diameter fluid flow pathways. Note oil coatings.

Figure AB-08. Calcite cement fault breccia . Fault provided major fluid flow conduit for dewatering of basin. Alternating composition of fluids moving along fault is recorded by inclusion-rich calcite cement, that was brecciated both syn- and post-emplacement.

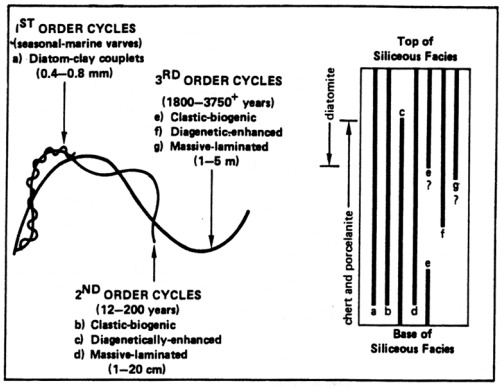

Figure 14. Schematic representation of the types and occurrences of cycles in the siliceous facies of the Monterey Formation. Numbers in years represent durations of the siliceous members of couplets within each type of cycle. Values in mm, cm and meters are ranges in thicknesses of these siliceous members. The column on the right shows the approximate distribution of each type of cycle within the siliceous facies; letters correspond to letters in parentheses designating different types of cycles. *Pisciotto & Garrison, 1981*

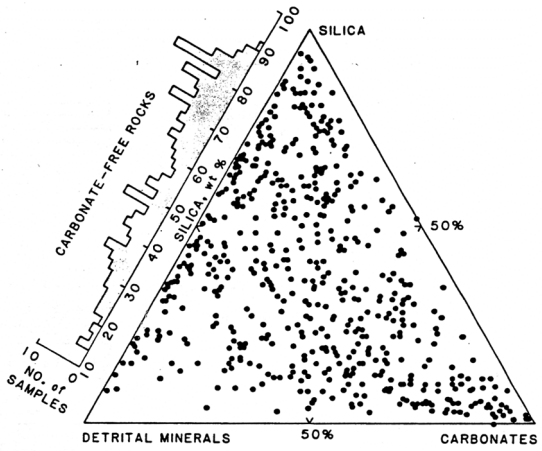

Figure 7. Diagram showing the wide variety of sedimentary compositions among individual beds in the Monterey Formation, Santa Barbara-Ventura and Santa Maria areas. Each data point represents a chemically analyzed sample, and the histogram represents the distribution of detritus-silica compositions of samples containing less than 1% carbonate minerals. Sedimentary components are expressed on an organic-matter-free basis, and apatite is included here with carbonates. From Isaacs (1987).

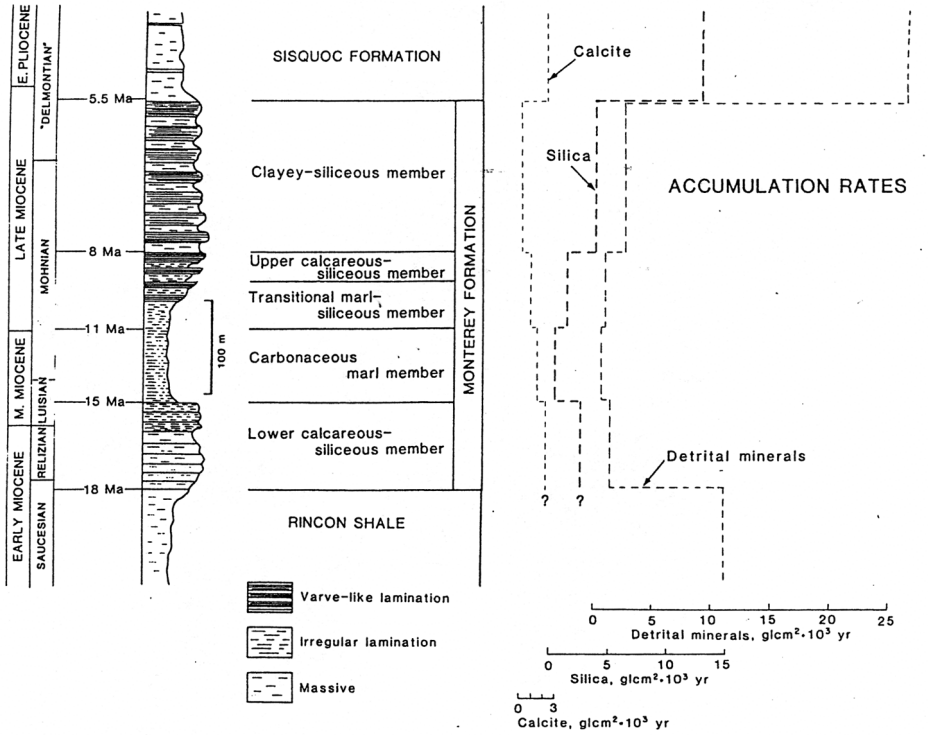

FIG. 2. Generalized lithostratigraphic column and accumulation rates of the Miocene sequence, Santa Barbara coastal area, California.
Isaacs, 1984

Figure AB-09. Although known as a siliceous unit, the Monterey is remarkably heterogeneous in composition . Cyclic variation is striking. It chiefly exists as silica-detrital alternations in the upper parts of the formation, but is more complex and heterogeneous in the middle and lower parts. The most biogenic-rich intervals accumulated at the slowest rates, undiluted by detritus.

ARROYO BURRO PART 2: FRACTURE & FAULT ANALYSIS

Outcrops of the Monterey Formation exposed along Arroyo Burro Beach provide outstanding analogs for fractured hydrocarbon reservoirs. There is plenty to see, and you are welcome to stroll along the beach at your own pace or join the group leaders for discussion. The main themes we would like to focus on are:

a.) mechanical stratigraphy and its effect on fracture/fault development
b.) orientations of fractures and faults with respect to fold geometry
c.) scaling of fracture and fault populations and resulting fracture architecture
d.) magnitude of strain accommodated by brittle deformation
e.) major pathways for fluid flow (fault –breccia –vein zones)
f.) fault-fracture envelopes
g.) fracture porosity and permeability; reservoir-scale fluid flow

Overview of Tectonics, Structural Style and Fold Geometry

Despite its relatively young geological age, the Miocene Monterey Formation in central coastal California displays an abundance of deformational structures at many scales (e.g., Grivetti, 1982; Snyder and others, 1983; Dunham and Blake, 1987; Narr and Suppe, 1991; Bartlett, 1994; Behl and Garrison, 1994; Gutiérrez-Alonso and Gross, 1997; Eichhubl and Boles, 2000a,b; Finn et al., 2003). This intense deformation may be attributed to the location of Miocene depositional basins with respect to subduction, microplate capture, and development of the San Andreas Transform system (Isaacs, 1980; Pisciotto and Garrison, 1981; Atwater, 1989; Nicholson et al., 1994). As a consequence of this tectonic activity, the entire southern block of the western Transverse Ranges rotated clockwise by ~ 90° since the middle Miocene (Crouch, 1979; Luyendyk and others, 1980; Hornafius, 1985). Presently the western Transverse Ranges is an actively developing fold and thrust belt characterized by rapid uplift, fault-related folding, and NNE-SSW directed shortening (e.g., Yeats, 1983; Namson and Davis, 1988).

In light of the Neogene tectonic activity along the California borderland, it should come as no surprise that rocks along the Santa Barbara and Santa Maria coastlines are intensely deformed. What makes structural development in the Monterey Formation so interesting and amenable for analysis is its diversity of rock types and thin to medium bedded stratification. Strong contrasts in mechanical properties often result in different styles of deformation (e.g., ductile versus brittle, faulting versus jointing) among different beds at the same outcrop, while bed thickness often limits the dimension, and hence scaling relations, of various fracture types. Added to the mix are the high levels of strain, resulting in the propagation of fractures and faults across bed boundaries and the development of brittle structures at a variety of scales.

Structural and tectonic maps of the western Transverse Ranges and Santa Maria fold and thrust belt (e.g., Fig. 6-10) reveal a series of E-W and ESE-WNW trending fold axes and reverse faults (Woodring and Bramlette, 1950; Dibblee, 1950, 1966; Sylvester and Darrow, 1979; Yeats, 1983; Shaw and Suppe, 1994) oriented approximately perpendicular to present-day maximum horizontal principal stress (S_H) as determined by earthquake focal mechanisms (Lee and others, 1979; Corbett and Johnson, 1982; Eaton, 1984) and borehole breakouts (Mount and Suppe, 1992; Wilde and Stock, 1997; Finkbeiner and others, 1997). Rapid Quaternary uplift and folding in the Ventura Basin (e.g., Yeats, 1977; 1983; Rockwell and others, 1988) as well as balanced cross sections across the Santa Maria fold belt (Namson and Davis, 1990), the western Transverse Ranges (Namson and Davis, 1988), and Santa Barbara Channel (Shaw and Suppe, 1994) all attest to an actively developing regional fold and thrust belt characterized by NNE-SSW directed shortening. Pure shear tectonic contraction is further supported by geodetic studies

that report 5 - 6.5 mm per year of convergence in the Santa Barbara region, with little or no rotational strain components (e.g., Feigl and others, 1993; Larsen and others, 1993). Structures within the Monterey Formation cannot by themselves conclusively determine whether the western Transverse Ranges continue to rotate clockwise as suggested by Jackson and Molnar (1990) and Luyendyk (1991), or whether the phase of simple shear block rotation was supplanted by present-day shortening as inferred from the aforementioned cross sections. However, mesostructures within the Monterey can be directly related to tectonic processes operating at upper crustal levels, especially with regards to development of the regional fold belt.

Looking SE from the parking lot at Arroyo Burro State Park, one can see the folded laminated beds of the Monterey Formation. The folds occur at many scales. The entire section along the beach is on the SW limb of the Mesa anticline, a regional first-order fold whose axis trends NW-SE, parallel to strike of the Mesa Fault and Lavigia Fault, mapped as vertical faults with inferred dip slip motion (Dibblee, 1966; 1986). Cross sections constrained by well control indicate that most of the E-W to NW-SE trending faults in the region are high angle reverse faults, with an unknown component of strike slip motion (Olson, 1982). The Lavigia Fault, mapped as a single strand at the surface north of Cliff Drive (Dibblee, 1966, 1986) is inferred to branch into two splays that intersect the coastline (Olson, 1982). The axis of the Mesa Anticline, a structure that produced oil from the Vaqueros Formation in the 1930's, is mapped offshore along strike of the northern strand of the Lavigia Fault (Hoyt, 1976; Olson, 1982). At Ellwood Beach, approximately 15 km to the west, the more easterly trending faults such as the More Ranch Fault display a net left-lateral - reverse oblique sense of motion (Bartlett, 1998).

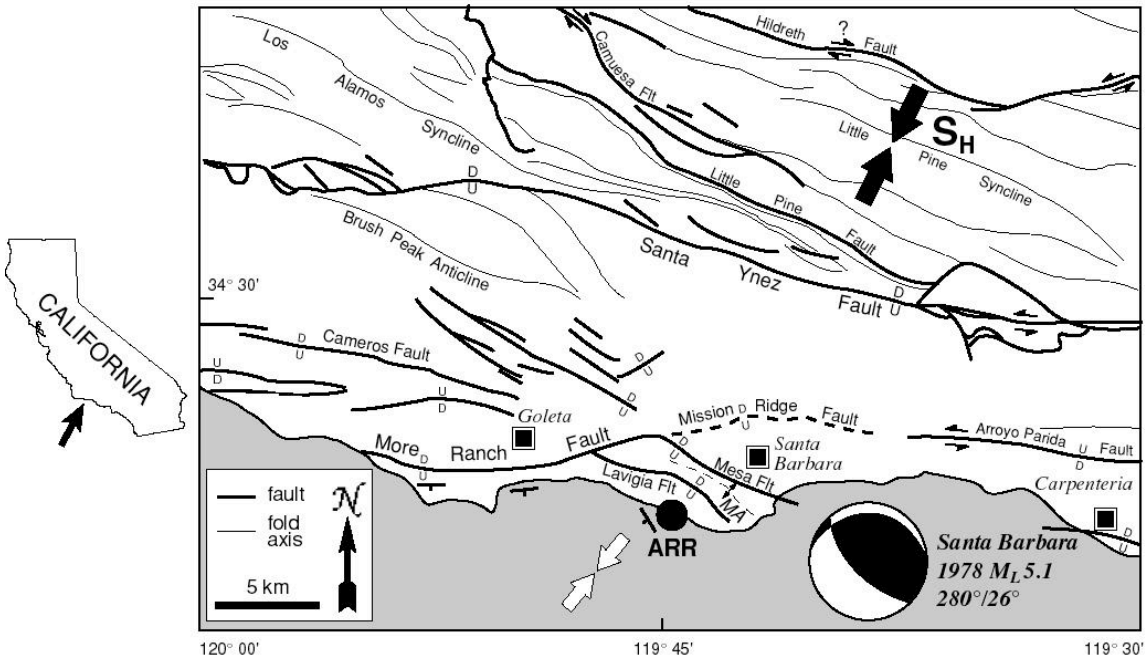

Figure AB-10. Tectonic and structural map of the Western Transverse Ranges in the Santa Barbara area (after Dibblee, 1966) showing location of Arroyo Burro section (ARR). Focal plane solution for the 1978 Santa Barbara earthquake (from Corbett & Johnson, 1982) is plotted along with SHMAX trend (black arrows) derived from borehole breakouts (Mount & Suppe) and structural trends. From Gross & Engelder (1995).

Folding in the Monterey Formation is controlled to a large extent by the presence of numerous thin (0.5 - 5 cm) bentonite and/or clay horizons that serve as detachments. Consequently, disharmonic folding in the Monterey Formation is quite common throughout the Santa Barbara and southern Santa Maria basins, especially among beds of different lithologies and different phases of silica diagenesis. Structural maps of Arroyo Burro beach reveal a series of second-order NW-SE trending folds in the

Monterey Formation, with wavelengths of ~ 200 meters (Fig. 6-02; Dibblee, 1966; Hornafius, 1994a; Gross and others, 1997). Projecting the Arroyo Burro exposures onto a NE-SW cross section, one can see the structural style is characterized by fault-related and detachment folding (Fig. 6-02). The numerous folds, thrusts and bedding plane faults observed in profile reflect a style of deformation found in many contractional fold and thrust belts. Bedding orientations measured along the 3.5 km transect are plotted as poles in a pi-diagram (Fig. 6-11). If the poles fall along a great circle, then the folds are cylindrical in shape and the normal to the best-fit great circle represents the fold axis (Ramsay and Huber, 1987). As one would expect from the numerous faults and contorted strata, there is considerable scatter in bedding orientation. However, the poles indeed cluster along a great circle, yielding a calculated fold axis trending 140° and plunging 6° to the SE. Thus, the folds at Arroyo Burro are cylindrical (i.e., their shape remains uniform along strike) with subhorizontal axes that trend parallel to regional structural trend. This is strong evidence indicating that folds in the Monterey Formation at Arroyo Burro are genetically related to, and formed in conjunction with, the western Transverse Ranges fold and thrust belt.

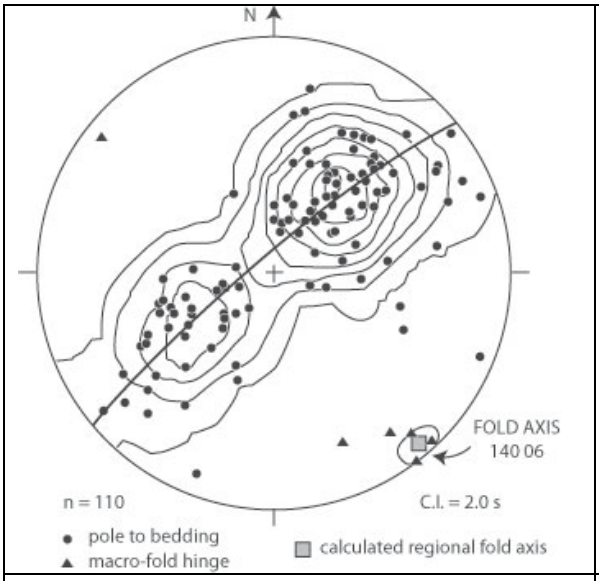

Fig. AB-11a. Pi diagram of poles to bedding showing best-fit cylindrical fold axis. Note the orientations of the main fracture and fault sets with respect to the fold axis.

Fig. AB-11b Photo of a small detachment fold near the main entrance to Arroyo Burro Beach State Park.

Stop #1 (Station A in some publications) – mechanical stratigraphy, fracture partitioning, fault scaling, fault-fracture mesh, GIS analysis.

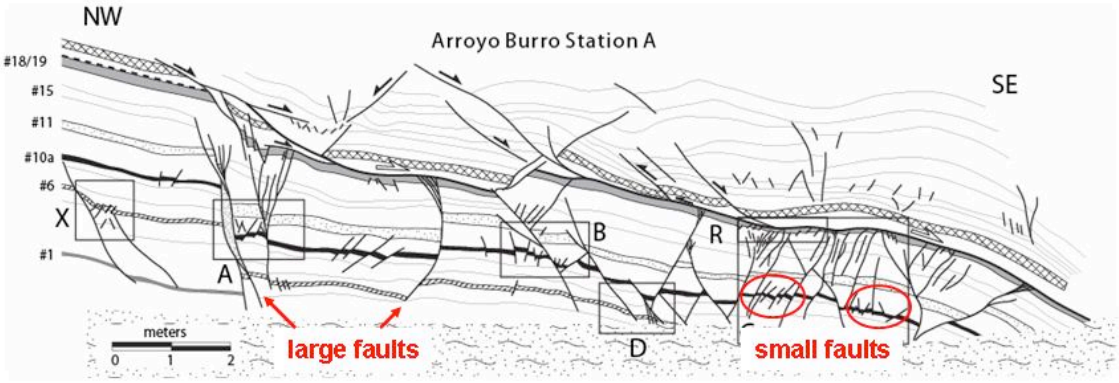

Fig. AB-12. Overview sketch of faults at Stop #1. From Gross et al (1997).

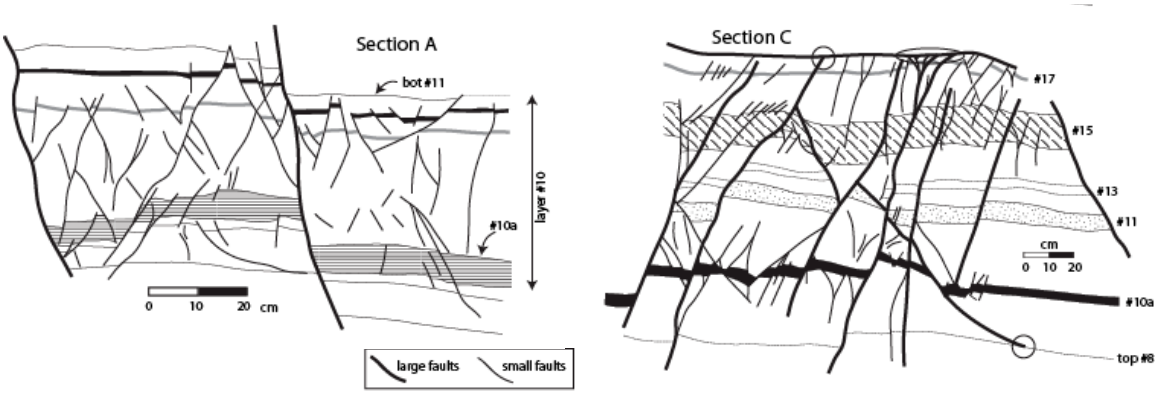

Fig. AB-13. Close-up sketches of portions of Stop #1. From Gross et al (1997).

Fig. AB-14. Example of a large fault at Stop #1. Note attenuation (thinning) of brittle porcelanite and dolostone beds, and smearing of shale within fault zone. Is this fault a conduit or seal?

Fig. B-15. Example of small faults at Stop #1

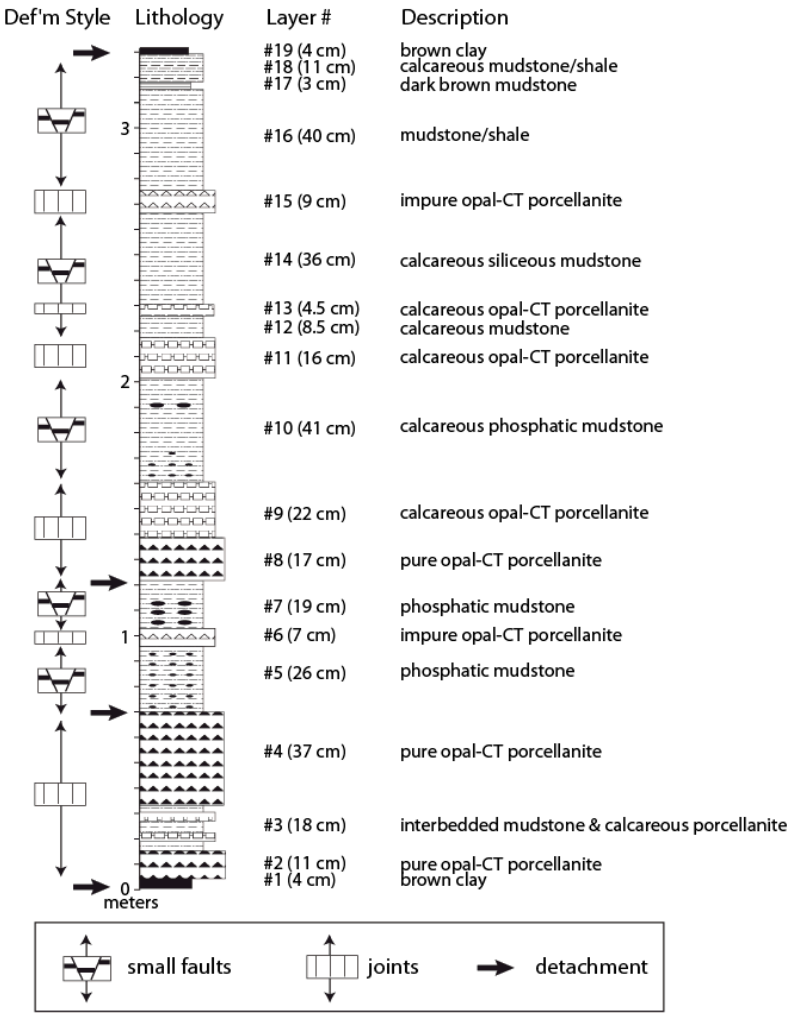

Fig. AB-16. Mechanical stratigraphy at Stop #1. From Gross et al (1997).

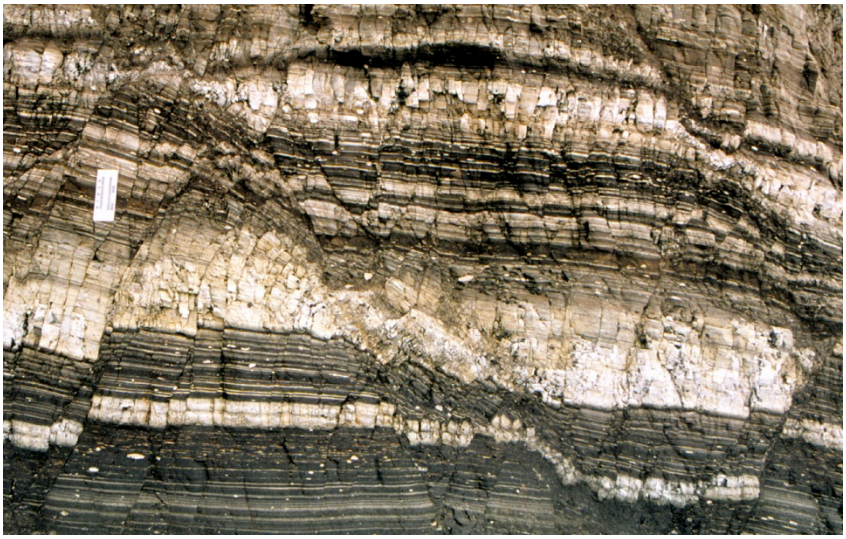

Fig. AB-17. Stop #1 photo showing fracture partitioning (faulting in mudstone vs. opening-mode fractures in porcelanite; refer to Fig. I-18 in Introduction chapter).

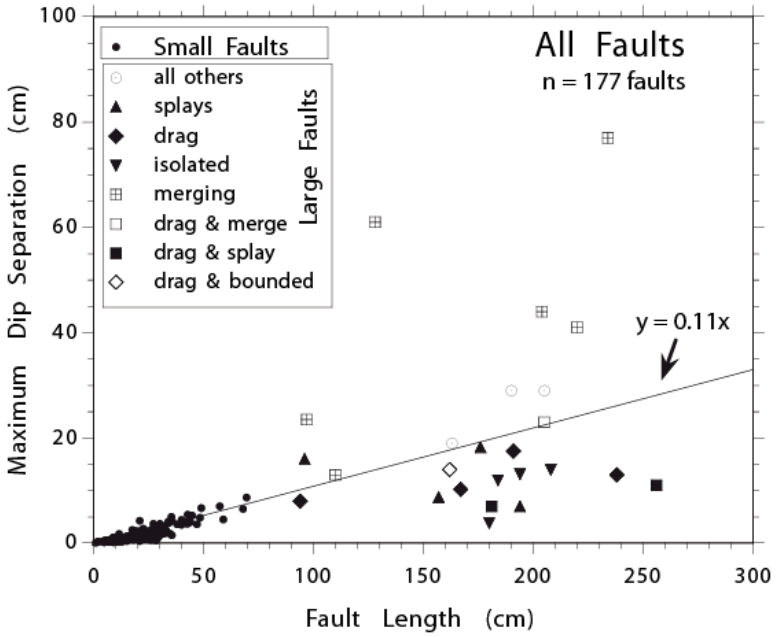

Fig. AB-18. Plot of fault length versus dip separation for normal faults at Stops #1 and #2. Note breakdown in linear scaling relationship for the larger, multi-layer faults. From Gross et al (1997).

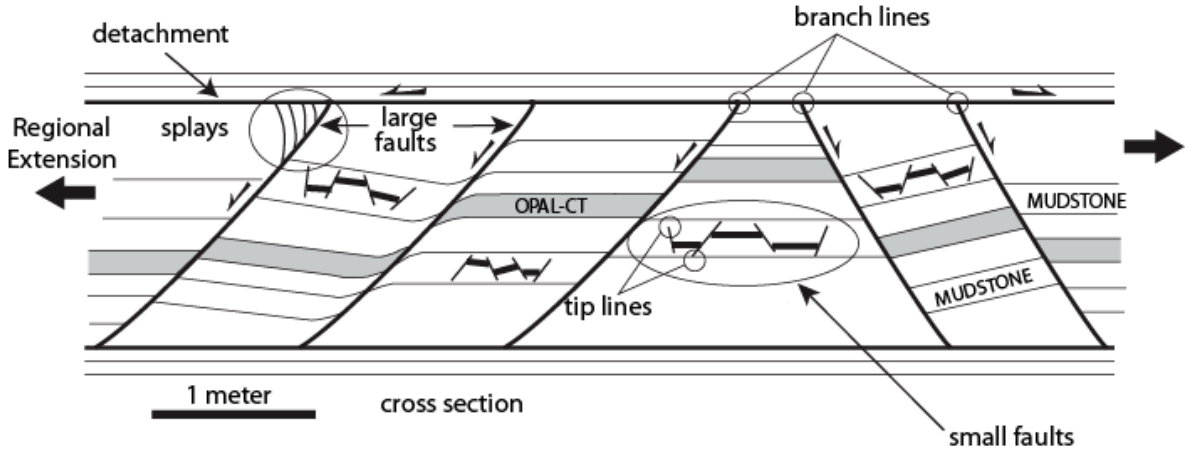

Fig. AB-19. Conceptual model to explain Displacement-Length scaling relations for faults at Arroyo Burro. From Gross et al (1997).

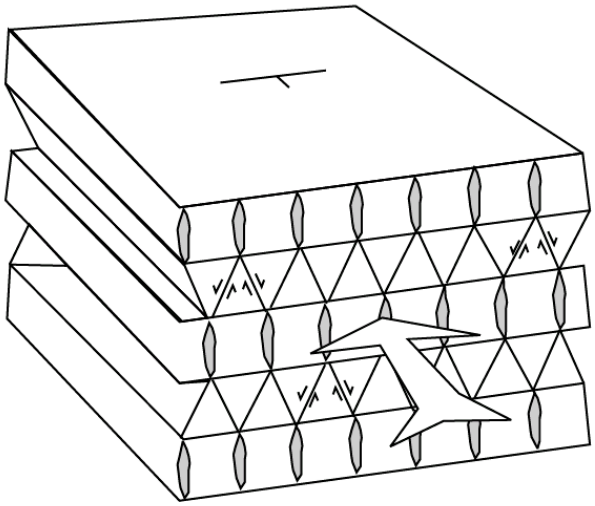

Fig. AB-20. Fault-fracture mesh proposed by Sibson (1996) to explain structural permeability at Arroyo Burro and other localities.

Geospatial (GIS) Analysis of Fractures At Stop #1 from Ghosh (2003):

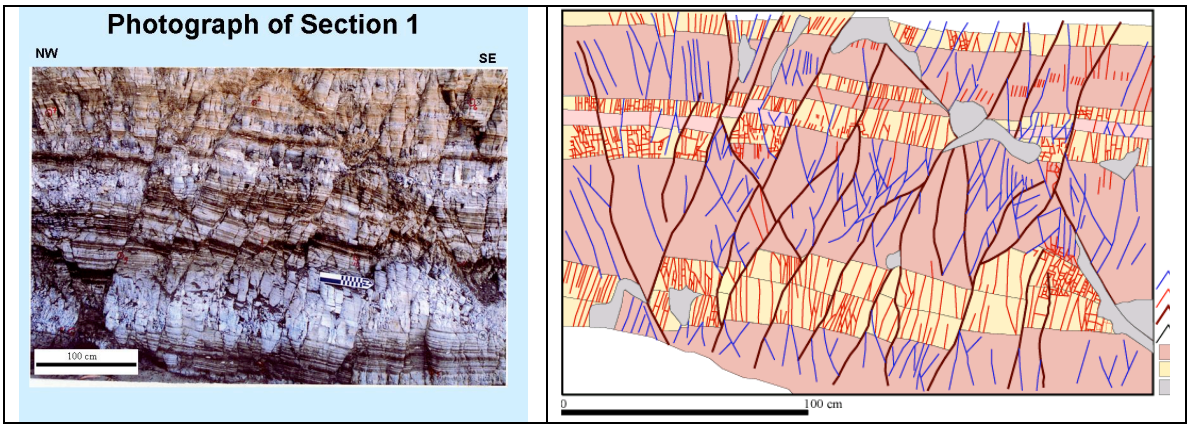

Fig. AB-21. Photo and digitized map of a portion of Stop #1 (Ghosh, 2003)

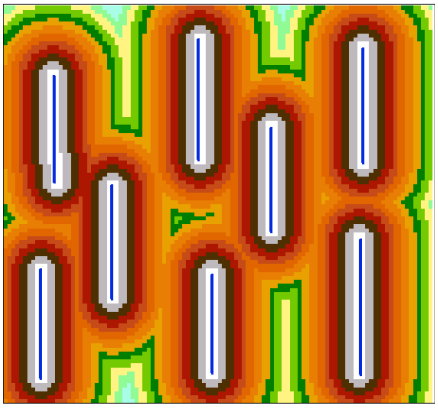

Fig. AB-22a. Distance buffer analysis around fractures.

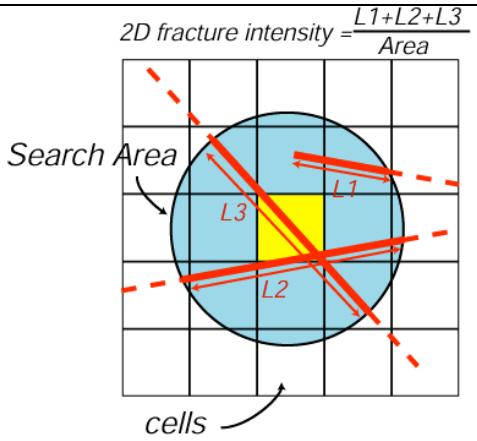

Fig. AB-22b. 2D fracture intensity analysis for cells in map.

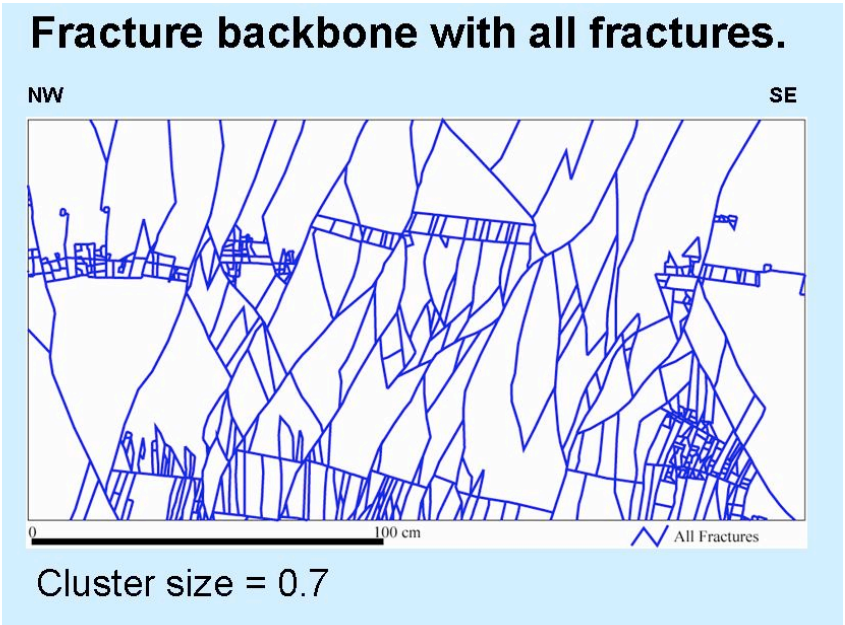

Fig. AB-23. Fracture backbone, representing all fractures that are interconnected across the domain of interest. (Ghosh, 2003)

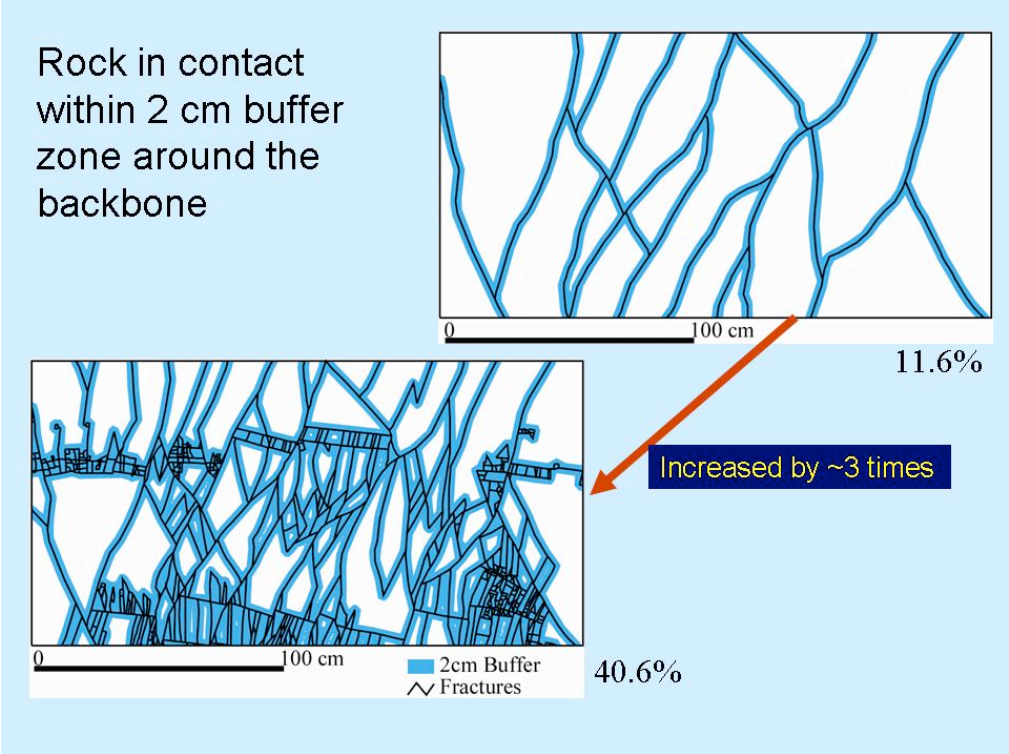

Fig. AB-24. Result of buffer analysis on fracture backbone, showing contribution of small fractures to flow if the matrix is accessible (Ghosh, 2003).

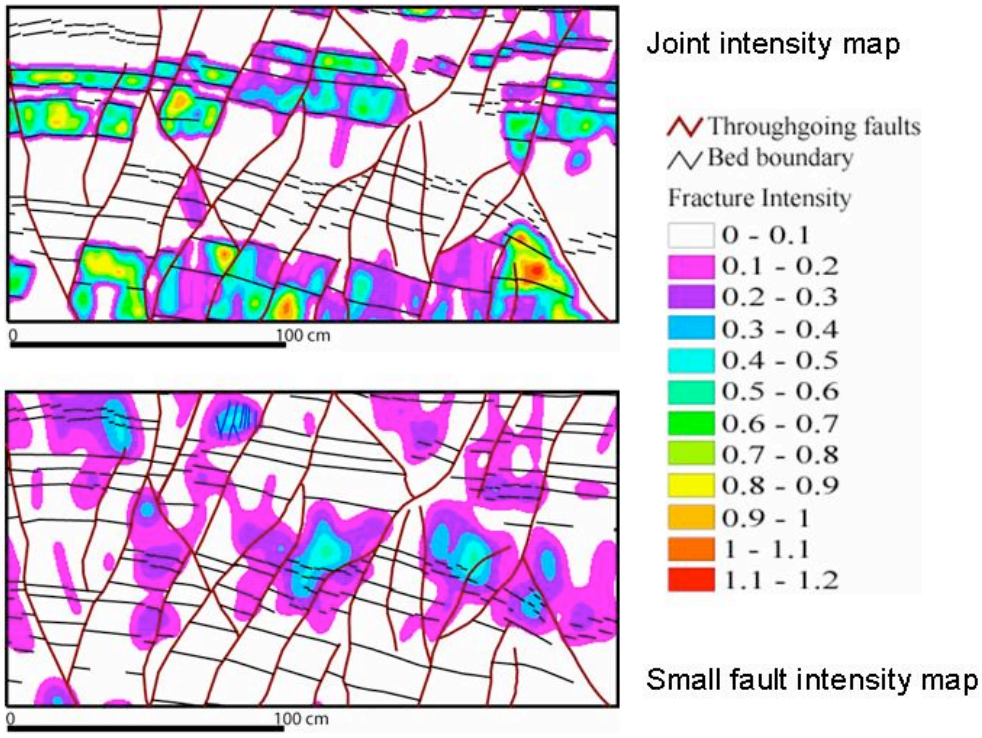

Fig. AB-25. Fracture intensity maps for joints and faults at Stop #1 (Ghosh, 2003).

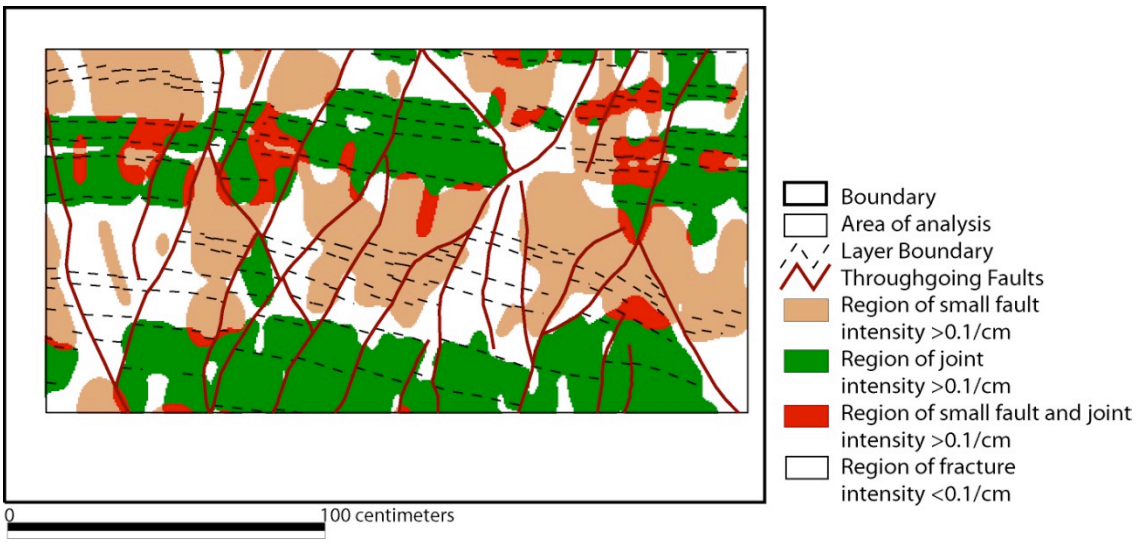

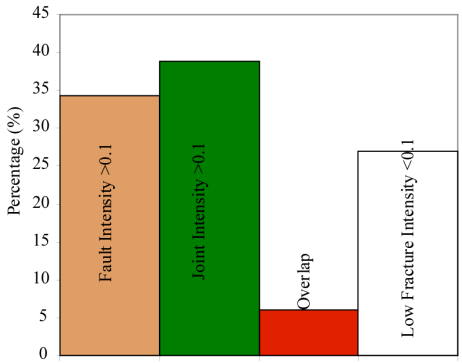

Fig. AB-26. Reclassified map of results of fracture/fault intensity analysis. Note how fracture partitioning can be quantified in terms of the fracture type and intensity within the mechanical stratigraphy (Ghosh, 2003).

Stop #2 (Station 7 in some publications) – faults & veins, measurement and calculation of fracture strain, fracture-fold mechanisms and relationships.

Fig. AB-27. Photo of overview of Stop #2; arrow points to subhorizontal detachment fault.

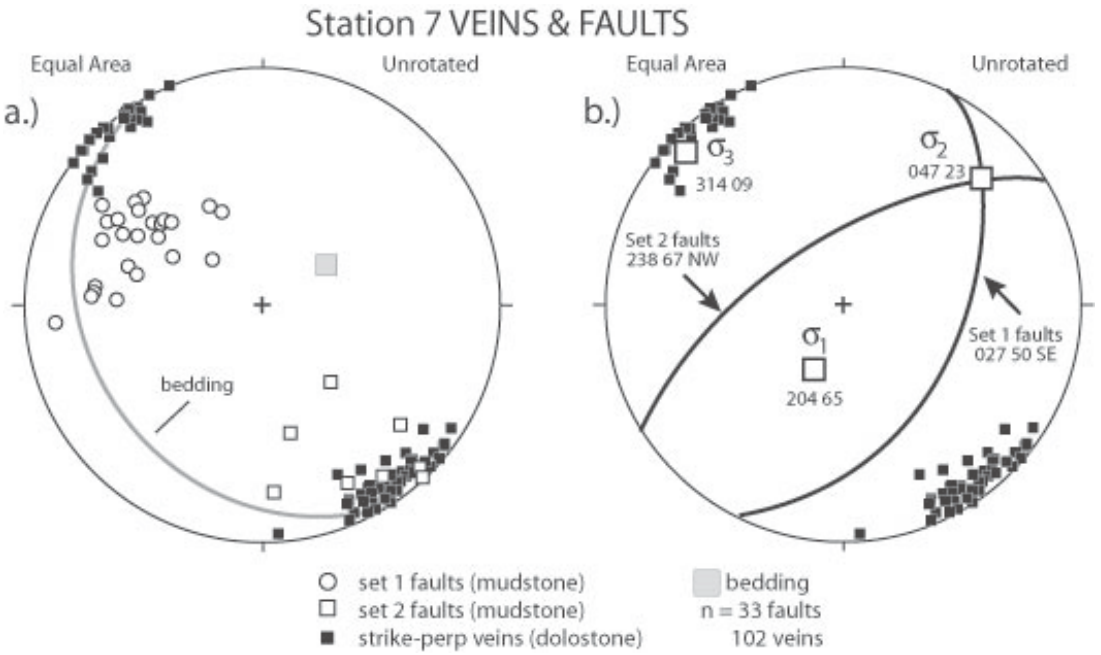

Fig. AB-28. Stereoplots of poles to joints and faults measured at Station 7, along with mean fault orientations and calculated principal stresses. Compare to fold axis derived from pi-diagram in Fig. 6-11a (Gross and Engelder, 1995).

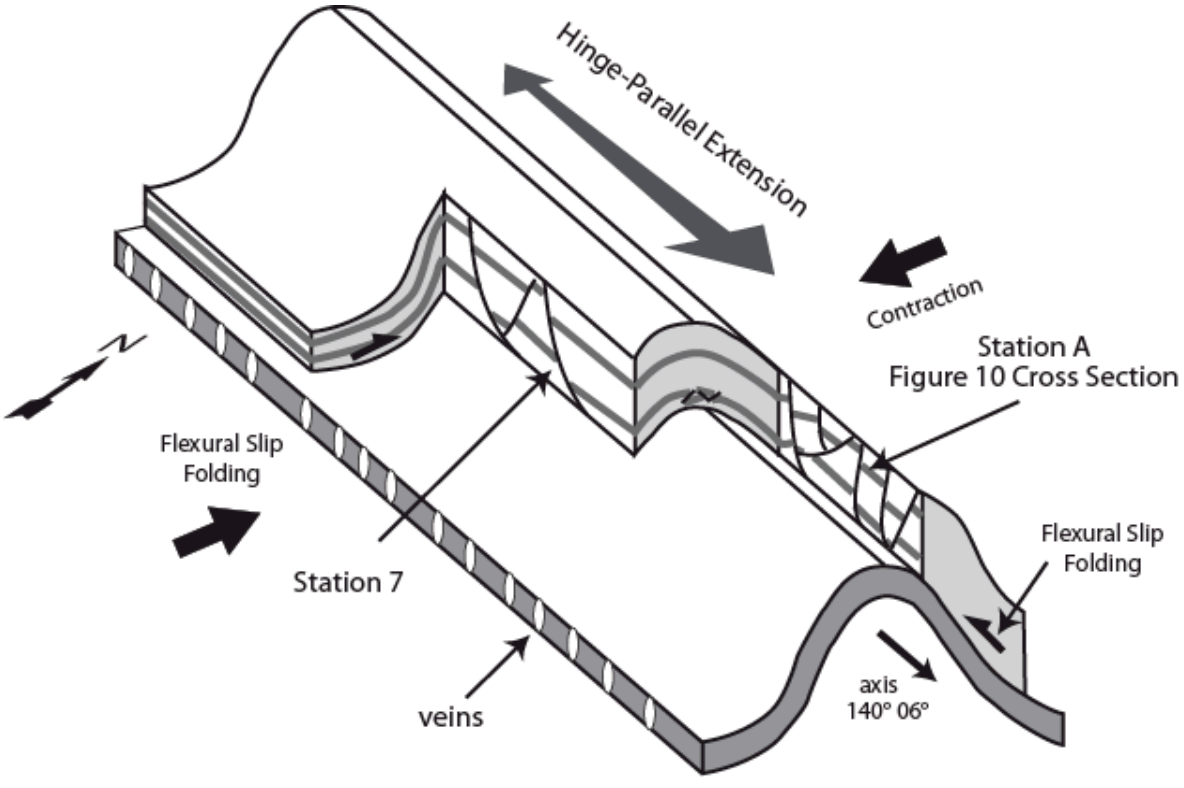

Fig. AB-29. Block diagram illustrating how joints (veins) and normal faults develop at Arroyo Burro with respect to fold geometry. These brittle structures accommodate extensional strain parallel to the fold axis, in response to regional NE-SW directed shortening. From Gross et al. (1997)

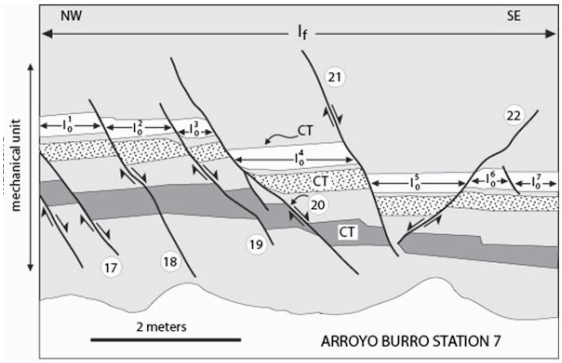

Fig. AB-30a. Sketch of a faults at Stop #2, illustrating how extensional strain was measured.

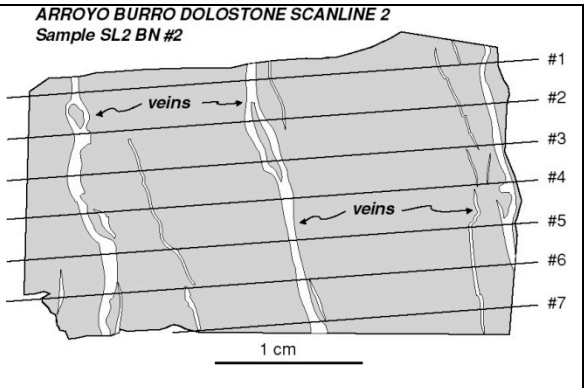

Fig. AB-30b. Sketch of veins in thin section from Stop #2, illustrating how strain was measured.

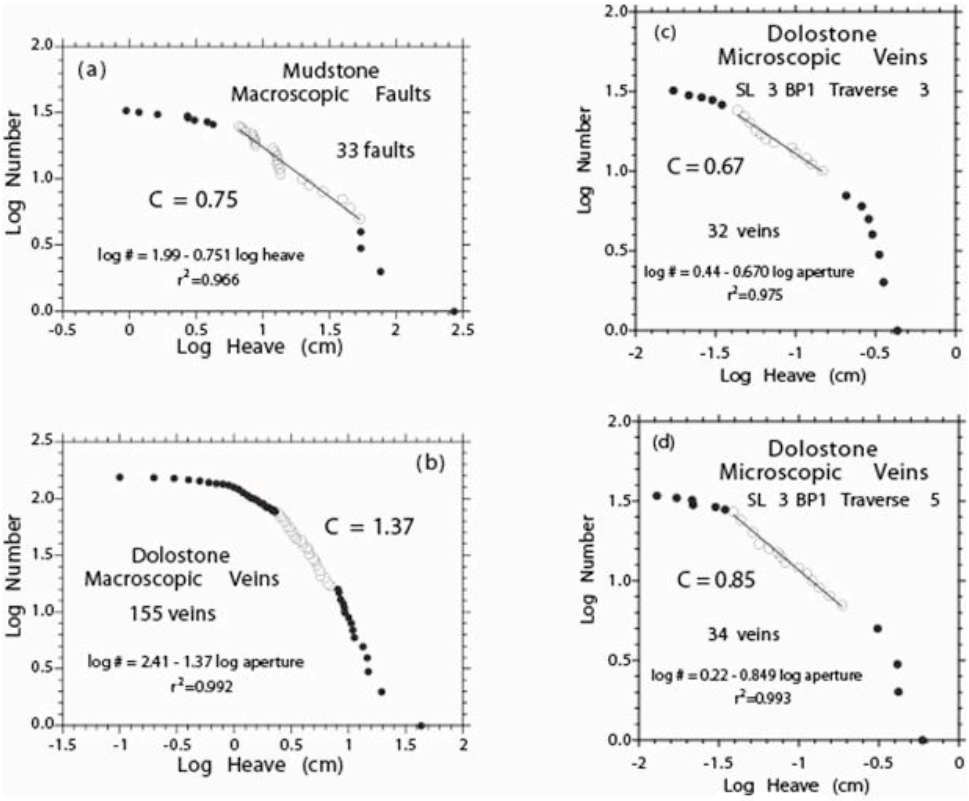

Fig. AB-31. Theoretical fault displacement population plots from Station #2, used to estimate the total extensional strain accommodated by faults and veins. From Gross and Engelder (1995).

Revised Strain Estimates (%):

Normal Faults	10.2 ± 1.0
Veins	9.7 ± 0.3

Stop #3 Tar-filled breccia / fault zone – throughgoing structural discontinuities, hydrocarbon pathways, focused fluid flow, fault-fracture envelopes, dilational fracturing, and high fluid pressures.

Fig. AB-32. Photo of tar-filled fault zone at Stop #3, with close-up of breccia. Note dilational nature of breccia and decrease in aperture and intensity of secondary veining away from the breccia zone (see Eichhubl and Boles, 1998).

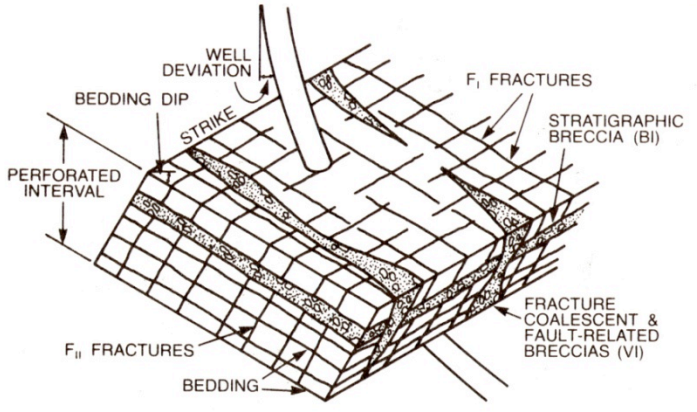

Fig. AB-33. Conceptual model of fracture/breccia flow in the Monterey Formation proposed by Belfield et al. (1983).

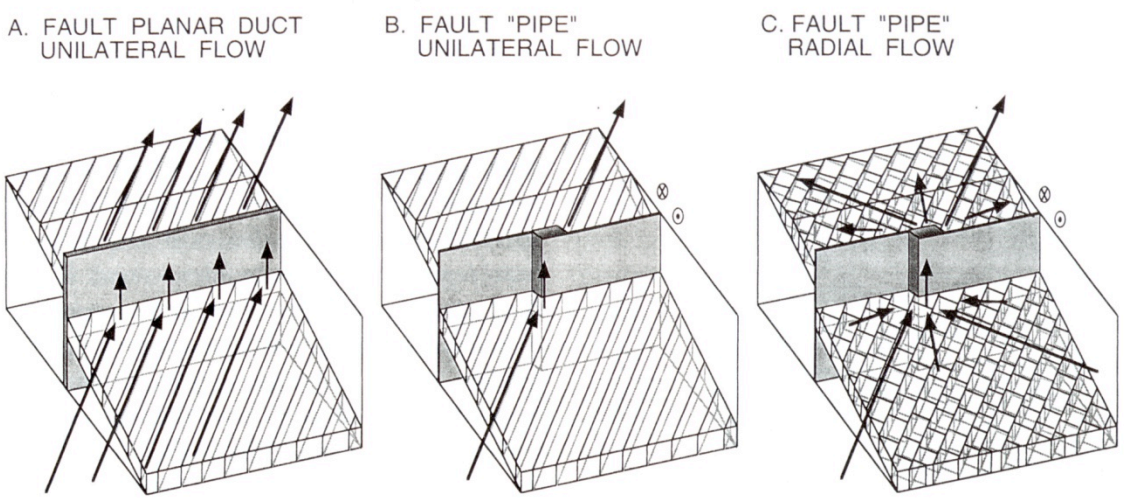

Fig. AB-34. Models for focused flow in the Monterey Formation proposed by Eichhubl and Boles (2000a).

Stop #4 Throughgoing dolostone vein – fracture cementation, multi-layer scaling.

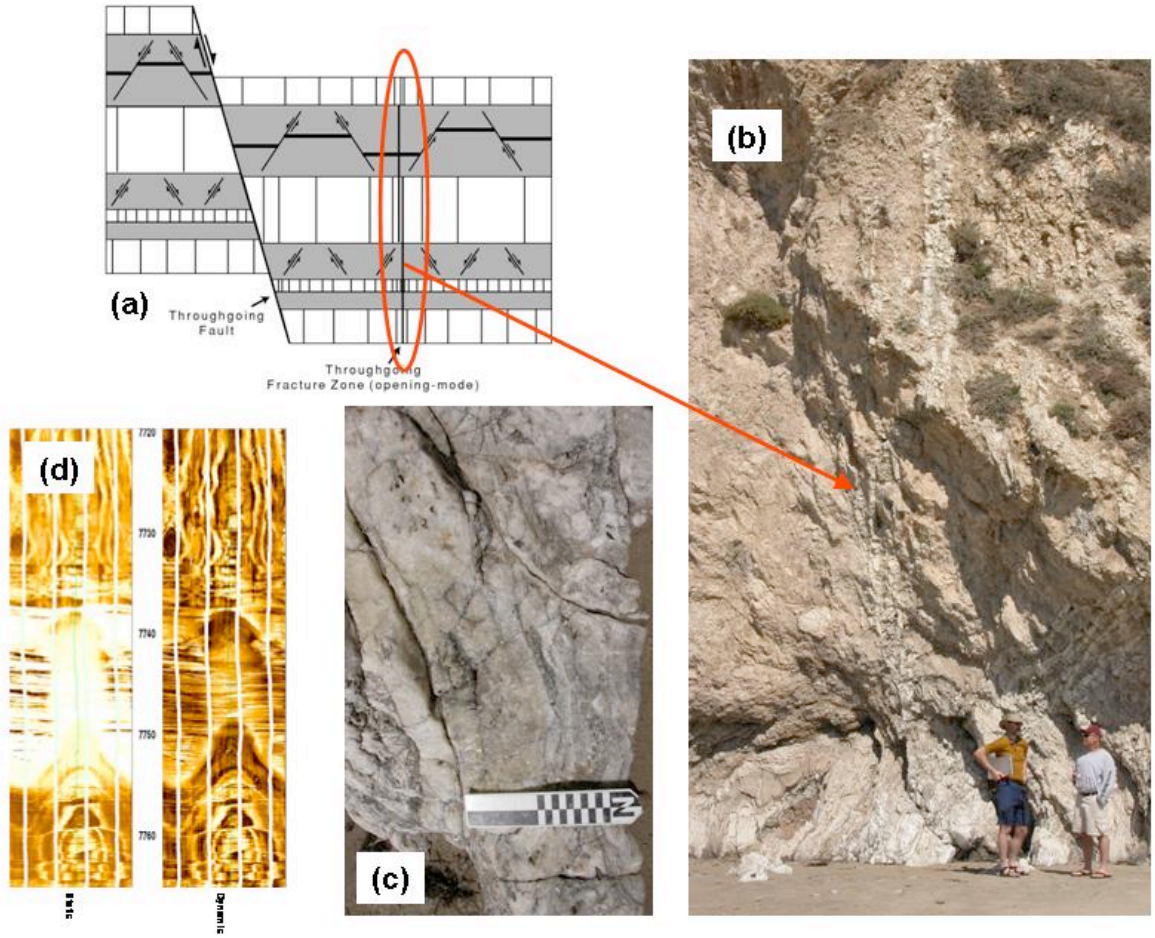

Fig. AB-35. Vertical dolostone vein at Stop #4. (a) Position in multi-scale hierarchy of the fracture network; (b) photo of vein; (c) close-up of vein fill; (d) example from image log of fractured dolostone interval.

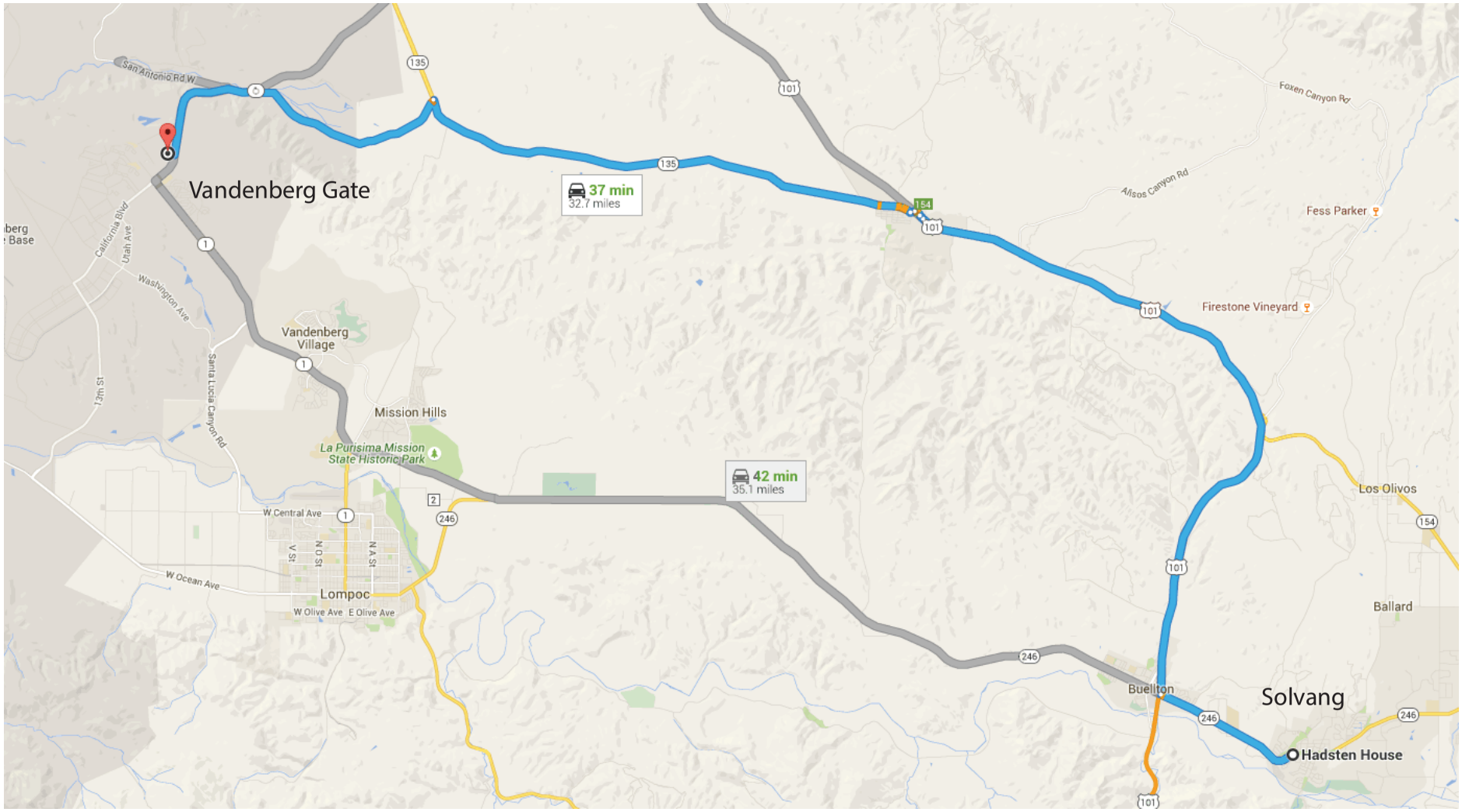

Day 3. Solvang to Vandenberg AFB gate.

Sandy beaches are closed June through September for Snowey Plover nesting season.

Monitoring and Management of the Endangered California Least Tern and the Threatened Western Snowy Plover at Vandenberg Air Force Base, 2013

Least Terns (left) and Snowy Plovers (right) breeding at Vandenberg Air Force Base

Point Blue Conservation Science

December 18, 2013

Executive Summary

Vandenberg Air Force Base (VAFB) contains approximately 13.8 linear miles of important coastal breeding habitat for the state and federally endangered California least tern (*Sternula antillarum browni*) and federally threatened Pacific coast population of the Western snowy plover (*Charadrius nivosus nivosus*). The California least tern is a small colonial seabird that breeds along the Pacific Coast. VAFB manages a least tern colony at Purisima Point, one of only three colonies between Monterey Bay and Point Conception. The Purisima Point least tern colony has been monitored annually since 1995. The Western snowy plover is a shorebird that breeds on coastal beaches from northern Washington to southern Baja California, Mexico. VAFB manages a breeding population of snowy plovers that is dispersed throughout much of the 13.8 miles of coastal beach habitat. The breeding population of snowy plovers has been monitored annually at VAFB since 1993. Staff at Point Blue Conservation Science monitored breeding least terns and snowy plovers at VAFB in 2013. This report summarizes least tern and snowy plover monitoring results from the 2013 breeding season within the context of VAFB's approximately 20-year time series for both species.

California Least Tern

The Purisima Point colony was visited at least five times a week throughout the breeding season. We first observed least terns at the colony on 13 May, which is late compared to historic arrival dates. Adult colony attendance increased quickly and remained consistent through the egg laying and incubation period. We estimate the 2013 breeding population to be 15 pairs which is 17% smaller than 2012 and 52% smaller than the 19-year mean. However, the 2013 breeding season was one of the most productive seasons on record. Hatching success (83%) was well above the 19-year average (59%) and fledging success (76%) was the second highest on record. Overall breeding success (1.27 fledglings per breeding pair) was also the second highest on record.

The Purisima Point least tern colony continues to be characterized by years of anomalously high and low reproductive success, with very few years consistent with the 19-year mean. Breeding productivity has been mostly above average since 2007, with two years of average to below average productivity (2011 and 2012). The breeding

population has not increased past the 19-year mean since 2005 and is even showing signs of a decreasing trend over the last three years (2011-2013). Least tern diet has also been variable since we began collecting diet samples in 2001. Our diet analyses have shown that least tern breeding productivity is highest when northern anchovy (*Engraulis mordax*) and/or rockfish (*Sebastes sp.*) dominate the diet. Abundance of both species is closely tied to oceanographic conditions. Since the winter of 2011, local oceanographic conditions have gone from La Niña (representing productive oceanic conditions) to El Niño neutral, with a brief warming period in 2012. The 2013 breeding may represent a return to productive conditions as both anchovy and rockfish were abundant in the diet.

Western Snowy Plover

The number of breeding snowy plovers observed and nests initiated in 2013 was similar to the long term mean. Clutch hatch success was higher than the long term mean, while fledging success was the highest on record. We attribute the high clutch hatch success in 2013 to lower predation rates compared to previous years while the increased fledging success likely due to increased wrack abundance (a food source for snowy plover prey) in 2013. Wrack abundance was significantly higher at most beach sectors in 2013 compared to 2012. Predators accounted for 20% of nest losses in 2013 compared to 37% in 2012 and 52% in 2011. The decrease in nest predation in recent years is primarily due to decreases in raven predation. Ravens took 18% of nests in 2011, 16% of nests in 2012, and <1% of nests in 2013.

Efforts to manage human activities at VAFB appear to be successful. Areas closed to recreational beach access have shown increased nesting effort and clutch hatch success when compared to adjacent open beach areas. Additionally, nesting effort base-wide has increased since closures were established in 2000. Overall, the time series data suggest that large scale processes (e.g., environmental variability) are governing breeding effort and fledging success, while more localized factors (e.g., predation) are governing clutch hatch success at VAFB. These results suggest that management of the snowy plover population on VAFB needs to occur at both base-wide and localized spatial scales, focusing on predators that are significantly impacting local beach sectors while using environmental and oceanographic information to manage VAFB's coastal ecosystem.

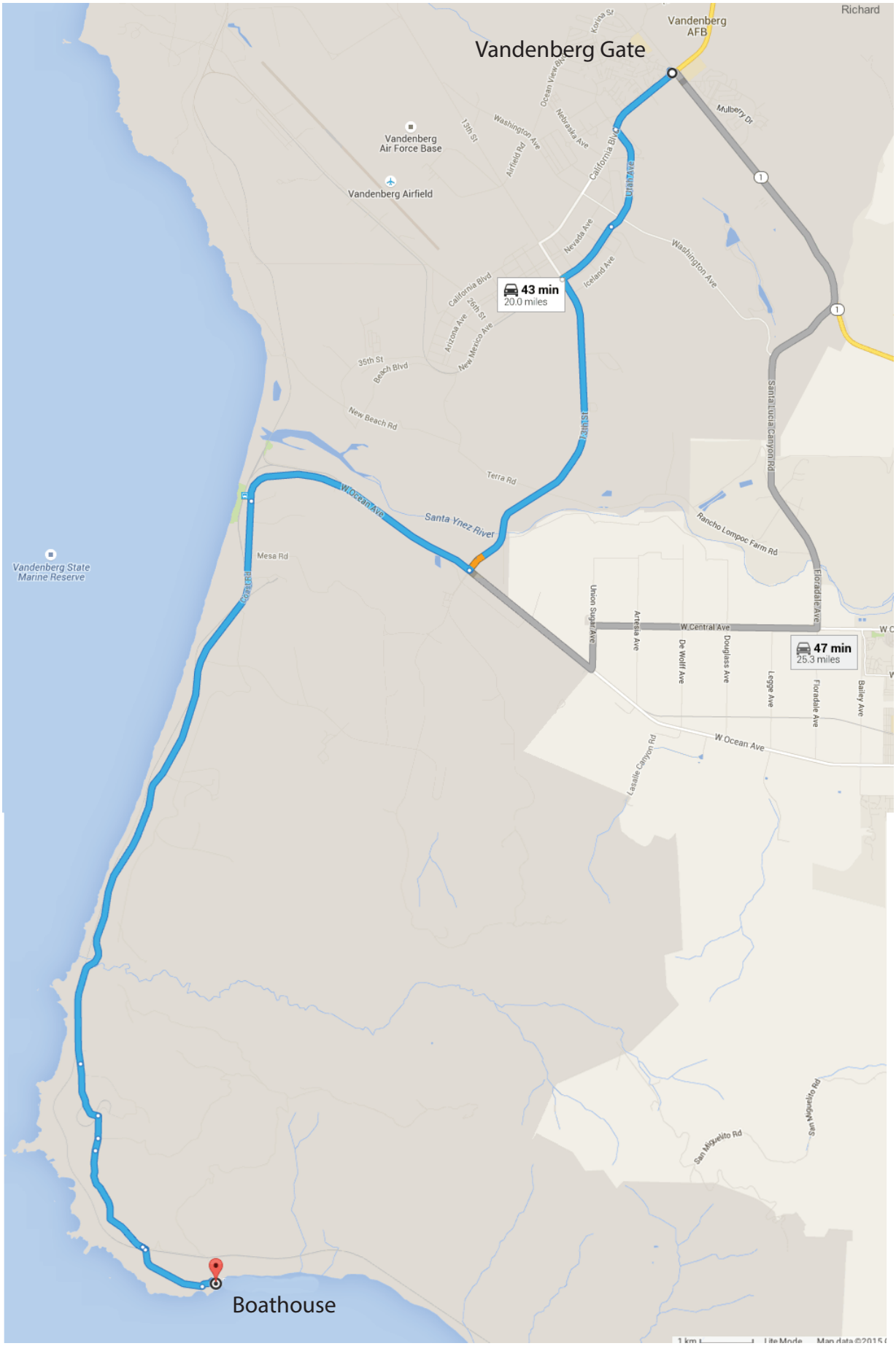

Day 3. Vandenberg AFB gate to Boathouse.

Vandenberg Air Force Base: Boathouse Section

Basin:
Southern edge of Santa Maria Basin

Formation/Members:
Monterey,
clayey-siliceous (upper siliceous)
upper calcareous-siliceous member

Notes:

- Upper calcareous-siliceous member of the Monterey Formation (east of Boathouse pier) consists of thickly interbedded black chert and tan dolomite, buff to white porcelanite, and shale.

- Similar to classic contorted, black, quartz-phase chert interbedded with dolostone exposures at Lions Head and Mussel Rock sections. Chert consists of thinly laminated quartz and dolomite ("tiger-stripe" chert).

- Note that only chert displays tight intraformational folding. Buckling, brecciation, and cementation structurally thickens initial stratigraphic thickness of chert beds.

- Upper, clayey-siliceous member of the Monterey Formation (west of Boathouse pier) consists of thin-bedded, laminated porcelanite, siliceous shale, plus minor chert, and dolomite.

- All silica is in the quartz-phase silica diagenetic grade.

- General lack of tar or oil in joints of brittle lithologies (chert and dolomite). Most early fractures are quartz- or dolomite-cemented, later ones are not oil-filled.
-

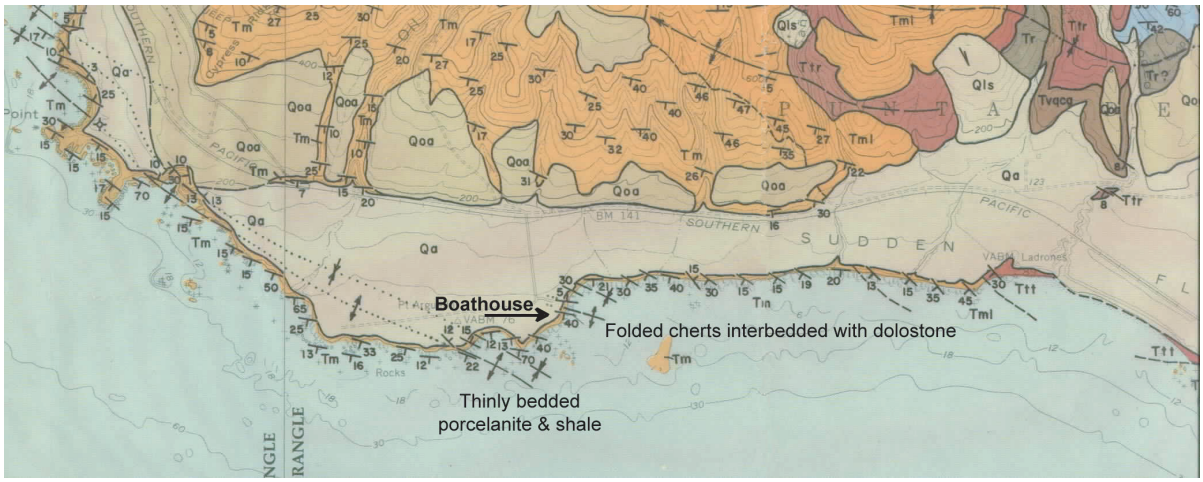

Figure BH-01. Geologic map of the Boathouse-Rodeo Canyon section area. Modified from (Dibblee and Ehrenspeck, 1988).

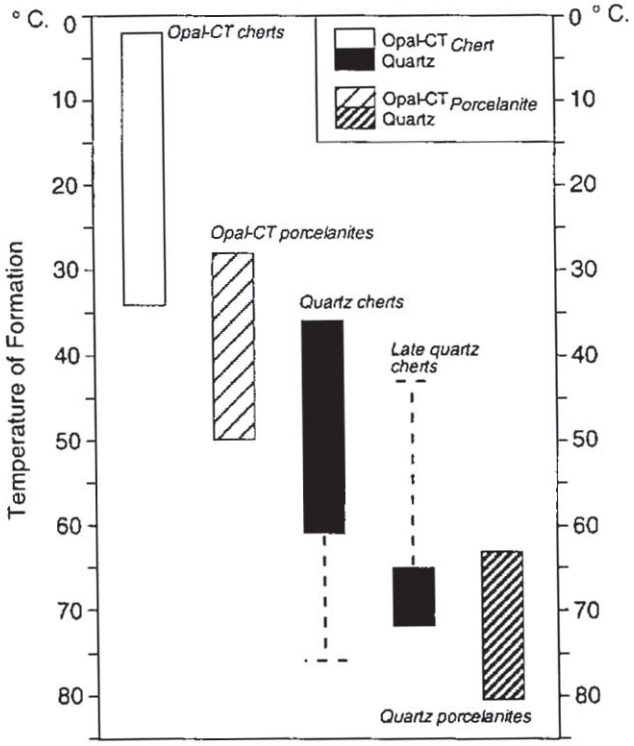

Figure BH-02. Sequence of silica diagenesis and chertification determined by integrated oxygen isotope, petrographic, and field relationship data, after Behl and Garrison (1994) and Behl (1998).

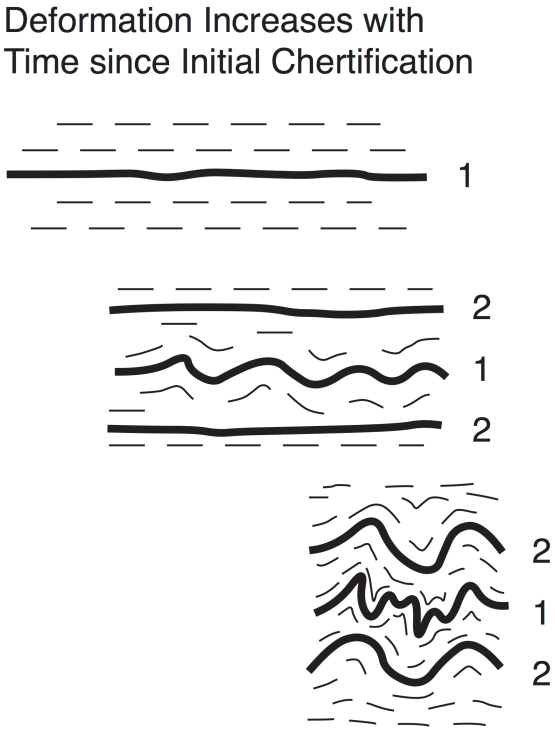

Figure BH-03. Cherts always show higher degree of deformation than associated shale, porcelanite, or dolomite. The earliest formed cherts show the greatest degree of macroscopic deformation (Behl and Garrison,1994: Behl, 1998).

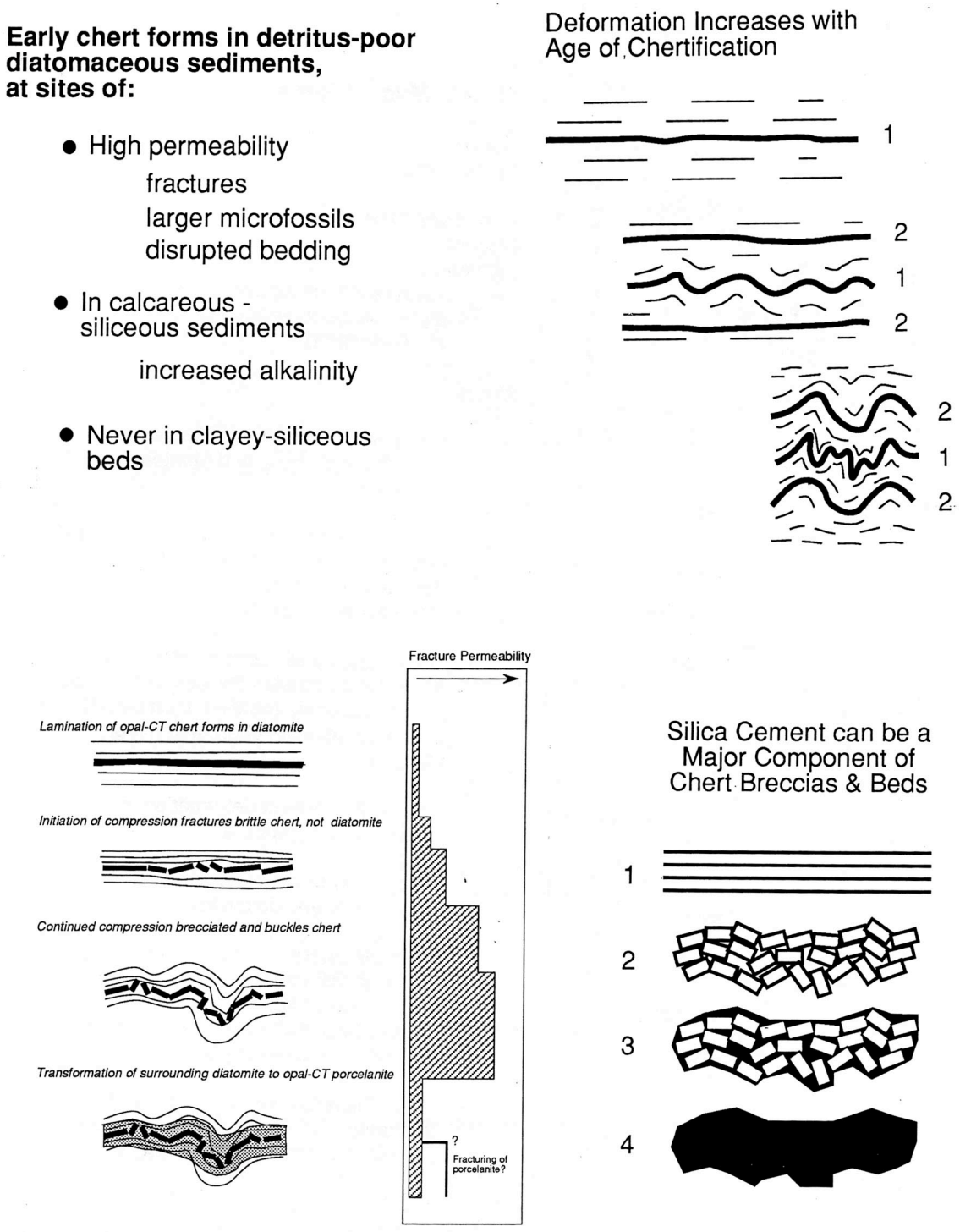

Fig. BH-4. Timing of chertification is critical the style of deformation, as well as the reservoir potential of the rocks. The earlier the chert becomes hard, brittle, and incompressible while still surrounded by extremely porous diatomaceous sediments, the greater the apparent contrast in degree of deformation of the different rocks. Fracture porosity is greatest during earlier stages of brecciation before individual laminations are cemented together.

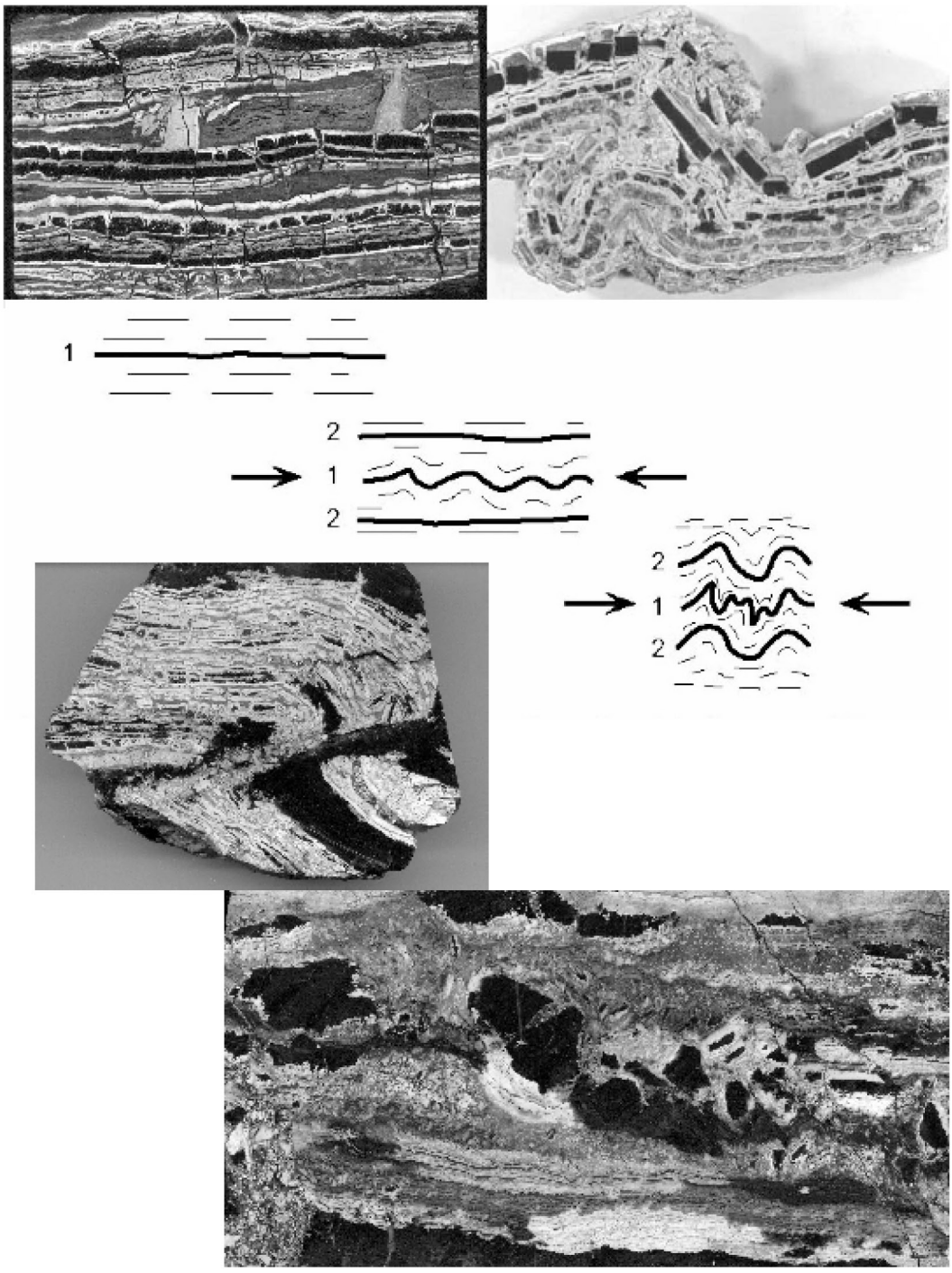

Figure BH-05. Stages of formation of a tightly cemented chert breccia. Initial jointing and boudinage of thin chert laminations. Shortening leads to rotation and bucking of chert laminations and beds, creating fracture porosity. Diffusion and advection of silica-rich pore-waters cements fragments. Continued diagenesis converts distinct fragments of opal-CT chert into homogeneous quartz chert, hiding evidence for early fragmented stage.

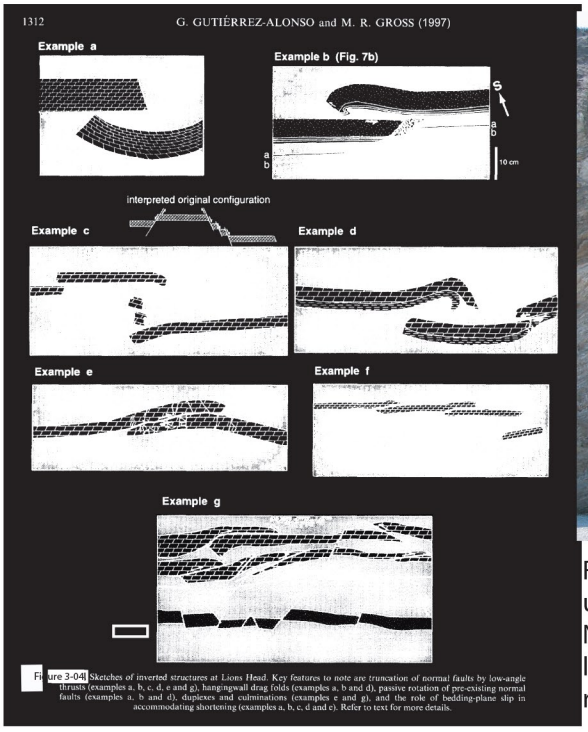

Figure BH-06. Thin-bedded porcelanite and siliceous shale of the upper clayey-siliceous member of the Monterey Formation. Note the kink-folds that involved several meters of strata, but lack of intrastratal folds. Highly convoluted folds are limited to rare chert beds in this member.

Figure BH-7. Thin- to medium-bedded porcelanite, chert, dolomite and shaleof the upper calcareous-siliceous member of the Monterey Formation in the Boathouse section.

Figure BH-8. Buckled and faulted quartz-phase chert between apparently undeformed dolostone beds. Petrographic analysis and field exposures show that the folding was initially accomplished by brittle deformation of opal-CT chert, later obscured by cementation and transformation to quartz.

Figure BH-9. Axis-perpendicular joint sets cut across chert folds, but pre-existing lineations from earlier phase of deformation are folded (fine structure slightly oblique to prominent fractures).

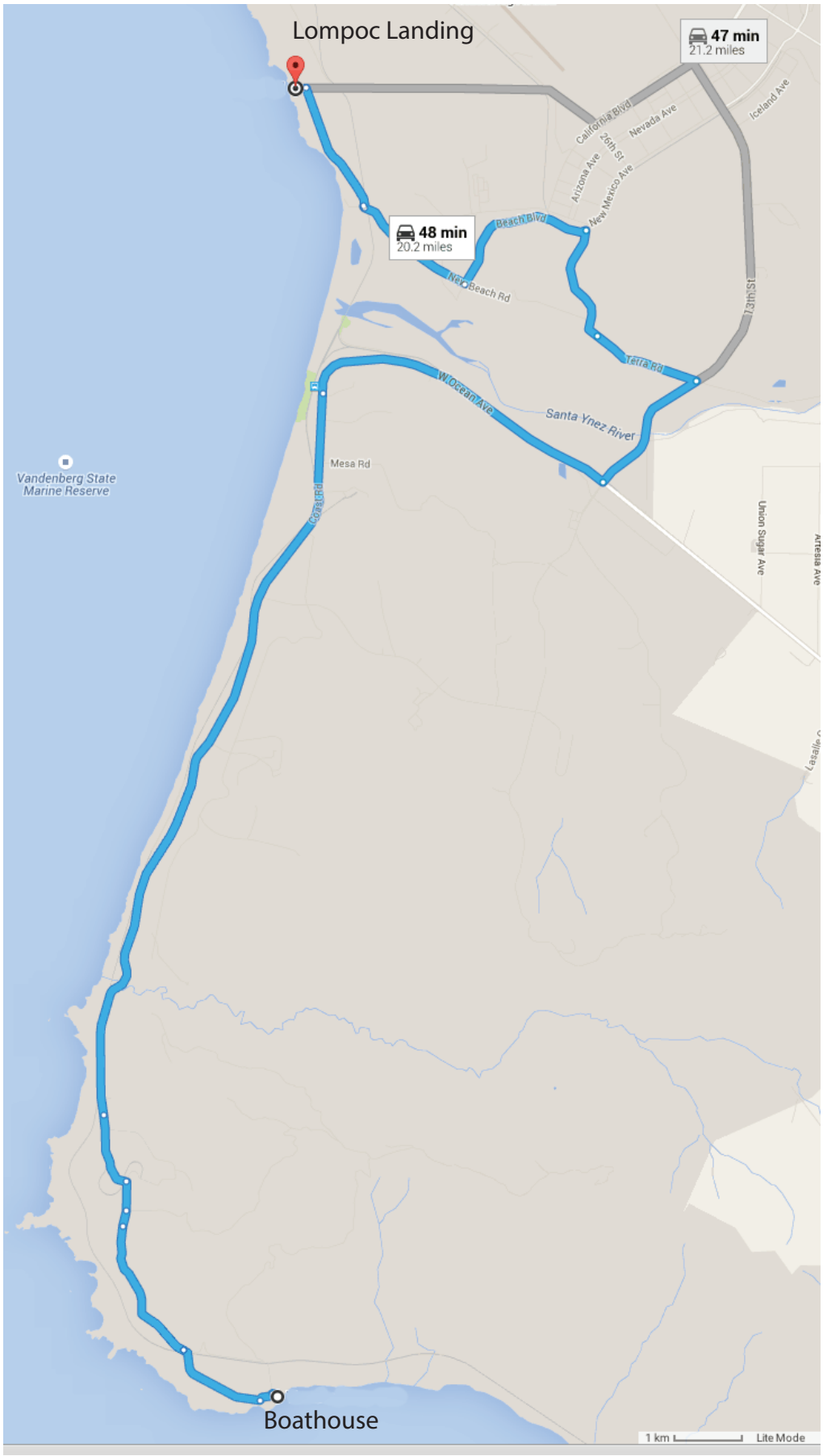

Day 3. Boathouse to Lompoc Landing.

Vandenberg Air Force Base: Lompoc Landing

Basin: Santa Maria

Formation/Members:

Monterey

Upper calcareous-siliceous member

Notes:

- Excellent exposure of exhumed oil reservoir of fractured chert and porcelanite, interbedded with siliceous shale and minor dolomite.
- Near crest of broad anticline south of the Lompoc-Purisima anticlinal trend.
- Most siliceous rocks are opal-CT phase in initial stage of conversion to quartz
- Bedding-confined opal-CT chert breccias consist of stacked chert laminations, shattered into cubes ~2-3 mm in diameter, similar to an angular gravel.
- Vertically cross-cutting breccias and joints provide stratigraphic connectivity and additional storage.
- Horizontal shortening and layer-parallel shear brittlely deform the chert, making it brecciate and buckle, giving rise to “contorted cherts”.
- Laminations of black-brown quartz chert only formed within layers and fragments of the purest opal-CT chert. Cementation and recrystallization to quartz obscures brittle origin of chert folds.
- Described in Dunham & Blake (1987) and Gutiérrez-Alonzo & Gross (1997).

Watch out for high surf!!!

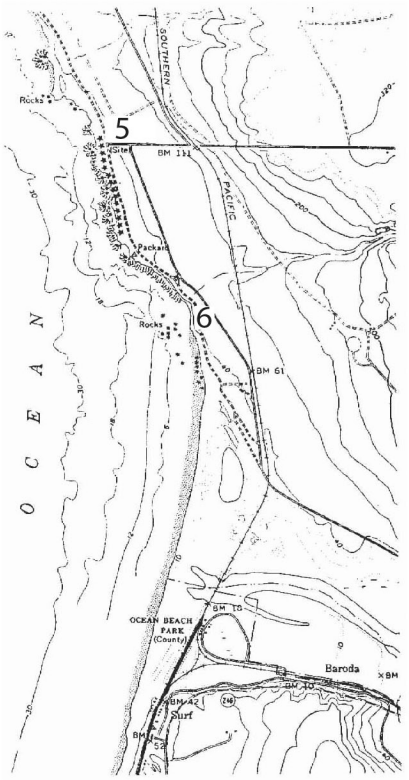

Figure LL-1. Location map for Lompoc Landing (5) and Wall Beach/North Surf (6).

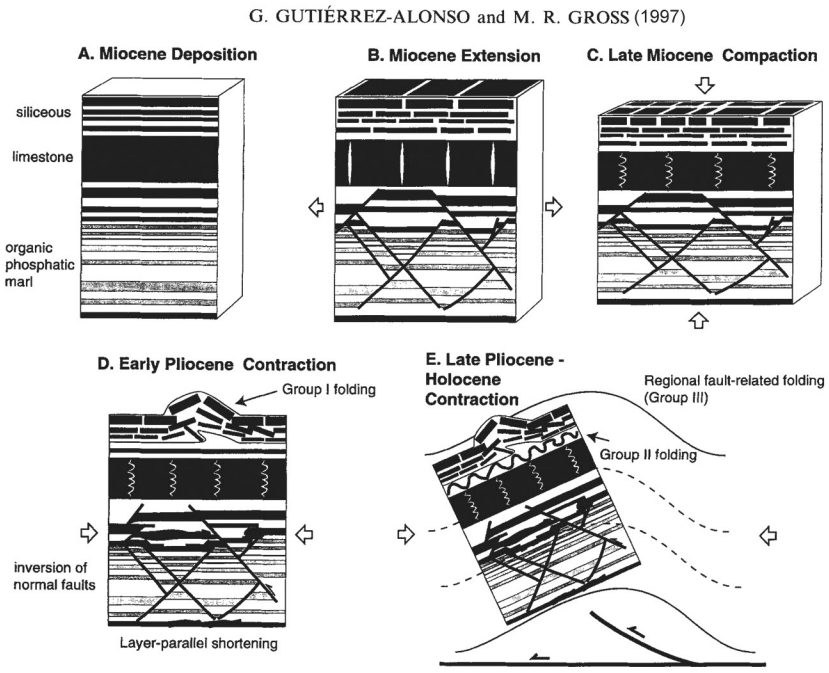

Figure LL-02. Model depicting sequence and timing of deformation events from the Miocene in the Monterey.

Figure LL-03. Several distinct, but irregular joint sets in chert and porcelanite.

Figure LL-04. Tar-saturated, brecciated shear zone cuts through stack of less brecciated opal-CT chert laminations, providing enhance vertical permeability.

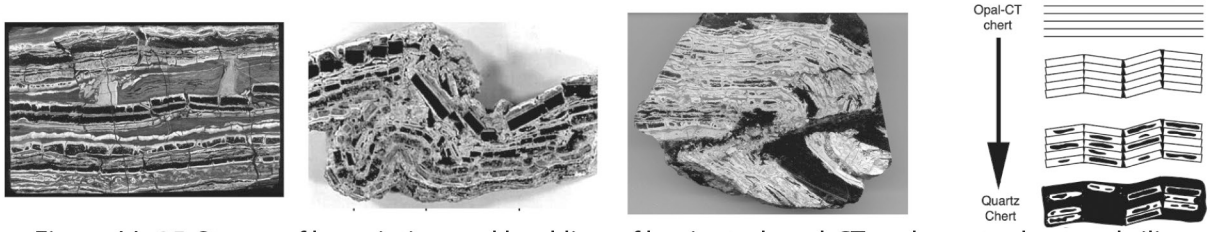

Figure LL-05. Stages of brecciation and buckling of laminated opal-CT and quartz chert and siliceous shale. White-weathering rock is opal-CT, black is quartz chert. Note how cementation and recrystallization of the opal-CT fragments to/with quartz is to obliterating the evidence for brittle deformation.

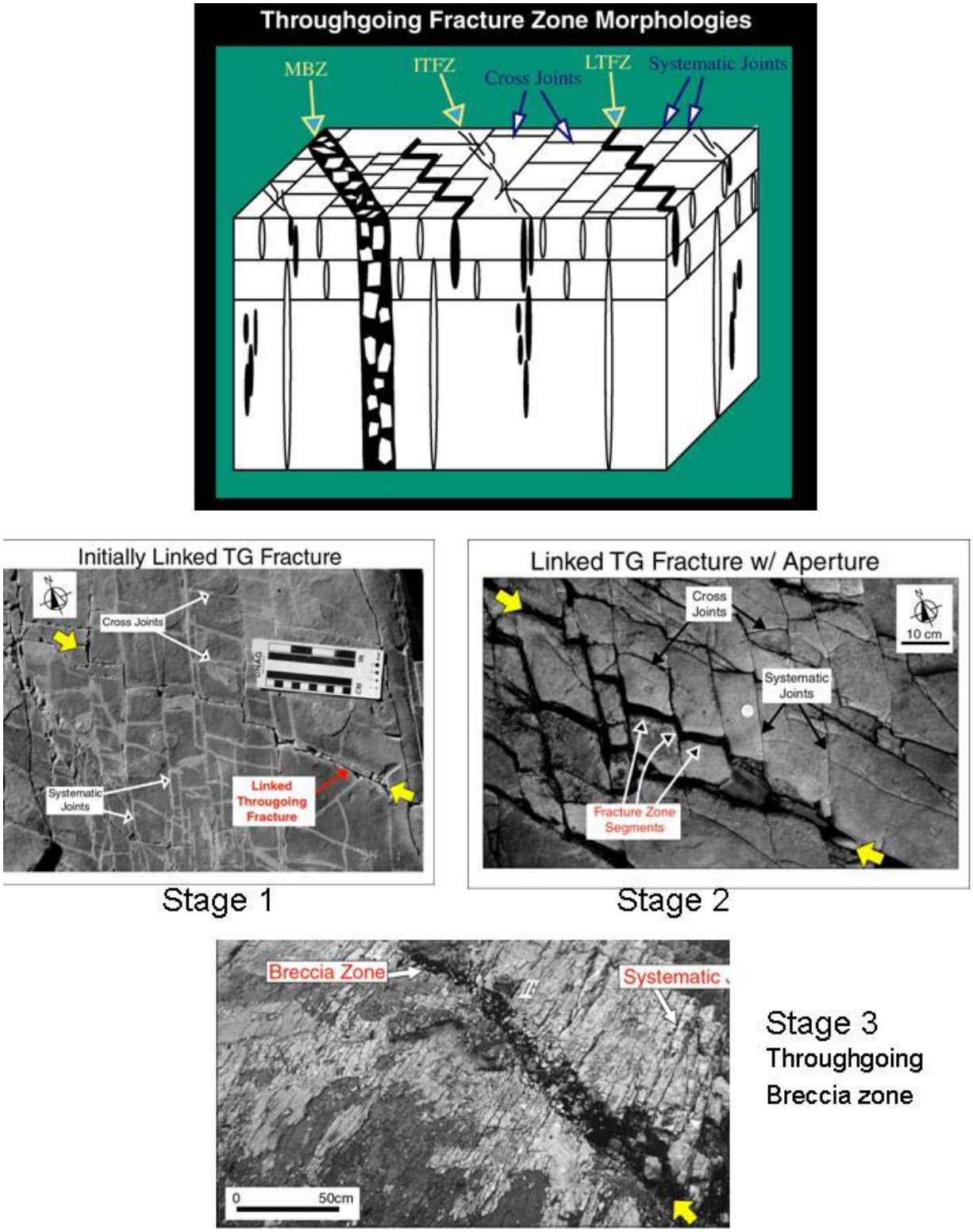

Figure LL-06. Morphologies of vertical (bed-normal) throughgoing fractures in the Monterey Formation at Lompoc Landing, showing stages and evolutionary development of these multi-layer structures. From Finn (2000) and Finn et al. (2003). Compare with bed-parallel breccia zones at Chico Martinez Creek.

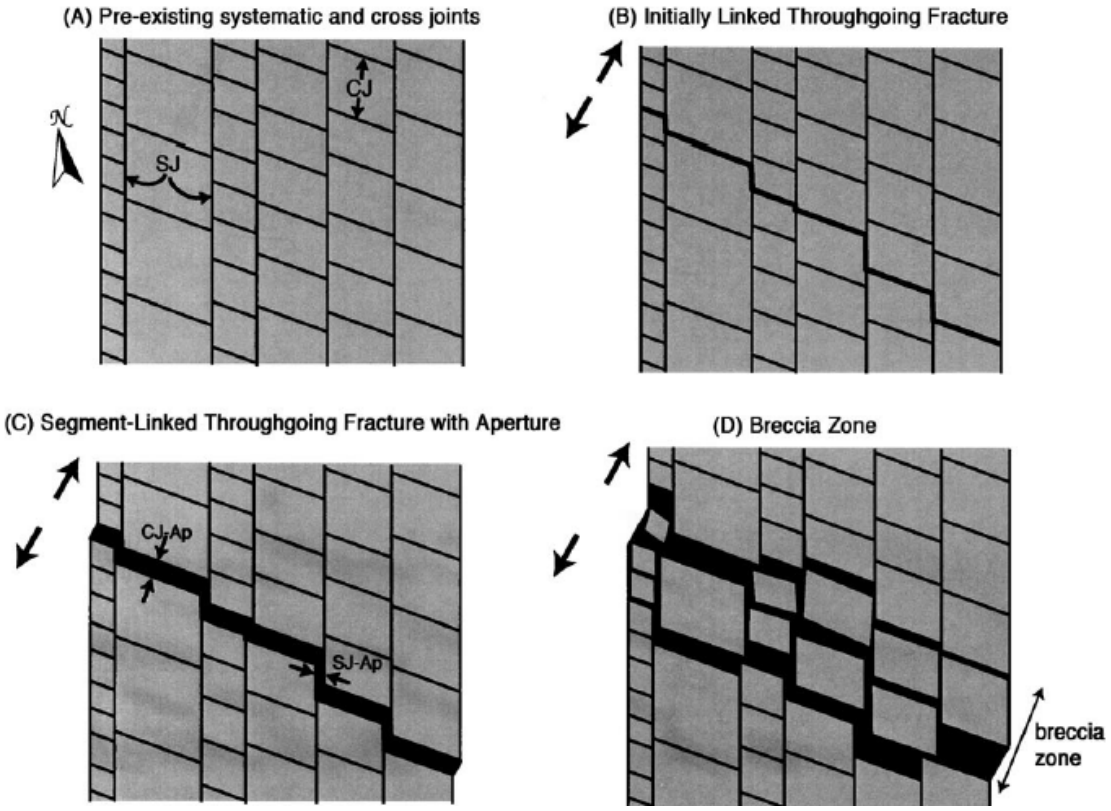

Figure LL-07. Conceptual model for development of breccia zones at Lompoc Landing due to extension normal to the trend of the throughgoing fracture. Breccia clasts are derived from joint-bounded blocks incorporated into the tar-filled matrix.From Finn et al. (2003).

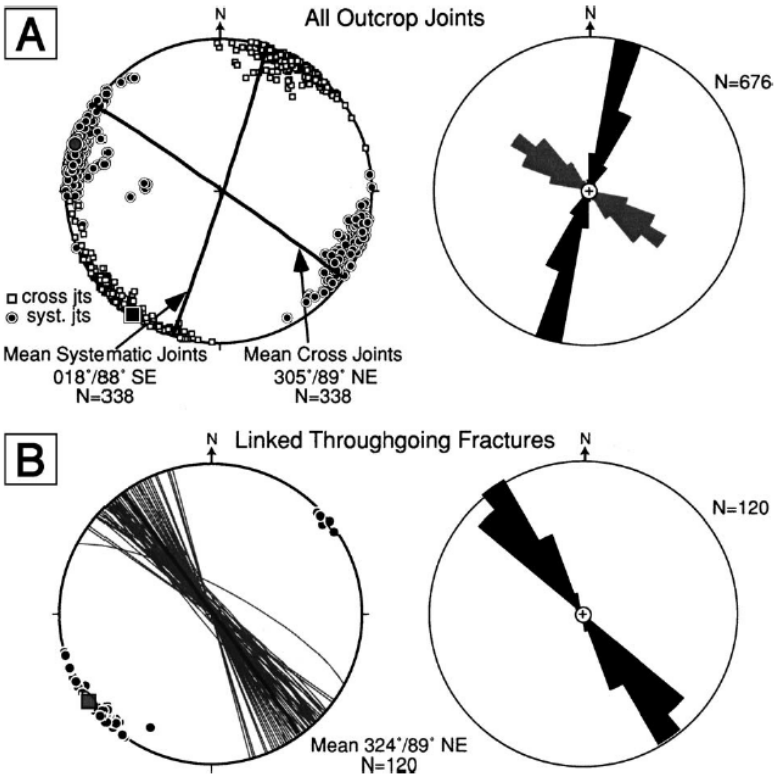

Figure LL-08. Stereoplots and rose diagrams of fracture data from Lompoc Landing, CA. (A) Orientations of bed confined joints. Systematic joints trend NNE–SSW and cross joints trend WNW–ESE. Note: 70° acute angle between trends and greater scatter in orientation for cross joints. (B) Orientations of linked throughgoing fractures. From Finn et al. (2003).